

**Sensitivity of inorganic aerosol impacts  
to US precursor emissions**

by

Jareth Ian Holt

A.B., Princeton University (2009)

Submitted to the Department of  
Earth, Atmospheric, and Planetary Science  
in partial fulfillment of the requirements for the degree of  
Doctor of Philosophy in Climate Physics and Chemistry

at the

MASSACHUSETTS INSTITUTE OF TECHNOLOGY

September 2016

© Massachusetts Institute of Technology 2016. All rights reserved.

Author .....  
Department of Earth, Atmospheric, and Planetary Science  
September 1, 2016

Certified by.....  
Susan Solomon  
Ellen Swallow Richards Professor of  
Atmospheric Chemistry and Climate Science  
Thesis Supervisor

Certified by.....  
Noelle E. Selin  
Associate Professor of Data, Systems, and Society,  
and Atmospheric Chemistry  
Thesis Supervisor

Accepted by .....  
Robert D. van der Hilst  
Schlumberger Professor of Earth and Planetary Sciences  
Head of Department of Earth, Atmospheric, and Planetary Sciences



# Sensitivity of inorganic aerosol impacts to US precursor emissions

by

Jareth Ian Holt

Submitted to the Department of Earth, Atmospheric, and Planetary Science  
on September 1, 2016, in partial fulfillment of the  
requirements for the degree of  
Doctor of Philosophy in Climate Physics and Chemistry

## Abstract

I present work on the relationship between inorganic atmospheric aerosol impacts and their precursor emissions from the United States of America. The inorganic aerosol ions nitrate ( $\text{NO}_3^-$ ), sulfate ( $\text{SO}_4^{2-}$ ), and ammonium ( $\text{NH}_4^+$ ) form from emissions of nitrogen oxides ( $\text{NO}_x$ ), sulfur dioxide ( $\text{SO}_2$ ), and ammonia ( $\text{NH}_3$ ). Emissions of  $\text{NO}_x$  and  $\text{SO}_2$  in the US have recently decreased, by 42% and 62% respectively for annual totals between 2005 and 2012, in response to economic, political, and technological developments. Under such large changes, the processes of aerosol formation may behave nonlinearly. The sensitivity of aerosol impacts to future emissions reductions – the change in a metric per unit change in emissions – can be very different from the sensitivity to past reductions. In this thesis, I use a chemical transport model to examine the sensitivities, changes in sensitivities, and the importance of nonlinear interactions for both health and climate impacts of inorganic aerosols.

The first section of this thesis focuses on surface concentrations of inorganic fine particulate matter ( $\text{PM}_{2.5}$ ), a relevant metric for human health. In winter,  $\text{PM}_{2.5}$  across the central US is primarily composed of ammonium nitrate, whose formation is highly dependent on thermodynamics. The recent  $\text{NO}_x$  and associated total nitrate ( $\text{HNO}_3 + \text{NO}_3^-$ ) reductions have made aerosol formation in this region limited by total nitrate availability. Future  $\text{NO}_x$  emissions reductions will thus have a much larger impact than they would have in the past. In summer,  $\text{SO}_4^{2-}$  aerosols dominate  $\text{PM}_{2.5}$ . The reduced  $\text{NO}_x$  emissions lead to higher peroxide concentrations and faster aqueous  $\text{SO}_2$  oxidation, without increasing sulfate wet deposition to the same degree. With faster oxidation, a larger fraction of the emitted  $\text{SO}_2$  forms sulfate and particulate matter, increasing the sensitivity of surface aerosol concentrations to  $\text{SO}_2$  emissions even as emissions themselves have decreased. These results suggest that  $\text{NO}_x$  and  $\text{SO}_2$  emissions reductions will continue to improve US air quality.

The second section of this thesis focuses on sensitivities of the direct radiative effect (DRE) of inorganic aerosols to US emissions, a key quantity for studying climate impacts. The DRE and changes in DRE in winter are largest over the ocean. The summertime DRE includes a long tongue of advected aerosols over the Atlantic as well

as a broad area of large DRE over the eastern US. As with surface concentrations, sensitivity of DRE to  $\text{NO}_x$  and  $\text{SO}_2$  emissions increased between 2005 and 2012, while sensitivity to  $\text{NH}_3$  emissions decreased. A simple scaling estimate of the DRE in the 2012 case from the 2005 DRE and sensitivities overestimates the magnitude of the DRE by  $10.3 \text{ mW m}^{-2}$  in January and  $21.4 \text{ mW m}^{-2}$  in July. These values are equivalent to underestimating the  $\text{SO}_2$  emissions reductions by 13.6% and 10.6%, respectively. These processes cause small errors for climate studies that assume scaling of aerosol radiative effects for current conditions, but greater errors could occur under future emission changes.

Thesis Supervisor: Susan Solomon

Title: Ellen Swallow Richards Professor of  
Atmospheric Chemistry and Climate Science

Thesis Supervisor: Noelle E. Selin

Title: Associate Professor of Data, Systems, and Society,  
and Atmospheric Chemistry

# Contents

<b>1</b>	<b>Introduction</b>	<b>11</b>
1.1	Motivation . . . . .	11
1.2	Outline . . . . .	15
<b>2</b>	<b>Methods</b>	<b>17</b>
2.1	Chemical transport model . . . . .	19
2.2	Model validation . . . . .	20
2.2.1	Measurement networks . . . . .	21
2.2.2	Model-measurement comparison . . . . .	22
2.3	Emissions . . . . .	26
<b>3</b>	<b>Sensitivities and nonlinearities</b>	<b>29</b>
3.1	Definitions . . . . .	29
3.2	Methods for estimating sensitivities . . . . .	32
3.2.1	Finite difference . . . . .	32
3.2.2	Complex step . . . . .	35
3.2.3	Direct decoupled . . . . .	37
3.2.4	Model Adjoint . . . . .	40
3.3	Comparison of estimates . . . . .	44
<b>4</b>	<b>Surface aerosol concentrations</b>	<b>47</b>
4.1	Introduction . . . . .	47
4.2	Methods . . . . .	49

4.3	Results . . . . .	50
4.3.1	Fine particulate concentrations . . . . .	50
4.3.2	Particulate sensitivities to emissions . . . . .	52
4.4	Underlying processes . . . . .	54
4.4.1	Thermodynamics of ammonium nitrate formation . . . . .	55
4.4.2	Kinetics of SO <sub>2</sub> oxidation . . . . .	57
4.4.3	Linearity of the system . . . . .	60
4.5	Discussion . . . . .	61
<b>5</b>	<b>Direct radiative effects</b>	<b>65</b>
5.1	Introduction . . . . .	65
5.2	Methods . . . . .	69
5.2.1	Chemical transport model GEOS-Chem . . . . .	69
5.2.2	Radiative transfer model RRTMG . . . . .	71
5.2.3	Off-line calculation validation . . . . .	72
5.3	DRE and its sensitivity to emissions . . . . .	75
5.3.1	Base-case DRE . . . . .	76
5.3.2	DRE sensitivities . . . . .	77
5.4	Discussion . . . . .	78
5.5	Conclusion . . . . .	82
<b>6</b>	<b>Conclusions</b>	<b>87</b>
6.1	Discussion . . . . .	87
6.2	Future work . . . . .	89
6.3	Final notes . . . . .	91
<b>A</b>	<b>Normalizing sensitivities</b>	<b>93</b>

# List of Figures

2-1	Scatterplot of model and IMPROVE concentrations. . . . .	24
2-2	Scatterplot of model and CSN concentrations. . . . .	25
4-1	Reference-case PM <sub>2.5</sub> concentrations in January. . . . .	51
4-2	Reference-case PM <sub>2.5</sub> concentrations in July. . . . .	52
4-3	PM <sub>2.5</sub> sensitivities to January emissions. . . . .	53
4-4	PM <sub>2.5</sub> sensitivities to July emissions. . . . .	55
4-5	Thermodynamic component of PM <sub>2.5</sub> sensitivities. . . . .	56
4-6	Histogram of daily-average PM <sub>2.5</sub> . . . . .	57
4-7	Aqueous fraction of total SO <sub>2</sub> oxidation. . . . .	59
4-8	Constant-sensitivity approximation compared to full model results. . . . .	60
5-1	Spatial comparison of on-line and off-line DRE estimates. . . . .	74
5-2	Scatterplot comparison of on-line and off-line DRE estimates. . . . .	75
5-3	Spatial maps of DRE in the base cases. . . . .	76
5-4	Vertical profiles of concentrations in the base cases. . . . .	85
5-5	Domain used for the profiles in figure 5-4 . . . . .	86
5-6	Sensitivities of domain-average DRE to each precursor emission. . . . .	86

THIS PAGE INTENTIONALLY LEFT BLANK

# List of Tables

2.1	Model-measurement statistics for January. . . . .	22
2.2	Model-measurement statistics for January, continued . . . . .	22
2.3	Model-measurement statistics for July. . . . .	23
2.4	Model-measurement statistics for July, continued. . . . .	23
2.5	US annual emissions (total without wildfires) in thousands of short tons for the years 2005 and 2012 along with the percentage change. .	27
2.6	Perturbations in US anthropogenic emissions of each species applied in the sensitivity simulations. . . . .	27
4.1	Emissions used for each simulation. . . . .	49
4.2	Changes in oxidant concentrations. . . . .	58
5.1	Domain-average DRE in the validation dataset. . . . .	73
5.2	Domain-average DRE in the base cases. . . . .	77
5.3	Fractional changes in DRE sensitivities between the 2005 and 2012 cases.	80

THIS PAGE INTENTIONALLY LEFT BLANK

# Chapter 1

## Introduction

### 1.1 Motivation

The chemistry of gases is central to atmospheric chemistry, but liquid and solid particles matter as well – as evidenced by clouds. These liquid and solid particles suspended in air are collectively called aerosol<sup>1</sup> and are a key focus of modern atmospheric chemistry. Part of the reason for that focus is that atmospheric particles can affect human health on national and international scales. Another reason is that particles scatter and absorb light, impacting climate. I will address both of these motivations in this thesis.

That particulates harm human health has been known for decades. In one of the earliest epidemiological studies, [Lave and Seskin \(1973\)](#) showed a strong association between mortality rate and air quality through a cross-sectional study of 117 metropolitan areas in the US between 1960 and 1961. They found that an increase of  $10 \mu\text{g m}^{-3}$  in mean particulate concentrations was associated with a mortality rate increase of 0.41 per 10,000. Of the variables considered for statistical regression, mean particulate levels were the third-largest determinant of mortality, behind the population fraction above 65 years of age and the non-white population fraction. [Dockery et al. \(1993\)](#) conducted a prospective cohort study within six US cities to establish

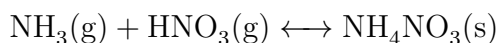
---

<sup>1</sup>The terms ‘aerosols’, ‘particulates’, and ‘particulate matter’ are commonly used to refer to the particles specifically (as opposed to the liquid/solid/gas combination) and I will use all of these terms equivalently.

a stronger link between *long-term* particulate exposure and mortality. They found that total *fine* particulate concentrations (particles with a diameter less than 2.5  $\mu\text{m}$ , abbreviated as  $\text{PM}_{2.5}$ ) were the variable most directly associated with mortality rates. These and other studies have established that  $\text{PM}_{2.5}$ , due to its ability to penetrate all the way into the alveoli of the lungs, is one of the most important atmospheric pollutants to control in order to limit mortality and morbidity. The WHO estimates that fine particulates cause 800,000 premature deaths per year worldwide (Cohen et al., 2006).

Similarly, the research linking atmospheric particulates to climate is decades old. Aitken (1882) first started measuring particle concentrations and their relation to visibility and cloud and fog formation. Ångström (1929) describes the link between net insolation and atmospheric dust concentrations, and McCormick and Ludwig (1967) even cites anthropogenic pollutants as one cause of the decline in global temperatures starting in the 1950s. In this thesis, I will focus on the direct radiative effect of primarily scattering aerosols. Other areas of aerosol-climate research include the effects of aerosols on cloud formation, brightness, and lifetime (Twomey, 1974; Albrecht, 1989) and absorbing, carbonaceous aerosols and their chemistry (Koch and Del Genio, 2010; Bond et al., 2013).

Aerosols in the atmosphere may have been directly emitted as their liquid or solid species (primary emission) or formed within the atmosphere from gaseous species (secondary formation). Aerosols can be further divided into carbonaceous aerosols (containing carbon); mineral dust and sea salt (containing alkali and trace metals); and inorganic aerosols. The inorganic aerosols are particles formed from the ions nitrate ( $\text{NO}_3^-$ ), sulfate ( $\text{SO}_4^{2-}$ ), and ammonium ( $\text{NH}_4^+$ ). These ions are commonly used in introductory chemistry to study acid-base reactions, and similar reactions form aerosols. The secondary formation can be direct, as with ammonium nitrate:



or it can involve water, as in the absorption of ammonia:



These acid-base reactions are all reversible and hence controlled by thermodynamics. Because species can readily transfer between gas and aerosol states, it is useful to refer to all species of a given oxidation state collectively. ‘Total nitrate’ thus refers to all N(V) species, i.e. the combination  $\text{HNO}_3(\text{g}) + \text{NO}_3^-(\text{aer})$ ; ‘total ammonia’ to  $\text{N}(-\text{III}) = \text{NH}_3(\text{g}) + \text{NH}_4^+(\text{aer})$ ; and ‘total sulfate’  $\text{S}(\text{VI}) = \text{SO}_4^{2-}(\text{aer}) + \text{HSO}_4^-(\text{aer})$ . These ‘total’ quantities are conserved as thermodynamic equilibrium is established, and changes in local temperature and relative humidity only affect the partitioning of the totals between their gas and aerosol phases.

The acid-base reactions described above explain how particles form from total nitrate, sulfate, and ammonia present in the atmosphere. However, ammonia is the only one of these species directly emitted into the atmosphere in large amounts. Sulfate can be directly emitted by fossil fuel combustion, but the majority of anthropogenic atmospheric sulfur comes from sulfur dioxide ( $\text{SO}_2$ ). Nitrate is formed from nitrogen oxides,  $\text{NO}_x = \text{NO} + \text{NO}_2$ , which are produced during combustion and other high-temperature industrial processes. To link fine particulate matter impacts on human health and climate to emissions, we have to understand both the kinetics that form nitrate and sulfate from  $\text{SO}_2$  and  $\text{NO}_x$  as well as the thermodynamics that form aerosol species from their gaseous precursors.

In linking human health and climate impacts of aerosols to anthropogenic emissions, and especially the emissions of a single country or region, we must also consider emissions coming from other sources and the resulting state of the atmosphere. For example, anthropogenic  $\text{NO}_x$  emissions could decrease the oxidation rate of dimethyl sulfide (DMS,  $(\text{CH}_3)_2\text{S}$ ), which is the primary non-volcanic, non-anthropogenic source of atmospheric sulfur. To focus on the impacts of a change in emissions from a given source – say, from a new regulation – we ask the question “given the current mix of emissions and atmospheric state, what is the effect of an *additional* amount of emissions from this source?”. That additional effect, the *sensitivity* to emissions, is

the focus of this thesis. Built into the definition of sensitivity is its dependence on a given baseline of emissions and resulting atmospheric chemical concentrations.

Sensitivity is a useful concept in health, economic, and policy studies. One example of a sensitivity has already been given: the sensitivity of mortality rates to  $\text{PM}_{2.5}$  exposure. In the study by [Lave and Seskin \(1973\)](#), the sensitivity is (.41 per 10,000) per ( $10 \mu\text{g m}^{-3}$ ) and appears as a coefficient in their statistical regression equations. They also express this sensitivity<sup>2</sup> as a 0.53% decrease in mortality rate per 10% decrease in mean  $\text{PM}_{2.5}$ . When these numbers are multiplied by the sensitivity of  $\text{PM}_{2.5}$  concentrations to emissions, i.e. the decrease in mean  $\text{PM}_{2.5}$  per decrease in emissions, the result is the sensitivity of the mortality rate to the emissions. This is the number that gauges the effectiveness of a regulation, or the benefits of a change in fuel sources, because it directly relates the effects that are important (mortality) to the levers that humans can control (anthropogenic emission rate). In addition, the sensitivity of mortality rate to  $\text{PM}_{2.5}$  concentrations should be independent of the sensitivity of  $\text{PM}_{2.5}$  concentrations to emissions (it doesn't matter how the  $\text{PM}_{2.5}$  was produced, just that someone was exposed to it) so these two aspects of the policy-relevant sensitivity can be studied independently.

As mentioned, the sensitivity is specific to the baseline chosen for emissions and atmospheric state. This implies that sensitivities can change as emissions change – that is, the system can be nonlinear. This further implies that the effectiveness of a policy, as measured by the sensitivity of outcomes to emissions, can also change as emissions and background state shift. The initial shift could be changes in another country's anthropogenic emissions; changes in natural emissions; meteorological changes in background state; or climatic changes in background state. The end result is that the most effective policy to enact today may not be the most effective policy to enact in 5 or 10 years. Determining where and by how much the sensitivities have changed is thus a key step in making informed decisions.

Between 2005 and 2012, US emissions of  $\text{NO}_x$  and  $\text{SO}_2$  decreased by 42% and 62%,

---

<sup>2</sup>They refer to this %-per-% expression as an 'elasticity', which is also the terminology within economics.

respectively. The decline in emissions has been attributed to several factors, including a transition from coal to natural gas for electricity generation; the recession following the Financial Crisis of 2009; and the enforcement of the Tier 2 vehicle emissions controls (Russell et al., 2012). Decreases of this magnitude could lead to a nonlinear system response and to a change in sensitivities between 2005 and now.

## 1.2 Outline

In this thesis, I use a chemical transport model to explore how the decline in US emissions can cause a change in the sensitivity of  $\text{PM}_{2.5}$  concentrations to US  $\text{NO}_x$ ,  $\text{SO}_2$ , and  $\text{NH}_3$  emissions. For human health impacts, I calculate the sensitivities of surface-level, total  $\text{PM}_{2.5}$  concentrations. For climate impacts, I combine the chemical transport model output with a radiative transfer model to develop radiative sensitivities. Throughout, I try to identify the processes that contribute most to the sensitivities *and* to the changes thereof.

The thesis is roughly divided into three parts. First, I discuss the computational model used (chapter 2) and compare the different conceptual models of sensitivity (chapter 3). These chapters define the overall framework for the sensitivity calculations applied in later chapters. Next, I apply this framework to surface  $\text{PM}_{2.5}$  concentrations (chapter 4). Here, some of the key mechanisms behind changes in sensitivity are identified. Afterward, I turn to radiative forcing and climate impacts of  $\text{PM}_{2.5}$  (chapter 5). Finally, I conclude this thesis (chapter 6) with a discussion of the importance and application of these results and how the work may be extended. The key results of chapter 4 have already appeared in the peer-reviewed literature (Holt et al., 2015). The key results of chapter 5 have been summarized in a paper about to be submitted for publication (Holt et al., 2016).

THIS PAGE INTENTIONALLY LEFT BLANK

# Chapter 2

## Methods

The sensitivity of species concentrations to emissions is most readily explored using computer simulations. This is not the only possible approach; for example, [Ansari and Pandis \(1998\)](#) and [West et al. \(1999\)](#) combine measurements with thermodynamic equilibrium models to estimate sensitivities. However, the thermodynamic approach can only produce sensitivities of aerosol concentrations to total nitrate, sulfate, and ammonia concentrations, not to precursor emissions. Simulations also do not need to be used in isolation. [Pinder et al. \(2008\)](#) and [Dennis et al. \(2008\)](#) generate statistical indicators of aerosol behavior from simulations and then apply those indicators to measurements to produce a hybrid sensitivity. These authors note that their approach is unable to generate sensitivities to  $\text{NO}_x$  emissions, and these emissions decreased by 42% between 2005 and 2012. Since emissions changed so much over such a short time, the aerosol response may have been nonlinear and measurement-derived sensitivity estimates would be inaccurate.

There is a diversity of modeling software available for simulating atmospheric chemistry. These models can be broadly grouped into three categories: box models, chemical transport models, and earth system/climate-chemistry models. Box models represent a homogeneous atmospheric boundary layer over a domain, with only one or a few distinct boxes. These models are useful for understanding atmospheric processes. [Vayenas et al. \(2005\)](#) use such a model to show how the different deposition rates of nitrate aerosol and nitric acid gas impact the total aerosol concentrations.

Chemical transport models (CTMs) divide their domains into a number of grid cells, allowing them to represent transport of chemical species across regions. The resolution of CTMs ranges from global models of  $15^\circ$  cells (MacLeod et al., 2011) to regional and local models of 2 km cells (Thompson and Selin, 2012). CTMs focus on the reactions of atmospheric chemical species and thus use prescribed meteorological fields (temperature, wind speed, precipitation, etc.) from climate or weather model forecasts or from meteorological reanalysis. Earth system models simulate meteorology and chemistry simultaneously and are thus able to represent impacts of chemical species on temperature, precipitation, cloud brightness, and other factors. However, these additional features require much more computational resources than CTMs. The type and resolution of a model limits what scientific questions the model can answer.

Estimating sensitivities in a consistent, policy-relevant way requires some care in the experimental design. ‘Design’ here includes deciding how to vary emissions to both calculate sensitivities and to represent the recent changes in sensitivities. It also includes accounting for model bias, determining what resolution is sufficient, and identifying the key processes driving the changes. In addition, there are multiple conceptions of the ‘sensitivity’, each with an associated implicit model of the response to emissions.

This chapter discusses the particular CTM used for this work and the design of simulations performed with that CTM. The CTM’s features are described in section 2.1. Simulations using the default settings are compared to observations of speciated aerosol concentrations over the US and also to other CTM performance studies in section 2.2. Section 2.3 describes the emissions inventory used in the model and specifies the emissions-scaling approach used for the sensitivity experiments that are the primary focus of this thesis.

## 2.1 Chemical transport model

I used the GEOS-Chem chemical transport model (Bey et al., 2001; Liu et al., 2001) version 9-02<sup>1</sup>. This model simulates ozone-NO<sub>x</sub>-hydrocarbon-aerosol chemistry (Park et al., 2004). The thermodynamic module ISORROPIA II (Fountoukis and Nenes, 2007), which determines the aerosol fractions of NO<sub>3</sub><sup>-</sup> and NH<sub>4</sub><sup>+</sup>, was incorporated into GEOS-Chem by Pye et al. (2009). While GEOS-Chem was originally developed to study global ozone distributions, it has expanded our understanding of regional atmospheric chemistry in the US (Henze et al., 2009; Heald et al., 2012; Walker et al., 2012; Zhang et al., 2012a) and atmospheric composition impacts on climate (Leibensperger et al., 2012a,b; Mickley et al., 2012; Heald et al., 2014).

GEOS-Chem combines the chemistry mechanism mentioned above with the Goddard Earth Observing System (GEOS) meteorological analysis. The analysis used for my simulations, GEOS-5.2.0, comes from the NASA Global Modeling and Assimilation Office. This analysis has a native horizontal resolution of 0.5° latitude by 0.67° longitude and 72 hybrid- $\sigma$  layers extending to 0.01 hPa. For the chemistry, the top 36 layers (upwards of 78.5 hPa, roughly 17.8 km) are re-gridded into 11 stratospheric layers. In both the native model and the chemical model, the bottom 32 layers (up to 150.4 hPa, 13.7 km) vary with the surface pressure. The meteorological fields have 3-hour resolution for two-dimensional quantities (e.g. surface latent heat flux) and 6-hour resolution for three-dimensional quantities (e.g. temperature). The GEOS-5.2.0 fields have an unusually low night-time boundary layer (Liu and Liang, 2010) that results in a high bias in non-photochemical species concentrations such as NO<sub>3</sub><sup>-</sup>. Walker et al. (2012) corrected this issue by defining a friction velocity-based minimum boundary layer height.

My simulations use both a global domain and a nested domain. The global domain has 2° × 2.5° horizontal resolution, a timestep of 30 minutes for chemical reactions, and a timestep of 15 minutes for tracer transport. The global simulations provide boundary conditions for the nested domain. The nested domain has the native 0.5° × 0.67°

---

<sup>1</sup>Available at <http://geos-chem.org/>

resolution of the meteorological fields and spans 140°-40° W and 10°-70° N. Nested simulations use timesteps of 20 minutes for reactions and 10 minutes for transport. Concentrations of key species are saved every 3 hours for most simulations, though the results presented are mostly monthly averages.

A key reaction for inorganic aerosols is the hydrolysis of  $\text{N}_2\text{O}_5$ . The rate of this reaction is important both for the nitrate produced and its effects on  $\text{NO}_x$  lifetime.  $\text{NO}_x$ , ozone and hydroxyl concentrations in the northern extra-tropics are particularly sensitive to the hydrolysis rate (Macintyre and Evans, 2010). The reaction rate has been shown to depend on aerosol nitrate and water content (Bertram and Thornton, 2009; Bertram et al., 2009; Chang et al., 2011) with higher nitrate concentrations limiting the further production of nitrate. An estimate of this limitation is included in this version (9-02) of GEOS-Chem.

Another relevant new feature of GEOS-Chem is interactive soil  $\text{NO}_x$  emissions. In addition to increasing the accuracy of the dependence of soil emissions on precipitation, soil moisture, and temperature, the soil  $\text{NO}_x$  module responds dynamically to the nitrogen loading on the soil (Hudman et al., 2012). This nitrogen loading includes both atmospheric deposition and the application of fertilizers. Thus while anthropogenic, non-agricultural  $\text{NO}_x$  emissions can be specified within the model, the natural and agricultural  $\text{NO}_x$  emissions cannot.

## 2.2 Model validation

This section evaluates the simulations that use default (i.e. 2005 base case) settings against two surface measurement networks in the US. The first network, the Interagency Monitoring of Protected Visual Environments (IMPROVE), reports speciated fine aerosol concentrations at a number of national parks across the US. The second network, the EPA Chemical Speciation Network (CSN), includes speciated concentrations at both rural and urban sites.

GEOS-Chem has previously been evaluated against ozone and hydrocarbon concentrations (Bey et al., 2001); wet and dry deposition networks (Liu et al., 2001;

Zhang et al., 2012a); aerosol component concentrations from ground sites (Heald et al., 2012; Walker et al., 2012); aerosol species from satellite retrievals (Ford and Heald, 2012); and aerosol optical depth from ground sites and satellite retrievals (Drury et al., 2010). It has also been compared to other chemical transport model predictions of aerosol concentrations in the AeroCom inter-comparison (Myhre et al., 2013). The evaluations reported here thus focus on the species and time periods most relevant to the current work.

### 2.2.1 Measurement networks

The IMPROVE network is a system of monitors at national parks across the US and is described by Malm et al. (1994). These monitors measure elements, inorganic ions, and carbonaceous characterization of fine aerosols, providing 24-hour average samples once every 3 days. Because of their placement within national parks, IMPROVE sites are ideal for studying background, regional-scale air composition, away from the direct influence of urban pollution. For the model-measurement comparison, the nitrate and sulfate concentrations from Module B are used as well as ammonium at the few sites with ammonium measurements. For January and July of 2005, 163 sites provide nitrate and sulfate data and 10 sites provide ammonium data.

The US Environmental Protection Agency (2014a) Chemical Speciation Network (CSN)<sup>2</sup> reports daily-average measurements of fine aerosol composition. Different sites have different data collection frequencies and record measurements either once every 3 days or once every 6 days. The CSN includes sites in towns and cities across the US; unlike the IMPROVE network, it is expected to measure urban-influenced air composition. For January and July of 2005, there are 253 CSN sites reporting concentrations for nitrate, sulfate, and ammonium.

---

<sup>2</sup>This has also been referred to as the Speciation Trends Network or Status and Trends Network (STN). The CSN is actually the combination of the EPA-funded STN sites plus additional, externally-funded, quality-controlled sites.

Jan		N	MB	ME	RMSE
NO <sub>3</sub> <sup>-</sup>	IMP	1549	1.36	1.75	3.30
NO <sub>3</sub> <sup>-</sup>	CSN	1252	1.82	3.06	4.71
SO <sub>4</sub> <sup>2-</sup>	IMP	1551	-0.10	0.65	1.07
SO <sub>4</sub> <sup>2-</sup>	CSN	1260	-0.84	1.27	1.75
NH <sub>4</sub> <sup>+</sup>	IMP	109	0.63	0.71	0.92
NH <sub>4</sub> <sup>+</sup>	CSN	1259	0.24	0.88	1.39

Table 2.1: Model-measurement comparison statistics for January. The column marked ‘N’ is the total number of valid measurements for the month across the US. The other columns, all in units of  $\mu\text{g m}^{-3}$ , are the mean bias, mean gross error, and root mean square error.

Jan		FB	FE	NMB	NME	MNB	MNE	$r^2$
NO <sub>3</sub> <sup>-</sup>	IMP	35.7	107.8	120.8	155.2	407.6	449.5	42.8
NO <sub>3</sub> <sup>-</sup>	CSN	25.8	79.3	61.1	102.5	122.4	154.8	15.3
SO <sub>4</sub> <sup>2-</sup>	IMP	17.8	62.7	-7.9	52.9	85.9	119.5	42.6
SO <sub>4</sub> <sup>2-</sup>	CSN	-43.0	59.2	-31.9	48.8	-23.2	50.3	27.5
NH <sub>4</sub> <sup>+</sup>	IMP	50.4	58.1	66.7	74.9	117.3	123.8	29.1
NH <sub>4</sub> <sup>+</sup>	CSN	8.5	48.7	14.6	53.3	39.9	68.7	20.8

Table 2.2: More model-comparison statistics for January. All statistics here are presented as percentages. The statistics are fractional bias, fractional gross error, normalized mean bias, normalized mean error, mean normalized bias, mean normalized error, and coefficient of determination (squared Pearson correlation).

## 2.2.2 Model-measurement comparison

Tables 2.1, 2.2, 2.3, and 2.4 provide summary statistics of the model-measurement comparison. Figures 2-1 and 2-2 show the comparison as scatterplots of model concentrations versus IMPROVE and CSN measurements, respectively. For all of these statistics, the modeled concentrations are taken as the values from the model grid cell containing the measurement site. The 3-hourly model output is averaged over the same single day as each measurement, providing as close a match in space and time as possible, following the recommendations of [Simon et al. \(2012\)](#). The resulting statistics thus appear weaker than when monthly averages are used, but they are actually much more robust indicators of model performance.

Our simulation agrees well with SO<sub>4</sub><sup>2-</sup> measurements. Compared to January IMPROVE measurements, the modeled SO<sub>4</sub><sup>2-</sup> concentrations have small bias (NMB=

Jul		N	MB	ME	RMSE
NO <sub>3</sub> <sup>-</sup>	IMP	1381	0.22	0.43	1.02
NO <sub>3</sub> <sup>-</sup>	CSN	1237	0.64	1.06	1.93
SO <sub>4</sub> <sup>2-</sup>	IMP	1381	-0.58	1.15	2.14
SO <sub>4</sub> <sup>2-</sup>	CSN	1245	-0.96	1.90	2.89
NH <sub>4</sub> <sup>+</sup>	IMP	27	-0.05	0.69	0.81
NH <sub>4</sub> <sup>+</sup>	CSN	1235	0.26	0.74	1.07

Table 2.3: As in table 2.1 for July.

Jul		FB	FE	NMB	NME	MNB	MNE	$r^2$
NO <sub>3</sub> <sup>-</sup>	IMP	-6.7	94.7	81.8	156.7	135.5	198.0	13.7
NO <sub>3</sub> <sup>-</sup>	CSN	18.8	88.4	91.4	151.1	148.4	192.7	7.2
SO <sub>4</sub> <sup>2-</sup>	IMP	-2.2	42.7	-20.1	39.9	15.0	49.5	70.9
SO <sub>4</sub> <sup>2-</sup>	CSN	-14.6	39.8	-18.5	36.7	-0.8	41.0	57.7
NH <sub>4</sub> <sup>+</sup>	IMP	-6.6	39.9	-2.5	35.4	4.9	39.9	38.6
NH <sub>4</sub> <sup>+</sup>	CSN	27.0	49.7	16.3	46.3	137.0	155.1	49.3

Table 2.4: As in table 2.2 for July.

7.9%) but with modest correlation ( $r^2=42.6\%$ ). In the northern Midwest, however, modeled January SO<sub>4</sub><sup>2-</sup> is low (NMB=-45%). In addition, the modeled January SO<sub>4</sub><sup>2-</sup> concentrations are considerably lower than the CSN measurements (NMB=-31.9%). For July SO<sub>4</sub><sup>2-</sup>, the spatial correlation is much higher ( $r^2=70.9\%,57.7\%$  for IMPROVE,CSN). In addition, the bias compared to CSN measurements is smaller than in January (NMB=-18.5%), but the bias compared to IMPROVE measurements is larger (NMB=-20.1%).

Modeled NO<sub>3</sub><sup>-</sup> concentrations are often much larger than the measurements. Compared to January IMPROVE measurements, there is a high bias (NMB=107.8%) but a similar correlation as with SO<sub>4</sub><sup>2-</sup> measurements ( $r^2=42.8\%$ ). Part of this high bias is linked to the low bias of modeled SO<sub>4</sub><sup>2-</sup> in the Midwest. The bias is lower for July NO<sub>3</sub><sup>-</sup> concentrations (NMB=81.8% compared to IMPROVE) but the correlation is also smaller ( $r^2=13.7\%$ ). The correlation with winter measurements provides some confidence that the major processes of nitrate formation are being captured by the model, but all of our results must take into account the model’s high nitrate bias.

There are few NH<sub>4</sub><sup>+</sup> measurements to compare to, but model performance for this species is encouraging. In January, model bias is high compared to IMPROVE

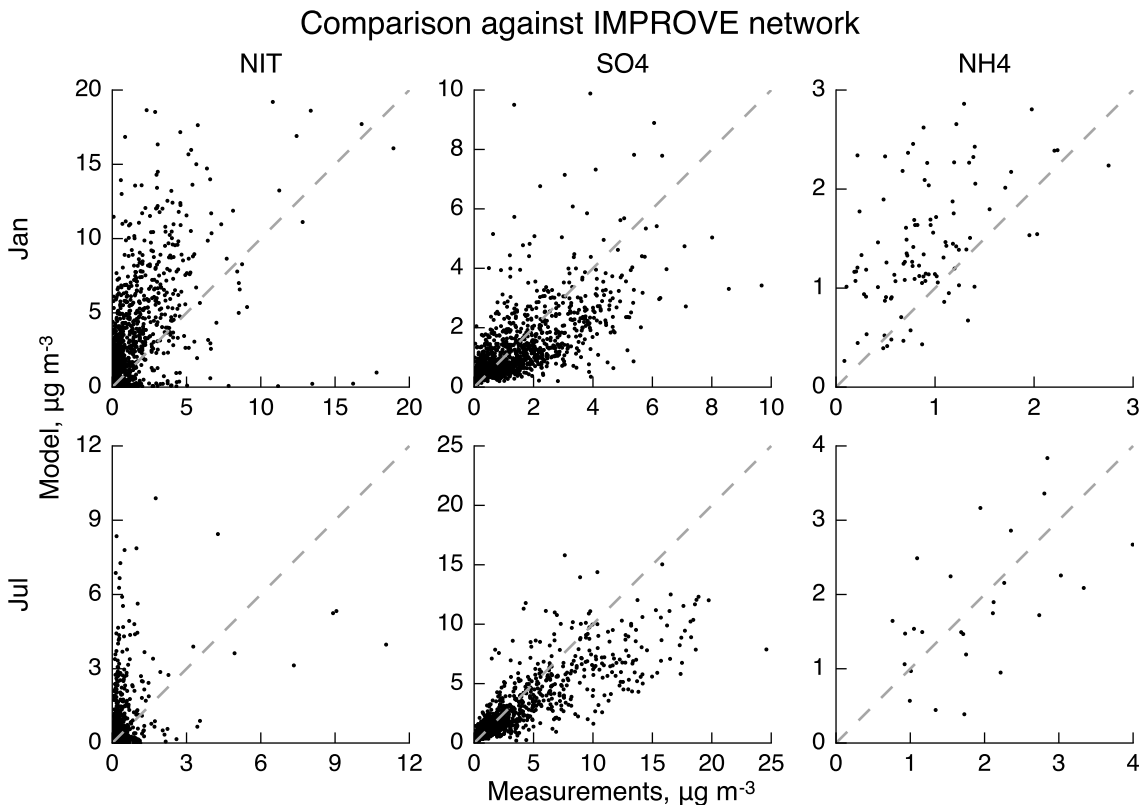


Figure 2-1: Scatterplot comparison of model and IMPROVE concentrations for each species. Each dot is a single measurement at a single site.

(NMB=66.7%) and modest compared to CSN (NMB=14.6%). The correlation is modest compared to both networks ( $r^2=29.1\%,20.8\%$  for IMPROVE,CSN). In July, the correlations are higher ( $r^2=38.6\%,49.3\%$  for IMPROVE,CSN) and the bias compared to IMPROVE is smaller (NMB=-2.5%).

The high bias of GEOS-Chem aerosol  $\text{NO}_3^-$  has been explored previously (Walker et al., 2012; Heald et al., 2012; Zhang et al., 2012a) but our comparison highlights a few interesting details. The modeled winter concentrations have a higher correlation with the rural IMPROVE measurements than with the more urban CSN measurements but the bias is larger as well. The spatial and temporal agreement with rural measurements suggests that the model captures the large-scale spatial structure of nitrate formation but overestimates  $\text{HNO}_3$  production or underestimates its atmospheric removal.

Simon et al. (2012) compare published performance statistics from a range of

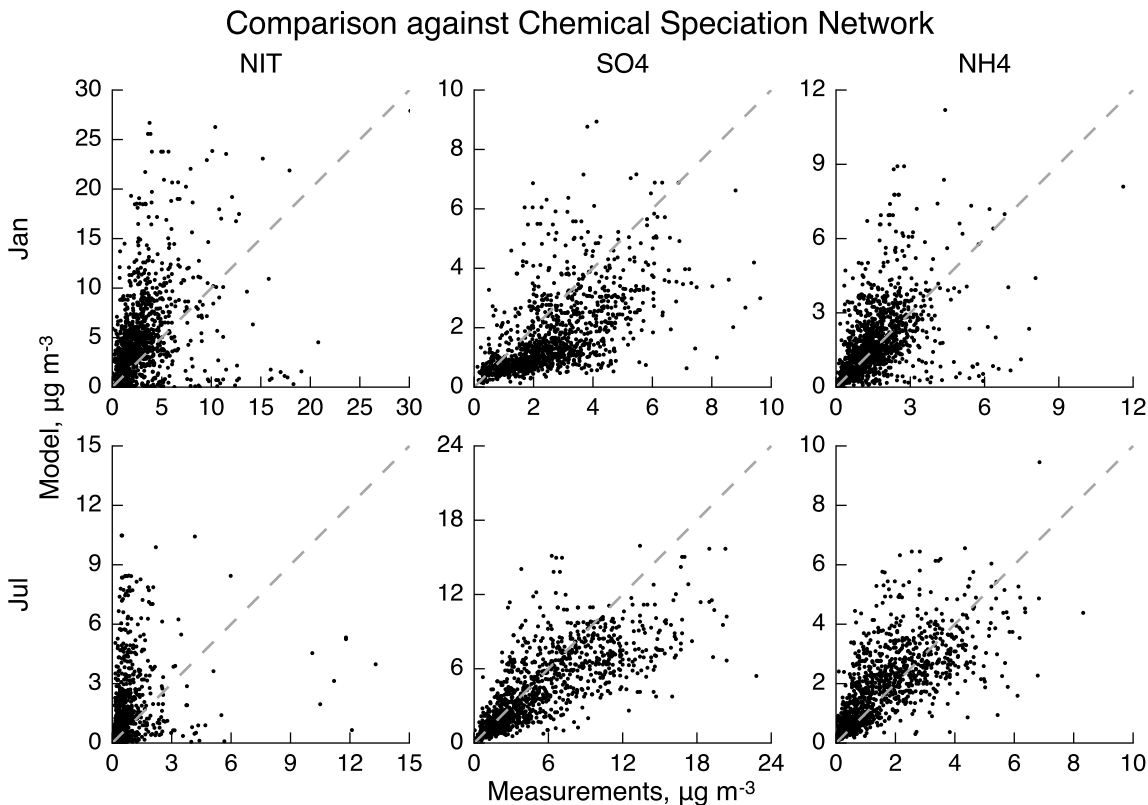


Figure 2-2: As in figure 2-1 but for the CSN measurements.

chemical transport models (not including GEOS-Chem). They find that modeled  $\text{SO}_4^{2-}$  is unbiased (NMB < 15%), whereas  $\text{NO}_3^-$  is biased high in winter (NMB 0% to 50%) and low in summer (-15% to -75%). Squared correlations for  $\text{SO}_4^{2-}$  and  $\text{NH}_4^+$  are between 25% and 60%, compared to 10%-45% for  $\text{NO}_3^-$ . Comparing their results to our statistics indicates that GEOS-Chem has a higher bias in winter  $\text{NO}_3^-$  than is typical but otherwise has a comparable performance to other models.

In chapter 4, the behavior of ammonium nitrate in the northern Midwest is highlighted. Over this region, the NMB of modeled  $\text{NO}_3^-$  compared to IMPROVE measurements is 109% and  $r^2 = 42\%$ , showing that GEOS-Chem estimates  $\text{NO}_3^-$  in this area better than in the national average. While sulfate biases are generally smaller than nitrate, modeled  $\text{SO}_4^{2-}$  is low in this area. Using the thermodynamic module of GEOS-Chem, increasing model  $\text{SO}_4^{2-}$  in this area would bring the  $\text{NO}_3^-$  bias down to 97%. Modeled  $\text{NO}_3^-$  is thus better simulated in this region, where its behavior is most important to our analysis, than in other parts of the US.

## 2.3 Emissions

GEOS-Chem uses emissions from the EDGAR and RETRO global inventories, along with several regional inventories (e.g. China, Europe). The regional inventories are scaled from their reference year according to national energy use statistics ([van Donkelaar et al., 2008](#)). The base simulation uses the reference year for the US regional inventory, 2005. This inventory, the EPA National Emissions Inventory for 2005 (NEI05), includes emissions of  $\text{NO}_x$ ,  $\text{SO}_2$ ,  $\text{NH}_3$ , several hydrocarbon species, and primary organic and inorganic aerosols. The summer  $\text{NH}_3$  emissions reported in NEI05 are scaled according to [Zhang et al. \(2012a\)](#) and are consistent with process-based  $\text{NH}_3$  emissions inventories ([Pinder et al., 2006](#)).

While the EPA only produces a full emissions inventory every few years, they provide national, annual total emissions estimates for every year ([US Environmental Protection Agency, 2014b](#)). Table 2.5 shows the emissions (total without wildfires) of several species for 2005, 2012, and the percent change (2012/2005 - 1). Only  $\text{NO}_x$  and  $\text{SO}_2$  emissions are changed between the 2005 and 2012 simulations as these are the largest changes among the various species. However, the 25.5% decrease in CO could also affect our results. This species only affects aerosol formation indirectly through oxidant concentrations, so its impacts should be smaller than the 25% decrease would suggest. I discuss the possible influence of CO and other organic emissions on my results in chapter 6. Since starting this work, the EPA has revised some of their emissions estimates, resulting in a smaller decline in NOx emissions and a larger decline in CO emissions between 2005 and 2012 than has been used for this study. Thus my simulations use -42% changes in  $\text{NO}_x$  and -62% changes in  $\text{SO}_2$  rather than the listed -33% and -64%.

I created two groups of simulations, based around high and low emissions, to test the influence of large-scale emissions reductions on  $\text{PM}_{2.5}$  sensitivity. In the high emissions base case, the default emissions for 2005 are used, including NEI05 for US emissions. In the low emissions base case, the total anthropogenic emissions of each species is decreased by the percentage given in table 2.5. Then, for each base case,

	NO <sub>x</sub>	SO <sub>2</sub>	NH <sub>3</sub>	CO	VOC	Primary PM <sub>2.5</sub>	Primary PM <sub>10</sub>
2005	20,261	14,490	3,799	80,646	15,885	4,919	20,497
2012	13,512	5,175	4,079	60,103	14,636	5,015	19,390
$(\frac{2012}{2005} - 1) \times 100$	-33.3	-64.3	+7.4	-25.5	-7.9	+2.0	-5.4

Table 2.5: US annual emissions (total without wildfires) in thousands of short tons for the years 2005 and 2012 along with the percentage change.

	NO <sub>x</sub> , Gg N	SO <sub>2</sub> , Gg S	NH <sub>3</sub> , Gg N
Jan	48.2	57.8	8.0
Jul	43.8	56.4	36.9

Table 2.6: Perturbations in US anthropogenic emissions of each species applied in the sensitivity simulations.

emissions of a given species were increased or decreased by a fixed amount, given in table 2.6. These perturbation have the same spatial and temporal structure as the base-case emissions. Their magnitude is based on a 10% change of the 2005 base case emissions for each month. The concentrations from these additional simulations are then used in the finite difference estimates of sensitivities for each base case.

Different simulations have different national total emissions but keep the same spatial and temporal structure as NEI05. This approach has two potential shortcomings. First, the emissions changes are due to factors that extend across economic sectors. A decrease in the use of coal for electricity generation would not impact transportation SO<sub>2</sub> emissions, for example. This would shift both the spatial and temporal (the diurnal and weekly cycles) structure of emissions. Second, emissions changes need not occur uniformly across the country. For these reasons, the scaling approach applied here is best suited to analyzing broad, continental-scale changes in the factors that control aerosol formation, such as thermodynamic limitation and oxidation rates. Fortunately, [Fioletov et al. \(2011\)](#), [Russell et al. \(2012\)](#), and [Tong et al. \(2015\)](#) show that NO<sub>2</sub> and SO<sub>2</sub> concentrations in different regions, as well as emissions from different sectors, are consistent with this scaling approach.

THIS PAGE INTENTIONALLY LEFT BLANK

# Chapter 3

## Sensitivities and nonlinearities

An atmospheric chemistry model like GEOS-Chem is complex. It has a wide variety of input parameters that can be varied in any given simulation, such as chemical rate constants, meteorological fields, and emission rates. There are also many different metrics that can be applied to summarize simulation output. Thus it is important to clarify the terms “sensitivity” and “nonlinearity” and how they describe the model’s response. Just as there are multiple ways to define sensitivity, there are multiple ways to estimate it as well, and the choice of method impacts the meaning of the results.

In this chapter, I compare different approaches to defining and estimating sensitivities. To make this comparison, the content of this chapter revolves around a system more abstract and general than my particular simulations. This system and the term “sensitivity” are defined in section 3.1. In section 3.2 I describe four different methods for estimating sensitivities. The applicability of these methods are compared in section 3.3.

### 3.1 Definitions

Atmospheric chemistry models simulate the distribution of several chemical species in space and time. The concentrations  $C_j(\mathbf{x}, t)$  of species  $j$  are the primary output fields of the model. (‘Fields’ here refers to the fact that the quantities vary in space and time.) Other key aspects of the model are input fields such as wind velocities

and emission rates; initial and boundary fields for the concentrations; and input parameters such as chemical rate constants. The model is defined by a differential equation that is first-order in time:

$$\frac{\partial C_j}{\partial t} = R_j(\mathbf{x}, t; \mathbf{C}, \mathbf{E}; \mathbf{K}), \quad C_j(\mathbf{x}_{\text{bnd}}, t) = B_j(\mathbf{x}_{\text{bnd}}, t), \quad C_j(\mathbf{x}, 0) = I_j(\mathbf{x}). \quad (3.1)$$

The source terms  $R_j$  represent advection, diffusion, surface deposition and emission, and chemical production and loss of species  $j$ . Hence, this term can depend explicitly on space and time; on the concentrations of all species; and the various input fields  $\mathbf{E}(\mathbf{x}, t)$  and parameters  $\mathbf{K}$ . On the boundary of the domain, where  $\mathbf{x} = \mathbf{x}_{\text{bnd}}$ , the concentrations and concentration gradients are specified by the boundary condition values  $B_j$ . At the start of a simulation, the initial concentration values  $I_j$  must also be specified. The resulting species concentrations  $C_j$  depend on space, time, and all output fields and parameters.

Sensitivities to parameters and sensitivities to fields are subtly different. For input *parameters*, which have no spatial or temporal variation, the sensitivity is the partial derivative

$$S_{j,k}(\mathbf{x}, t) = \frac{\partial C_j(\mathbf{x}, t)}{\partial K_k}. \quad (3.2)$$

Specifically, this is ‘the sensitivity of output  $C_j$  at  $(\mathbf{x}, t)$  to parameter  $K_k$ ’. This phrasing is important as I will be describing sensitivities related to multiple outputs and inputs, though the phrase can be shortened if the particular output or input is implicit. The sensitivity to this parameter states that if a new simulation were run with the parameter increased to  $K_k + \Delta K_k$ , the concentrations would be approximately

$$C'_j(\mathbf{x}, t) \approx C_j(\mathbf{x}, t) + S_{j,k}(\mathbf{x}, t) \cdot \Delta K_k.$$

For input *fields*, the sensitivity is given by the variational derivative ([Gelfand and Fomin, 1963](#))

$$S_{j,k}(\mathbf{x}, t; \mathbf{y}, s) = \frac{\delta C_j(\mathbf{x}, t)}{\delta E_k(\mathbf{y}, s)}. \quad (3.3)$$

This would be called ‘the sensitivity of output  $C_j$  at  $(\mathbf{x}, t)$  to the field  $E_k$  at  $(\mathbf{y}, s)$ ’. If a new simulation were run with the value of this field increased by  $\Delta E_k(\mathbf{y}, s)$  then

the concentrations would be

$$C'_j(\mathbf{x}, t) \approx C_j(\mathbf{x}, t) + \int d\mathbf{y} ds S_{j,k}(\mathbf{x}, t; \mathbf{y}, s) \cdot \Delta E_k(\mathbf{y}, s).$$

The need to integrate over the changes in inputs, rather than multiply, is one of the defining features of the variational derivative. It also distinguishes sensitivities to parameters from sensitivities to fields.

The sensitivity describes the system response to small variations in the inputs around a particular baseline. For larger variations in inputs, the accuracy in using the sensitivity to estimate system response depends on higher-order derivatives. If these derivatives all vanish for some input, then the system is ‘linear’ in that input. In a linear system, the equations above for  $C'_j$  become exact, regardless of the size of the variations in inputs. A less strict condition is that these equations hold when only one parameter is varied, in which case the system is ‘semi-linear’ in that parameter.

A simple emission-loss system demonstrates these concepts. The system is defined by

$$\frac{dC}{dt} = E(t) - kC, \quad C(0) = I$$

where  $k$  is a loss rate,  $E(t)$  is a variable source, and  $I$  is the initial value. The system output is  $C(t)$  and it has two input parameters  $k, I$  and one input field  $E$ . This system has the analytic solution

$$C(t) = Ie^{-kt} + \int_0^t ds E(s) \cdot e^{-k(t-s)}$$

and its various sensitivities are

$$S_{C,k}(t) = \frac{\partial C(t)}{\partial k} = -t \cdot Ie^{-kt} - \int_0^t ds E(s) \cdot (t-s)e^{-k(t-s)}$$

$$S_{C,I}(t) = \frac{\partial C(t)}{\partial I} = e^{-kt}, \quad S_{C,E}(t; s) = \frac{\delta C(t)}{\delta E(s)} = e^{-k(t-s)}\Theta(t-s).$$

Here,  $\Theta(t-s)$  is the step function, which is zero if  $t < s$  and one if  $t \geq s$ .

The sensitivities for this emission-loss model quantify some of the intuitive features of the system. A large loss rate  $k$  will produce low concentrations, so the sensitivity to  $k$  is negative. Because of the loss rate, the influence of emissions and concentrations in

the remote past on current concentrations is small. This waning influence is reflected in the exponential decay of  $S_{C,I}$  and  $S_{C,E}$  with time. This system is semi-linear in  $I$  and  $E$  but nonlinear in  $k$ ; if  $k$  is fixed, then the system is fully linear. The linearity expresses the fact that a given increase in emissions leads to the same increase in concentrations, regardless of the baseline emission rate. That is, the difference in concentrations between emission rates of 100 and 101 is the same as the difference in concentrations between 20 and 21 or 1000 and 1001. This is in contrast to  $\text{CH}_4$ , for example, whose atmospheric lifetime depends on concentrations. While this system is simple, it shows both how sensitivities are (in principle) calculated and how input parameters and fields must be treated differently.

## 3.2 Methods for estimating sensitivities

Sensitivities can be directly and explicitly calculated in the simple, concrete example system provided in the previous section. In more complicated systems – both large computational models and real phenomena – the sensitivity to inputs can only be estimated. In this Section I describe four methods for estimating sensitivities: finite differences, complex step, direct decoupling, and model adjoint. These four methods have different levels of accuracy, theoretical limitations, and computational resource burdens, and I compare these methods at the end of this Section. In addition, their results have subtly different meanings; these meanings and their implications are explored in section 3.3.

### 3.2.1 Finite difference

The finite difference method is the most general way to estimate sensitivities to input parameters. The partial derivative in equation (3.2) is replaced by the finite difference

$$S(K_0) \approx \frac{C(K_0 + \Delta h) - C(K_0 - \Delta h)}{2\Delta h}.$$

All that is required for this estimate of the sensitivity is that we can measure the output at both  $K_0 - \Delta h$  and  $K_0 + \Delta h$ . Because values on either side of  $K_0$  are used,

this is referred to as the central finite difference. Typically, the output would also be measured at the baseline value of  $K_0$ , resulting in three measurements. The one-sided finite differences

$$S(K_0) \approx \frac{C(K_0 + \Delta h) - C(K_0)}{\Delta h} \approx \frac{C(K_0) - C(K_0 - \Delta h)}{\Delta h}$$

can also be used.

The accuracy of the finite difference method as an estimate of sensitivity is related to the size of the deviation  $\Delta h$  and to higher-order derivatives of the function. Formally, if  $C$  is three times continuously differentiable with respect to the input parameters, then the central finite difference has an accuracy

$$\left| S - \frac{C(K_0 + \Delta h) - C(K_0 - \Delta h)}{2\Delta h} \right| \leq (\Delta h)^2 \cdot \frac{1}{3!} \max_{|\alpha|=3} \max_{\mathbf{K} \in B} |D^\alpha C(\mathbf{K})|.$$

The last term on the right-hand side denotes the maximum of all third-order derivatives of  $C$  in an area containing all three values  $K_0 - \Delta h, K_0, K_0 + \Delta h$ . Since this estimate is proportional to  $(\Delta h)^2$ , it is second-order accurate. The one-sided finite differences have an accuracy

$$\left| S - \frac{C(K_0 + \Delta h) - C(K_0)}{\Delta h} \right| \leq \Delta h \cdot \frac{1}{2!} \max_{|\alpha|=2} \max_{\mathbf{K} \in B} |D^\alpha C(\mathbf{K})|$$

which is only first-order. The higher accuracy of the central finite difference makes it preferable to the one-sided difference in many applications, despite requiring an additional measurement. If  $C$  is only twice differentiable, then the central finite difference is only first-order accurate like the one-sided difference; if  $C$  is only once differentiable, then neither difference is guaranteed to be accurate.

The above equations for the accuracy of the finite difference rest on the assumption that the outputs vary smoothly with the inputs. Real systems are not guaranteed to behave smoothly, exhibiting chaotic behavior, phase transitions, and other critical phenomena. In addition, complicated models – even deterministic computational models – have noise and uncertainty. If each of the measurements represent the ‘true’ value of the output plus noise  $\epsilon$ , then an extra term  $\epsilon/\Delta h$  is added to the central finite difference accuracy and  $2\epsilon/\Delta h$  to the one-sided difference. Choosing the size of  $\Delta h$

when designing an experiment thus requires balancing the accuracy of the sensitivity estimate ( $\sim (\Delta h)^2$ ) and the limitations of noise ( $\sim (\Delta h)^{-1}$ ). Crucially, the accuracy of the finite difference estimate *cannot* always be increased by using smaller  $\Delta h$ .

The finite difference method can sometimes be extended to calculating sensitivities to input fields. In a computational model, the input field effectively becomes a set of input parameters: one for every spatial and temporal grid point the field is defined on. However, two additional simulations are required for each parameter when using central finite differences (one simulation with one-sided differences). If there are  $N$  space-time points for the field, then  $2N$  simulations are required to calculate sensitivities to an input field. This approach can work for models that can be run quickly. For example, [Muller and Mendelsohn \(2007, 2009\)](#); [Muller et al. \(2011\)](#); [Muller \(2011\)](#) apply finite differences to a source-receptor model of air quality, generating sensitivities to 6 emitted species from 10,000 spatial points (US counties and point sources). For larger models, the resource requirements are too great to apply this approach directly.

A different approach to sensitivities to input fields is to use scaling parameters. The input field is deconstructed into specified base fields:

$$E(\mathbf{x}, t) = \sum_k K_k \cdot E_k(\mathbf{x}, t), \quad \Delta E(\mathbf{x}, t) = \sum_k \Delta K_k \cdot E_k(\mathbf{x}, t).$$

This replaces the input field  $E$  with additional input parameters  $K_k$ . [Caiazzo et al. \(2013\)](#); [Fann et al. \(2009\)](#) use this approach, treating the base fields  $E_k$  as the distribution of sources from a given economic sector (e.g. electric power generation, road transportation). I also use this approach, with the base fields being all anthropogenic sources of a given species. Changes in the parameters  $K_k$  then reflect overall increases or decreases in that economic sector, whether due to economic downturn or new national emission regulations. Unfortunately, this approach cannot easily address changes in the spatial or temporal distribution in a sector's emissions, as might come from regional regulations.

### 3.2.2 Complex step

The complex step method employs a similar approximation as the finite difference method but using complex numbers as inputs. This approach was made computationally tractable by [Squire and Trapp \(1998\)](#); see [Constantin and Barrett \(2014\)](#) for a review of applications.

Suppose the output  $C$  is infinitely differentiable in a parameter  $K$  for values of  $K$  within the radius of convergence  $\delta$  around a baseline value  $K_0$ . Then  $C$  is exactly equal to its Taylor series in this same area:

$$C(x) = \sum_{j=0}^{\infty} \frac{1}{j!} \frac{d^j C}{dK^j}(K_0) \cdot (K - K_0)^j = \sum_{j=0}^{\infty} a_j (K - K_0)^j.$$

The real function  $C$  can be extended to a unique complex function

$$\eta(z = x + ih) = \sum_{j=0}^{\infty} a_j (z - K_0)^j$$

for any value of  $z = x + ih$  within the radius of convergence. In particular:

$$\begin{aligned} \eta(K_0 + i\Delta h) &= \sum_{j=0}^{\infty} a_j (i\Delta h)^j \\ \operatorname{Re}\{\eta(K_0 + i\Delta h)\} &= \sum_{j \text{ even}} a_j \binom{j}{j/2} (-1)^{j/2} (\Delta h)^j \\ C(K_0) = a_0 &= \operatorname{Re}\{\eta(K_0 + i\Delta h)\} - (\Delta h)^2 \cdot \sum_{\substack{j \geq 2 \\ j \text{ even}}} a_j \binom{j}{j/2} (-1)^{j/2} (\Delta h)^{j-2} \\ \operatorname{Im}\{\eta(K_0 + i\Delta h)\} &= \sum_{j \text{ odd}} a_j \binom{j}{\frac{j-1}{2}} (-1)^{(j-1)/2} (\Delta h)^j \\ S(K_0) &= \frac{\operatorname{Im}\{\eta(K_0 + i\Delta h)\}}{\Delta h} - (\Delta h)^2 \cdot \sum_{\substack{j \geq 3 \\ j \text{ odd}}} a_j \binom{j}{\frac{j-1}{2}} (-1)^{(j-1)/2} (\Delta h)^{j-3}. \end{aligned}$$

Evaluating the function using a single, *complex* input thus provides a second-order estimate of both the value of  $C$  and its sensitivity to the parameter.

The theoretical limitations of the complex step method are related to the differentiability of the function. A real-valued function of real-valued inputs can only be associated with a complex function if the real function is infinitely differentiable (an-

alytic). This is a much more stringent requirement than the single differentiability of the finite difference method. This restriction is compounded when multiple input variables are considered. In addition, the complex function associated with the real function is only well-defined within a radius of convergence around  $K_0$ . It can be extremely difficult to prove that a given system has this analytic behavior and find its radius of convergence; in practice, these facts have to be assumed to be true to proceed.

The complex step method requires formulating a model in a way that allows for complex inputs, which can be a practical limitation to its use. If each of the calculations within the model is based on an analytic function, then the end result should also be analytic. Basic operations (e.g. addition and multiplication) extend naturally to complex numbers, but other operations (e.g. logarithms and inverse trigonometric functions) require different algorithms for dealing with complex-valued inputs. Checking and replacing such algorithms in large computational models can be onerous and error-prone, but these changes do not fundamentally change how the model represents transport, deposition, or other physical processes. Thus the complex step method is unintrusive, in terms of changing how the model operates, compared to the direct decoupled and adjoint methods detailed below.

One feature of the complex step method is that it can use much smaller values of  $\Delta h$  than is available for the finite difference method. In the finite difference method, the results from two model runs are subtracted from each other. The baseline values from each run cancel but the numerical noise does not. The inability to cancel out the noise leads to an error term proportional to  $1/\Delta h$ , restricting  $\Delta h$  from being made too small. In the complex step method, only one model run is used and the noise primarily affects the value of  $C(K_0)$ ; there is no ‘cancellation error’ in estimating the sensitivity. As a result,  $\Delta h$  can be made very small, increasing the accuracy of the estimates of both  $C(K_0)$  and  $S$ . This is fortunate because  $\Delta h$  now impacts the estimated value of  $C(K_0)$ . In the complex step method,  $\Delta h$  both *can* be made small (to increase the accuracy of the sensitivity estimate) and it *has to* be made small (to make the estimate of the actual value accurate).

In terms of resource use, the complex step method is similar to the finite difference method, requiring an additional model run for each sensitivity. However, since small values of  $\Delta h$  are needed and real-valued quantities are replaced by complex-valued ones, applying the complex step method replaces single-precision, real variables with double-precision, complex ones. This change in variables quadruples the memory needed to run the model and to store the results. In addition, some core algorithms are, counterintuitively, less accurate for double-precision variables than for single-precision, especially those algorithms that have to be fundamentally altered to handle complex variables. On modern, massively parallel computer architectures, the additional resource use is not a large deterrent to using the complex step method, but it can be an issue for high-resolution models with many chemical species.

### 3.2.3 Direct decoupled

Whereas the finite difference and complex step methods estimate sensitivities *post facto* from simulations, the direct decoupled method treats the sensitivity as an additional dynamical quantity within the model. Taking a partial derivative of equation (3.1) with respect to a parameter  $K_k$  gives

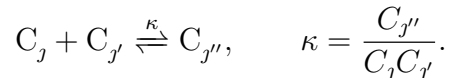
$$\frac{\partial}{\partial t} S_{j,k}(\mathbf{x}, t) = \frac{\partial}{\partial K_k} R_j(\mathbf{x}, t; \mathbf{C}, \mathbf{E}; \mathbf{K}) = \frac{\partial R_j}{\partial K_k} + \sum_{\ell} \frac{\partial R_j}{\partial C_{\ell}} \cdot S_{\ell,k}.$$

That is, the sensitivities  $S_{j,k}$  satisfy a dynamical equation similar to that of  $C_j$ . The first term on the right-hand side is nonzero when  $K_k$  is a physical parameter such as wind speed or reaction rate constant. The second term represents coupling between the various chemical species. For example, if  $C_j$  reacts with  $C_{j'}$  with a rate constant  $\kappa$ , then there are corresponding terms

$$R_j = -\kappa C_j C_{j'}, \quad \sum_{\ell} \frac{\partial R_j}{\partial C_{\ell}} \cdot S_{\ell,k} = -\kappa C_{j'} \cdot S_{j,k} - \kappa C_j \cdot S_{j',k}$$

in the dynamical equation for the sensitivity  $S_{j,k}$ . When these terms are present, the sensitivity for species  $C_j$  is affected by the sensitivities for all other species  $C_{j'}$ . In short, reactions spread sensitivities across all species in the model.

An additional level of complexity is added when some species, such as the inorganic aerosol components, are in chemical equilibrium with each other. Consider an equilibrium



The partial derivative of the equilibrium expression with respect to a parameter  $K_k$  satisfies

$$\begin{aligned} \frac{1}{\kappa} \frac{\partial \kappa}{\partial K_k} &= \frac{C_j C_{j'}}{C_{j''}} \cdot \frac{\partial}{\partial K_k} \frac{C_{j''}}{C_j C_{j'}} = \frac{C_j C_{j'}}{C_{j''}} \cdot \frac{C_j C_{j'} \cdot S_{j'',k} - C_{j''} \cdot (S_{j,k} C_{j'} + C_j S_{j',k})}{(C_j C_{j'})^2} \\ &= \frac{S_{j'',k}}{C_{j''}} - \frac{S_{j,k}}{C_j} - \frac{S_{j',k}}{C_{j'}}. \end{aligned}$$

This equation shows that the sensitivities of the equilibrium species are also in equilibrium with each other. The term on the left-hand side is obviously nonzero if the parameter  $K_k$  is directly related to the equilibrium constant, but it can also be nonzero for other reasons. In particular, atmospheric aerosols are often highly concentrated, non-ideal solutions and  $\kappa$  can depend on species concentrations. [Zhang et al. \(2012b\)](#) describe how non-ideal solutions can be treated within the DDM framework from both theoretical and computational perspectives.

The direct decoupled method has not, to my knowledge, been used to calculate sensitivities to fields except by using the scaling parameter approach.<sup>1</sup> The variational derivative of equation (3.1) is

$$\frac{\partial}{\partial t} S_{j,k}(\mathbf{x}, t; \mathbf{y}, s) = \sum_{\ell} \frac{\partial R_j}{\partial C_{\ell}} S_{\ell,k}(\mathbf{x}, t; \mathbf{y}, s) + \frac{\partial R_j}{\partial E_k} \cdot \delta(\mathbf{x} - \mathbf{y}, t - s) \quad (3.4)$$

where  $\delta(\mathbf{x} - \mathbf{y}, t - s)$  is the Dirac delta-function.<sup>2</sup> This delta-function term primarily determines the initial condition

$$S_{j,k}(\mathbf{x}, s; \mathbf{y}, s) = \frac{\partial R_j}{\partial E_k}(\mathbf{x}, s) \cdot \delta(\mathbf{x} - \mathbf{y})$$

without otherwise affecting the dynamics of the sensitivities. There are computational

<sup>1</sup>See [Hakami et al. \(2003\)](#); [Hakami \(2004\)](#) for applications of scaling parameters within DDM.

<sup>2</sup>The delta-function is actually a ‘generalized distribution’ that is zero whenever  $(\mathbf{x}, t) \neq (\mathbf{y}, s)$  but infinite at that point in such a way that its integral over space and time is one.

obstacles to evolving sharply-peaked functions (such as field sensitivities) in time. However, these obstacles have been addressed by work on heat transfer and other key differential equations. Equation (3.4) is (again, to my knowledge) the first description of a method for applying the direct decoupled method to field sensitivities.

There are several advantages to using the direct decoupled method to estimate sensitivities. First, while the above equations appear complicated, incorporating them into existing models can be relatively straightforward. Chemical transport models are already designed to solve advection-reaction-diffusion equations for many chemical species simultaneously, so the dynamical sensitivities are added on to an existing framework. Second, the resulting sensitivities are exact, at least in theory. Unlike the finite difference and complex step methods, there is no additional parameter  $\Delta h$  to be chosen. Third, this basic method can be extended to a wide variety of input parameters. In many models, physical parameters such as wind speeds and rate constants are defined in externally-produced files. It may be inconvenient or unwise to attempt to vary these inputs in the ways required by the two previous methods. Using the direct decoupled method, the sensitivities to these parameters can be calculated without having to directly alter the files that specify them. Finally, this approach can be directly extended to higher-order sensitivities (Hakami, 2004) without much additional resource use. I will return to this point momentarily.

One disadvantage of the direct decoupled method is the additional resources required to calculate sensitivities. The reaction term in the above equation suggests that the sensitivities to a given parameter have to be computed for *all* chemical species, not just those desired for later study. Two chemical species may not react directly with each other but their sensitivities become coupled through a chain of reactions. Thus calculating sensitivities to a parameter using the direct decoupled method *doubles* the number of dynamical quantities and hence approximately doubles the memory requirements. However, the actual implementation of the above equation involves a matrix factorization of  $\partial R_j / \partial C_k$ , which tends to be the limiting computational constraint. Yang et al. (1997) finds that including sensitivities to 20 parameters increases the model run time by only 80%. Fortunately, the same

factorization applies to sensitivities of all orders (Hakami, 2004). Thus higher-order sensitivities do not add much to CPU demands or total model run time but they do multiply the memory demands. Due to these memory demands, the direct decoupled method is more cumbersome for models with large numbers of active chemical species (e.g. GEOS-Chem, 90 species) than for models with fewer active species (e.g. CB05 in CAMx, 50 species).

### 3.2.4 Model Adjoint

The adjoint method, like the direct decoupled method, uses a dynamical equation for the sensitivity. In contrast to the three previous approaches, however, the adjoint method focuses on ‘inverse’ sensitivities and naturally extends to sensitivities to input fields. The key quantity in the adjoint method is the sensitivity of *current* concentrations to *previous* concentrations. This quantity is a matrix of variational derivatives

$$(A(\mathbf{y}, s; \mathbf{x}, t))_{j,j'} = \frac{\delta C_j(\mathbf{x}, t)}{\delta C_{j'}(\mathbf{x} - \mathbf{y}, t - s)}$$

where the primary dependent variables  $(\mathbf{y}, s)$  denote the distance from the secondary variables  $(\mathbf{x}, t)$ . In particular, as  $s$  increases,  $t - s$  decreases and  $A$  represents a dependence on quantities further and further back in time. For this reason,  $A$  is referred to as an ‘inverse’ or ‘backwards’ sensitivity, whereas the results of the previous sections are ‘forward’ sensitivities.

Deriving the equation that the inverse sensitivity satisfies is difficult; see Errico (1997); Plessix (2006) for details and computational implementations. The result is

$$\begin{aligned} \frac{\partial A_{j,j'}}{\partial s}(\mathbf{y}, s; \mathbf{x}, t) &= \sum_{j''} A_{j,j''}(\mathbf{y}, s; \mathbf{x}, t) \cdot \frac{\partial R_{j''}}{\partial C_{j'}}(\mathbf{x} - \mathbf{y}, t - s) \\ &\quad + \int d\mathbf{z} A_{j,j'}(\mathbf{z}, s; \mathbf{x}, t) \cdot \frac{\delta R_{j'}(\mathbf{x} - \mathbf{z}, t - s)}{\delta C_{j'}(\mathbf{x} - \mathbf{y}, t - s)}. \end{aligned}$$

The first term on the right-hand side is related to chemical reactions between species. A reaction  $C_1 \xrightarrow{k} C_2$  resulting in a rate  $-kC_1$  of loss from species 1 and gain to species

2 contributes

$$\frac{\partial A_{1,1}}{\partial s} = -k(A_{1,1} - A_{1,2}), \quad \frac{\partial A_{2,1}}{\partial s} = -k(A_{2,1} - A_{2,2}), \quad \frac{\partial A_{1,2}}{\partial s} = \frac{\partial A_{2,2}}{\partial s} = 0$$

to the various terms of  $\mathbf{A}$ . The integral in the dynamical equation for  $\mathbf{A}$  looks obtuse. Fortunately, only *functionals* of  $C_{j'}$  – advection and diffusion – contribute to this term. Their contributions to the sensitivities are<sup>3</sup>

$$\begin{aligned} R_{j'}(\mathbf{x}, t) &= -\nabla_{\mathbf{x}} \cdot (\mathbf{u}_{j'}(\mathbf{x}, t)C_{j'}(\mathbf{x}, t)) + \nabla_{\mathbf{x}} \cdot (\mathbf{D}_{j'}(\mathbf{x}, t) \cdot \nabla_{\mathbf{x}}C_{j'}(\mathbf{x}, t)) \\ \frac{\partial A_{j,j'}}{\partial s}(\mathbf{y}, s; \mathbf{x}, t) &= -\mathbf{u}_{j'}(\mathbf{x} - \mathbf{y}, t - s) \cdot \nabla_{\mathbf{y}}A_{j,j'}(\mathbf{y}, s; \mathbf{x}, t) \\ &\quad + \nabla_{\mathbf{y}} \cdot (\mathbf{D}_{j'}(\mathbf{x} - \mathbf{y}, t - s) \cdot \nabla_{\mathbf{y}}A_{j,j'}(\mathbf{y}, s; \mathbf{x}, t)). \end{aligned}$$

When these terms are added back into the above equation, the result is an advection-reaction-diffusion equation for the inverse sensitivities:

$$\begin{aligned} \frac{\partial A_{j,j'}}{\partial s} + \mathbf{u}_{j'}(\mathbf{x} - \mathbf{y}, t - s) \cdot \nabla_{\mathbf{y}}A_{j,j'} - \nabla_{\mathbf{y}} \cdot (\mathbf{D}_{j'}(\mathbf{x} - \mathbf{y}, t - s) \cdot \nabla_{\mathbf{y}}A_{j,j'}) \\ = \sum_{j''} A_{j,j''}(\mathbf{y}, s; \mathbf{x}, t) \cdot \frac{\partial R_{j''}}{\partial C_{j'}}(\mathbf{x} - \mathbf{y}, t - s). \end{aligned} \quad (3.5)$$

The sensitivities to input fields and input parameters can be calculated from  $\mathbf{A}$ :

$$\begin{aligned} S_{j,\ell}(\mathbf{y}, s; \mathbf{x}, t) &= \frac{\delta C_j(\mathbf{x}, t)}{\delta E_\ell(\mathbf{y}, s)} = A_{j,j'}(\mathbf{x} - \mathbf{y}, s; \mathbf{x}, t) \cdot \frac{\partial R_\ell}{\partial E_\ell}(\mathbf{y}, s) \\ S_{j,k}(\mathbf{x}, t) &= \frac{\partial C_j(\mathbf{x}, t)}{\partial K_k} = \sum_{j'} \int d\mathbf{y} ds A_{j,j'}(\mathbf{y}, s; \mathbf{x}, t) \cdot \frac{\partial R_{j'}}{\partial K_k}(\mathbf{x} - \mathbf{y}, t - s). \end{aligned}$$

The sensitivity  $\mathbf{A}$  defined above is a useful theoretical quantity but it cannot be calculated in practice. For a model with  $S$  species and  $N$  spatial points there are  $S^2N^2M(M+1)/2$  components of  $\mathbf{A}$  at the  $M^{\text{th}}$  time step. As with the direct decoupled method, the sensitivities of different species become coupled through chains of reactions. Due to advection and diffusion, the concentration of one species at one location can depend on the concentration of a different species at a different location. Finally, the sensitivities depend on the trajectory of the system through

---

<sup>3</sup>These equations apply to unbounded domains. For bounded domains, there are additional terms that incorporate the sensitivities to boundary conditions.

time, potentially going back arbitrarily far. Therefore none of the  $\sim (SNM)^2$  terms in  $\mathbf{A}$  can be ignored except in very specific systems. For models with any level of spatial or temporal resolution ( $N, M$  large), it is infeasible to calculate  $\mathbf{A}$  directly.

Instead, the adjoint method calculates the sensitivity of an ‘objective function’ to various inputs. In data assimilation, the objective function might be the model-measurement mismatch

$$J = \sum_{i,j} (C_j(\mathbf{x}_i, t_i) - C_{i,j}^{\text{meas}})^2$$

whereas in regulatory analysis, it might be the national, annual exposure to a specific pollutant

$$J = \int d\mathbf{x} dt C_0(\mathbf{x}, t).$$

The objective function is a scalar function or functional of the model outputs; it produces a single number from the output of a single model run. The sensitivity of the objective function to a specific concentration is

$$\begin{aligned} B_j(\mathbf{x}, s) &= \frac{\delta J}{\delta C_j(\mathbf{x}, T-s)} = \sum_{j'} \int d\mathbf{y} dt \frac{\delta J}{\delta C_{j'}(\mathbf{y}, t)} \cdot \frac{\delta C_{j'}(\mathbf{y}, t)}{\delta C_j(\mathbf{x}, T-s)} \\ &= \sum_{j'} \int d\mathbf{y} dt \frac{\delta J}{\delta C_{j'}(\mathbf{y}, t)} \cdot A_{j',j}(\mathbf{y} - \mathbf{x}, s + t - T; \mathbf{y}, t) \end{aligned}$$

where  $T$  denotes the end of the simulation. Applying equation (3.5) to  $B_j$  gives

$$\begin{aligned} \frac{\partial B_j}{\partial s}(\mathbf{x}, s) - \mathbf{u}_j(\mathbf{x}, T-s) \cdot \nabla_{\mathbf{x}} B_j(x, s) - \nabla_{\mathbf{x}} \cdot (\mathbf{D}_j(\mathbf{x}, T-s) \cdot \nabla_{\mathbf{x}} B_j(x, s)) \\ = \sum_{j''} B_{j''}(x, s) \cdot \frac{\partial R_{j''}}{\partial C_j}(\mathbf{x}, T-s). \end{aligned} \tag{3.6}$$

This is an advection-diffusion-reaction equation like equation (3.5). However,  $\mathbf{B}$  has only one index for each species, location, and time whereas  $\mathbf{A}$  had two indices; the number of components is reduced from  $(SNM)^2$  to  $SNM$ . Again, the sensitivity of

the objective function to an input follows from **B**:

$$S_j(\mathbf{x}, s) = \frac{\delta J}{\delta E_j(\mathbf{x}, T - s)} = B_{j'}(\mathbf{y}, t) \cdot \frac{\partial R_{j'}}{\partial E_j}(\mathbf{x}, T - s)$$

$$S_k = \frac{\partial J}{\partial K_k} = \sum_{j'} \int d\mathbf{y} ds B_{j'}(\mathbf{y}, s) \cdot \frac{\partial R_{j'}}{\partial K_k}(\mathbf{y}, T - s).$$

The adjoint sensitivities have several key features. First, they are inverse sensitivities. In equation (3.6), the velocity is flipped compared to typical advection. The sensitivities “swim upstream”, seeking out the key factors upwind of the current location. Second, like with the direct decoupled method, the adjoint sensitivities satisfy an advection-diffusion-reaction equation and can be integrated into an existing model framework. Third, the adjoint sensitivities to input *fields* are the primary quantities, whereas sensitivities to input parameters can be cumbersome to calculate. This is the only method designed specifically to study field sensitivities, making adjoint modeling a uniquely powerful tool.

The computational resource demand of an adjoint model is related to how these equations are applied. Before calculating the sensitivities, the model first has to be run forward, using the baseline inputs, and the matrices  $\partial R_{j'}/\partial C_j$  saved. Afterwards, the adjoint model (equation (3.6)) is run and the sensitivities **B** are output. In terms of memory, the matrices have  $S^2NM$  components and the sensitivities have  $SNM$ . Thus the adjoint model requires an order of magnitude more memory than the forward model (11 GB per simulation week in GEOS-Chem (Henze et al., 2007)). In terms of CPU time, the backward model takes  $\sim 2 - 10$  times as long to run as the forward model (Henze et al., 2007). Finally, the  $\partial R_{j'}/\partial C_j$  matrices are not typically explicitly calculated in forward models. Automated differentiation software has made the task of computing these matrices in large models feasible, but creating an adjoint of a model is still a difficult enterprise. Due to these constraints, only certain modeling groups have created adjoint versions of their models.

### 3.3 Comparison of estimates

The four approaches just described give subtly different insights into the systems they analyze. The direct decoupled and adjoint methods provide an exact sensitivity whereas the finite difference and complex step methods provide a sensitivity estimate. (The complex step method can provide a very accurate estimate, but it is still an estimate.) Conversely, only the finite difference method uses additional, fully non-linear simulations; the other methods can only estimate the actual system response to changes in inputs based on the value of the sensitivity. This difference affects the generality of the results. In addition, the adjoint method calculates the sensitivity of an objective function. Sensitivities of one objective function (e.g. population-average exposure) can differ considerably from those of another objective function (e.g. at-risk population exposure), also affecting the generality of adjoint models.

Each method is suited to different numbers of inputs and outputs. The adjoint method focuses on field sensitivities (many inputs) but has to limit its scope to a single objective function (one output). The finite difference and complex step methods provide sensitivities for all chemical species (many outputs) but for only one input parameter per simulation (one input). The direct decoupled method calculates sensitivities to several input parameters at once but is typically limited in both the number of parameters and the number of active chemical species (several inputs, several outputs).

These four methods also require different modifications to the underlying model. The finite difference method can be employed without changing critical code but input files have to be altered and managed. The complex step method requires changing variable types and checking that each subroutine of the model is complex-compatible. The direct decoupled method can be built on the existing advection-diffusion-reaction framework but the calculation of the reaction Jacobian  $\partial R_j / \partial C_j$  must be added to the base code. The adjoint method requires calculating and saving the reaction Jacobian as well as running the model backwards in time.

From these considerations, I have chosen to use the finite difference method for this

work. The fundamental policy questions are about how impacts (either population exposure to pollution or aerosol radiative effects) respond to emissions. The adjoint method could be used to describe the impacts of emissions from a particular area, which my parameter-scaling, finite-difference approach cannot. However, the adjoint approach would then not be able to show spatial resolution in the impacts. Some of my key results – nitrate condensation in the Midwest, radiative effect differences between land and ocean – could not be directly addressed with the adjoint approach. The complex step method for GEOS-Chem was developed concurrently with the work in this thesis ([Constantin and Barrett, 2014](#)) and could become a key tool in future work.

THIS PAGE INTENTIONALLY LEFT BLANK

# Chapter 4

## Surface aerosol concentrations

Reproduced in part with permission from J. Holt, N. E. Selin, and S. Solomon. Changes in inorganic fine particulate matter sensitivities to precursors due to large-scale US emissions reductions. *Environmental Science and Technology*, 49(8):4834-4841, 2015. Copyright 2015 American Chemical Society.

### 4.1 Introduction

Fine particulate matter ( $\text{PM}_{2.5}$ ) adversely affects cardiovascular and respiratory functioning (Pope, 2000) and is a key focus of air quality policies such as the National Ambient Air Quality Standards (NAAQS). Designing effective policies requires knowledge of how near-surface concentrations of  $\text{PM}_{2.5}$  respond to changes in precursors - its sensitivity to emissions.

Studies of health and economic impacts of emissions often apply estimates of  $\text{PM}_{2.5}$  sensitivities to parameterize how air quality responds to emissions. Muller and co-workers (Muller and Mendelsohn, 2007; Muller et al., 2011; Muller, 2011) use the integrated assessment model APEEP to calculate marginal damages (in US dollars per ton) by increasing emissions from one source by one ton and tracing impacts on human health, agriculture, and other vulnerable structures. The base case in APEEP uses the EPA 2002 National Emissions Inventory (NEI02), but Muller et al. (2011) implements the 2005 inventory (NEI05). Fann et al. (2012, 2013) use the

CAMx Particle Source Apportionment Technology to attribute  $\text{PM}_{2.5}$  concentrations to emissions from each economic sector. Their simulations use NEI05 and projections for 2016 based on proposed air quality rules. Similarly, [Fann et al. \(2009\)](#) use NEI02 with projections for 2015 as the emissions inventory for EPA Response Surface Model of air quality ([US Environmental Protection Agency, 2006](#)). In these studies, the projections based on then-proposed rules exhibit 30% decreases in national  $\text{NO}_x$  and  $\text{SO}_2$  emissions between 2001 and 2010 ([US Environmental Protection Agency, 2006](#)). These emissions actually decreased by 34% and 53%, respectively, and  $\text{NH}_3$  emissions increased by 17%. Whether sensitivities calculated using older (2002 and 2005) emissions, or even past estimates of current emissions, are sufficiently accurate for health and economic impact assessment depends on the nonlinear response of  $\text{PM}_{2.5}$ .

Several chemical mechanisms affect how  $\text{PM}_{2.5}$  forms from its precursor emissions.  $\text{NH}_3$  is the primary basic species, forming ammonium ( $\text{NH}_4^+$ ) in particles to neutralize acidic nitrate ( $\text{NO}_3^-$ ) and sulfate ( $\text{SO}_4^{2-}$ , formed from  $\text{SO}_2$ ).  $\text{PM}_{2.5}$  sensitivities to  $\text{NH}_3$  emissions are large, and it has been argued that reducing  $\text{NH}_3$  is a cost-effective strategy to reduce  $\text{PM}_{2.5}$  ([Ansari and Pandis, 1998](#); [Takahama et al., 2004](#); [Pinder et al., 2007](#); [Makar et al., 2009](#); [Henze et al., 2009](#); [Paulot and Jacob, 2013](#)). Sulfate is not volatile like  $\text{NH}_3$  and  $\text{HNO}_3$ , but it influences the ambient acidity and hence how much  $\text{HNO}_3$  can condense into  $\text{NO}_3^-$ .  $\text{PM}_{2.5}$  concentrations can even increase as  $\text{SO}_4^{2-}$  concentrations decrease, by allowing more  $\text{HNO}_3$  to condense ([Ansari and Pandis, 1998](#); [West et al., 1999](#)). However, multiple reactions oxidize  $\text{SO}_2$  into  $\text{SO}_4^{2-}$ , and each reaction responds differently to  $\text{NO}_x$  and hydrocarbon concentrations ([Manktelow et al., 2007](#); [Leibensperger et al., 2011](#)).

In this chapter, I evaluate the influence of large  $\text{NO}_x$  and  $\text{SO}_2$  emissions changes (comparable to those that occurred in the US between 2005 and 2012) on  $\text{PM}_{2.5}$  sensitivities and identify the most important nonlinear processes. Lower  $\text{NO}_x$  emissions lead to higher  $\text{SO}_2$  sensitivities across the US and to higher  $\text{NO}_x$  sensitivities in winter in cold, humid regions such as the northern Midwest. Lower  $\text{NO}_x$  and  $\text{SO}_2$  emissions also yield smaller sensitivities to  $\text{NH}_3$ . Our results suggest that the benefits of  $\text{NO}_x$  reductions could be much larger now that emissions are lower, especially in

winter (when  $\text{NH}_3$  emissions were thought to be dominant). We also show that  $\text{SO}_2$  controls are still effective, despite  $>60\%$  reductions nationally. The potential changes identified highlight the need to review the sensitivities used in health, economic, and policy studies and consider a multipollutant approach to air quality policy.

## 4.2 Methods

The configuration of the chemical transport model used for these results was described in Chapter 2. To summarize, I ran GEOS-Chem for January and July using 2005 meteorology for each emissions case. The emissions cases include base cases with US total anthropogenic emissions matching either the 2005 or 2012 EPA totals. For each of the three precursor species, emissions of that precursor were either increased or decreased by a fixed amount over the 2005 or 2012 reference to generate 6 more cases for each year. The total emissions in the reference cases and the changes applied to each precursor are provided in Table 4.1.

	2005 total		2012 total		Perturbation	
	Jan	Jul	Jan	Jul	Jan	Jul
$\text{NO}_x$ , Gg N	626.9	582.8	424.5	399.2	48.2	43.8
$\text{SO}_2$ , Gg S	424.7	417.1	245.5	242.2	57.8	56.4
$\text{NH}_3$ , Gg N	139.9	451.8	140.6	454.8	8.0	36.9

Table 4.1: Anthropogenic emissions (in kilotonnes,  $\text{kt} = 1 \times 10^6 \text{ kg} = \text{Gg}$ ) of inorganic  $\text{PM}_{2.5}$  precursors over the North American domain. The first two groups show total emissions – including Canada and Mexico – in the 2005 and 2012 base cases. The last group shows the change in US emissions that was applied to calculate the sensitivities, and is identical to table 2.6.

Similarly, the different ways to calculate and express sensitivities were compared in Chapter 3. For surface concentrations, I calculate  $\text{PM}_{2.5}$  sensitivities as the unnormalized finite difference

$$S(c) = \frac{\text{PM}_{2.5}(E(c) + \Delta E) - \text{PM}_{2.5}(E(c) - \Delta E)}{2 \times \Delta E} \quad (4.1)$$

where  $c$  is the reference year (2005 or 2012) with national-total emissions mass  $E(c)$ ;  $\Delta E$  is the mass change in emissions; and  $\text{PM}_{2.5}(E)$  is the  $\text{PM}_{2.5}$  concentration in the

simulation with emissions  $E$ . Emissions of other species are fixed at their baseline values for that case. The resulting sensitivities have units of  $\text{ng m}^{-3} \text{kt}^{-1}$ , where kt denotes 1000 metric tonnes ( $1 \times 10^6$  kg or 1 Gg) of emissions.

## 4.3 Results

The results of these simulations are divided into two parts. The first subsection describes the  $\text{PM}_{2.5}$  concentrations in the 2005 and 2012 base cases, highlighting the improvements in air quality that have already been made. The second subsection describes the  $\text{PM}_{2.5}$  sensitivities in these cases, showing how different emissions reductions may further improve air quality.

### 4.3.1 Fine particulate concentrations

The individual components and total inorganic  $\text{PM}_{2.5}$  concentrations are shown in figures 4-1 and 4-2 for January and July, respectively. The concentrations in the base cases for high (2005) and low (2012) emissions are the first two columns; the third column is their difference, shown to highlight the changes.

January  $\text{PM}_{2.5}$  peaks in the northern Midwest and is elevated over the eastern US. Northern Midwest  $\text{PM}_{2.5}$  is primarily composed of  $\text{NH}_4^+$  and  $\text{NO}_3^-$ . Only in the southeastern US is  $\text{SO}_4^{2-}$  a majority of the  $\text{PM}_{2.5}$  concentrations. National average  $\text{NO}_3^-$ ,  $\text{NH}_4^+$ , and  $\text{PM}_{2.5}$  concentrations in the low emissions case are 7.7%, 9.5%, and 11.6% lower than in the high emissions case, respectively. However, these decreases are not uniform across the US. The area around Kentucky, Ohio, and Virginia shows higher aerosol  $\text{NO}_3^-$  in the low emissions case than in the high emissions case. Higher  $\text{NO}_3^-$  is offset by lower  $\text{SO}_4^{2-}$ , so total  $\text{PM}_{2.5}$  concentrations are  $<0.15 \mu\text{g m}^{-3}$  higher in the low emissions case than the high emissions case.

July  $\text{PM}_{2.5}$  concentrations are generally lower than in winter but still higher over the eastern US than the western US. The largest mass contribution to summer  $\text{PM}_{2.5}$  comes from  $\text{SO}_4^{2-}$ , followed by  $\text{NH}_4^+$ .  $\text{SO}_4^{2-}$ ,  $\text{NH}_4^+$ , and total  $\text{PM}_{2.5}$  are all  $\sim 40\%$  lower in the low emissions case than in the high emissions case, compared to 62% lower

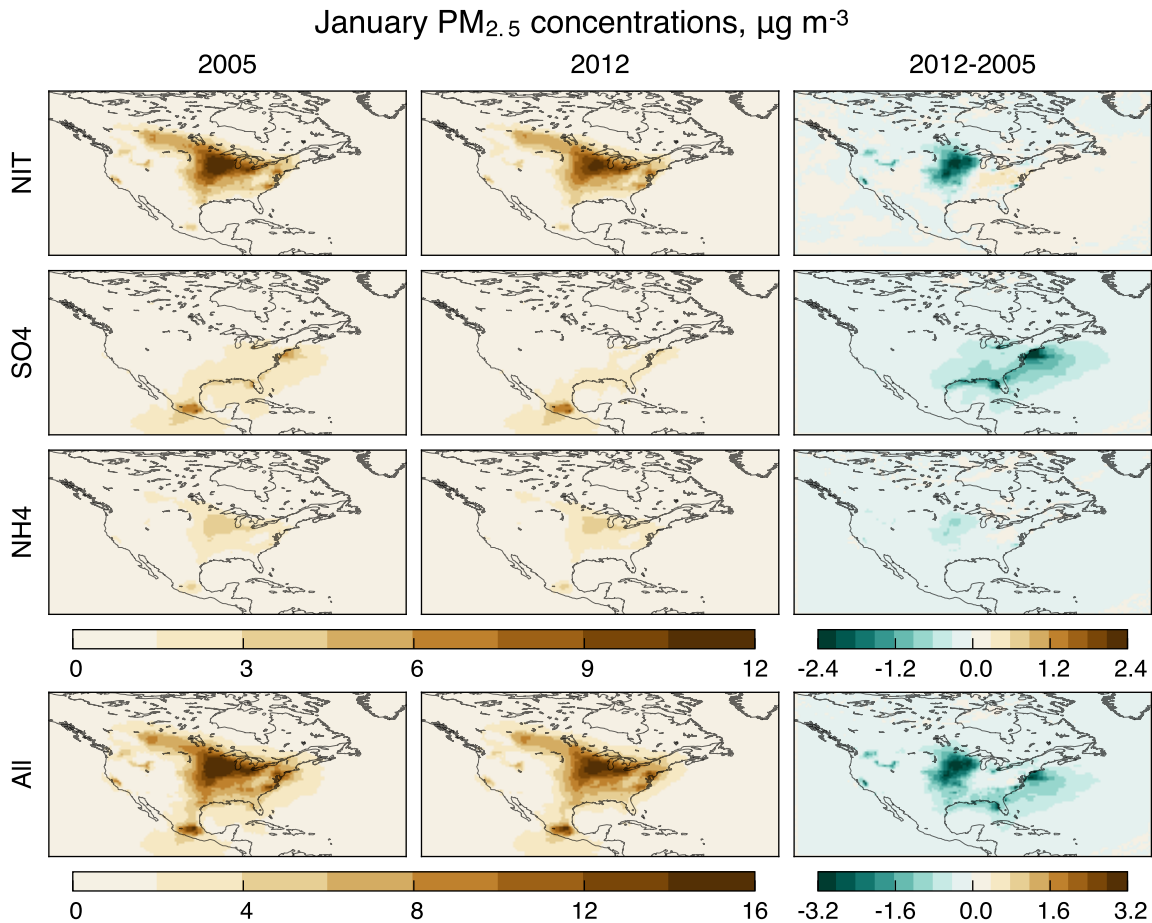


Figure 4-1: Surface-level mass concentrations of each component of PM<sub>2.5</sub> and the total (bottom row) in the reference cases. The left and middle columns show the 2005 and 2012 cases, respectively; the right column shows their difference.

SO<sub>2</sub> emissions. Some urban and regional areas (San Diego, New Orleans, Atlanta, Houston/Eastern Texas, Philadelphia/New Jersey, North Carolina, Illinois-Indiana-Ohio) show substantial summer aerosol NO<sub>3</sub><sup>-</sup> concentrations, up to  $5 \mu\text{g m}^{-3}$ . Aerosol NO<sub>3</sub><sup>-</sup> levels in these regions are lower in the low emissions case by 30.5% on average, compared to 42% lower NO<sub>x</sub> emissions. However, model-measurement correlations of summer NO<sub>3</sub><sup>-</sup> concentrations are small ( $r^2 = 13.7\%$ ,  $7.2\%$  compared to IMPROVE and CSN, respectively).

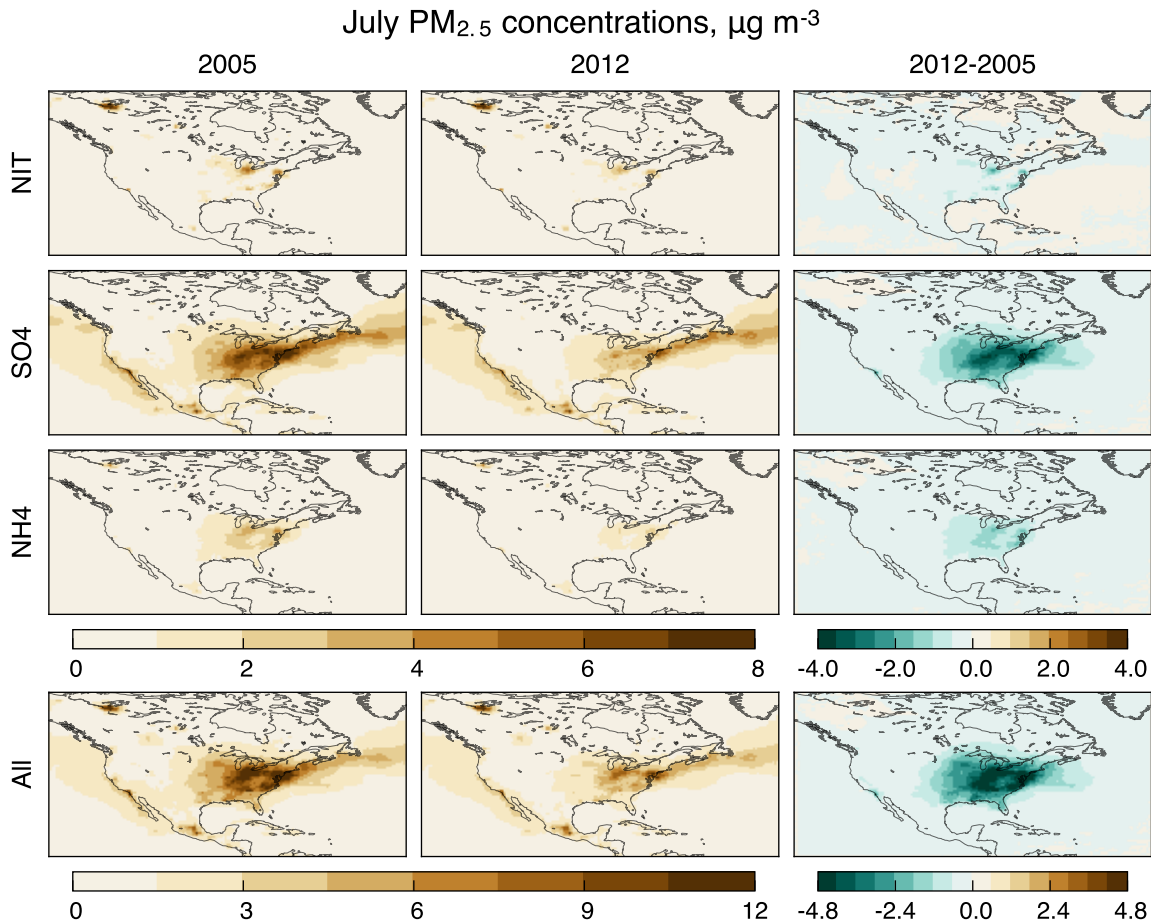


Figure 4-2: As in figure 4-1, but for July.

### 4.3.2 Particulate sensitivities to emissions

Here we describe the sensitivities of PM<sub>2.5</sub> to the different precursor emissions, as computed using equation 4.1. The resulting monthly-mean maps are shown in figures 4-3 and 4-4 for January and July, respectively.

January PM<sub>2.5</sub> is most sensitive to NH<sub>3</sub> emissions in both the high and low emissions cases. Sensitivity to NH<sub>3</sub> peaks in the northern Midwest at values of  $112 \text{ ng m}^{-3} \text{ kt}^{-1}$  in the high emissions case. In comparison, maximum winter sensitivities to NO<sub>x</sub> and SO<sub>2</sub> are  $0.1$  and  $10.5 \text{ ng m}^{-3} \text{ kt}^{-1}$ , respectively, over land. Over the southeastern US and the mid-Atlantic coast, winter sensitivities to SO<sub>2</sub> are prominent and can be up to 10% of the (local) sensitivity to NH<sub>3</sub>. We find slight ( $<0.35 \text{ ng m}^{-3} \text{ kt}^{-1}$ ) negative sensitivities to winter SO<sub>2</sub> emissions near the eastern

Great Lakes. The high sensitivities to  $\text{SO}_2$  emissions off the Atlantic coast are important for aerosol radiative effects and will be explored more in Chapter 5.

The differences in January sensitivities between the high and low emissions cases show two policy-relevant features. First, sensitivities to  $\text{NH}_3$  are much smaller in the low emissions case: 29% smaller in the national average and up to 72% smaller in the northern Midwest. In contrast, January sensitivities to  $\text{NO}_x$  are larger in the low emissions case: 210% larger in the national average. The changes in  $\text{NH}_3$  and  $\text{NO}_x$  sensitivities are also highly spatially correlated ( $r^2 = 95\%$ ). Second, average sensitivities to January  $\text{SO}_2$  emissions are 48% larger in the low emissions case over land. There are some local exceptions, such as the northeast US, that show slightly smaller sensitivities in the low emissions case, as well as the coastal region's large reduction in sensitivity.

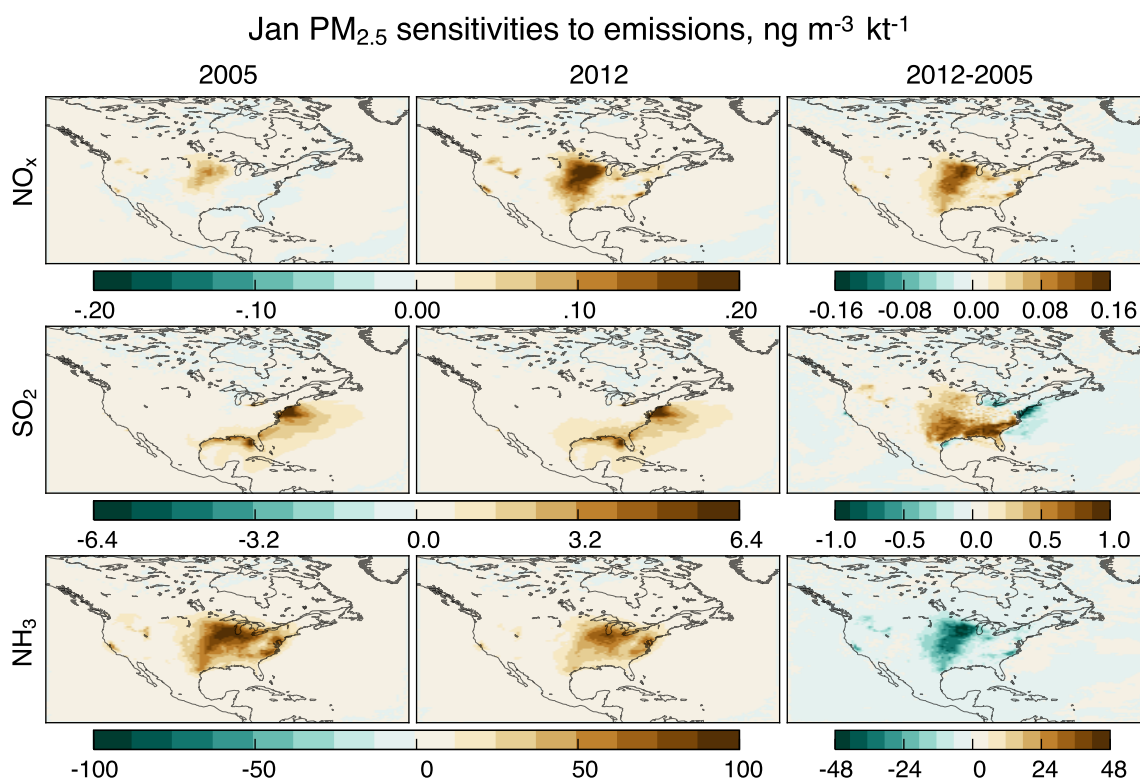


Figure 4-3: Sensitivity of surface-level inorganic  $\text{PM}_{2.5}$  mass concentrations to January emissions of  $\text{NO}_x$  (top),  $\text{SO}_2$  (middle), and  $\text{NH}_3$  (bottom) emissions. The units for  $\text{NO}_x$  emissions are  $\text{ng m}^{-3} (\text{kt N})^{-1}$ ; for  $\text{SO}_2$  and  $\text{NH}_3$  emissions, the denominators are  $\text{kt SO}_2$  and  $\text{kt NH}_3$ .

In contrast to January, the July sensitivities to different precursors have a smaller range of magnitudes. July  $\text{PM}_{2.5}$  sensitivities to  $\text{SO}_2$  emissions (figure 4-4, middle row) are high across the eastern US and peak in the Ohio River Valley. Sensitivities to  $\text{SO}_2$  are larger in the low emissions case than the high emissions case at nearly every grid point: 24% larger in the national average and up to 98% larger in the eastern US. In the high emissions case, summer sensitivities to  $\text{NH}_3$  emissions are large around the Great Lakes region, eastern Pennsylvania, and a few urban regions. These regions also have high summer sensitivities to  $\text{NO}_x$  emissions, though the magnitudes are different: peak summer sensitivities to  $\text{NH}_3$  and to  $\text{NO}_x$  in the Great Lakes region are 15.3 and  $0.14 \text{ ng m}^{-3} \text{ kt}^{-1}$ , respectively. Summer sensitivities to  $\text{NH}_3$  are 45% smaller on average in the low emissions case than the high emissions case.

Summer sensitivities to  $\text{NO}_x$  emissions are evident around the Great Lakes and a few localized areas on the Atlantic and Gulf coasts. Unlike  $\text{NH}_3$ , the sign of changes in sensitivity to summer  $\text{NO}_x$  emissions varies: the Great Lakes region and some urban areas have larger sensitivities in the low emissions case, whereas the southeastern US has smaller sensitivities. In grid cells where sensitivity to  $\text{NO}_x$  is larger in the low emissions case, it is 25% larger on average; in cells where the sensitivity is smaller, it is 17% smaller on average. The summer sensitivities to  $\text{NO}_x$  and to  $\text{NH}_3$  are spatially correlated ( $r^2 = 82\%$  in the 2005 case) whereas the *changes* in sensitivities are not.

## 4.4 Underlying processes

We investigated several processes that could contribute to differences in  $\text{PM}_{2.5}$  sensitivities between the high and low emissions cases. In this section, we focus on two particularly important aspects. First, the thermodynamics of ammonium nitrate formation determines winter sensitivities throughout the Midwest. Second, the kinetics of  $\text{SO}_2$  oxidation help explain changes in sensitivity to both  $\text{NO}_x$  and  $\text{SO}_2$  emissions across the eastern US in both seasons. In section 4.4.3, we describe how well a linear model based on the high emissions case sensitivities predicts the  $\text{PM}_{2.5}$  concentrations in the low emissions case, showing how sensitivity changes impact the performance

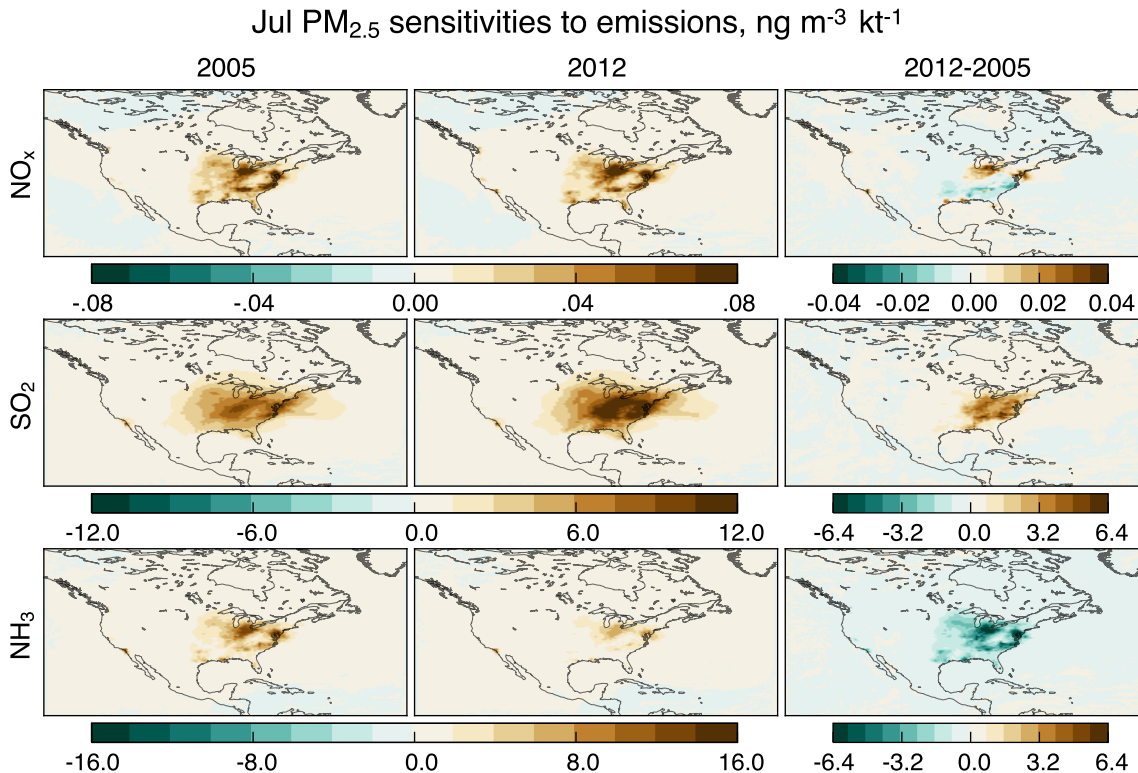


Figure 4-4: As in figure 4-3, but for July emissions.

of a simplified model.

#### 4.4.1 Thermodynamics of ammonium nitrate formation

Cold and humid environments, such as the northern Midwest in winter, promote condensation of NH<sub>3</sub> and HNO<sub>3</sub> into PM<sub>2.5</sub>. NH<sub>4</sub><sup>+</sup> and NO<sub>3</sub><sup>-</sup> concentrations are high in this region (figure 4-1) as are sensitivities to NH<sub>3</sub> and NO<sub>x</sub> emissions (figure 4-3). The differences in NO<sub>x</sub> and NH<sub>3</sub> sensitivities between the high and low emissions cases are highly correlated ( $r^2 = 95\%$ ) and opposite. In addition, PM<sub>2.5</sub> concentrations in this region are similar in the high and low emissions cases – 18 and 16  $\mu\text{g m}^{-3}$ , respectively.

To focus on thermodynamic effects, we used ISORROPIA II (Fountoukis and Nenes, 2007), the thermodynamic module in GEOS-Chem, to explore how PM<sub>2.5</sub> concentrations vary with total available HNO<sub>3</sub> and NH<sub>3</sub>. SO<sub>4</sub><sup>2-</sup> concentration, temperature, and relative humidity are fixed at their average values between 89 and 97°

W and 39.75 and 45.25° N:  $1.23 \mu\text{g m}^{-3}$ ,  $-8.4^\circ\text{C}$ , and 83%. Figure 4-5 shows total  $\text{PM}_{2.5}$  under these conditions. There is a line at which the system is neutral with respect to  $\text{NH}_3$ , i.e. where there is exactly enough  $\text{NH}_3$  to fully neutralize both the  $\text{SO}_4^{2-}$  and  $\text{NO}_3^-$ , and this neutrality line distinctly separates nitrate-limited and nitrate-saturated regimes. Below the line,  $\text{PM}_{2.5}$  concentrations depend strongly on  $\text{HNO}_3$  concentrations (nitrate-limited); above the line,  $\text{PM}_{2.5}$  concentrations depend only on  $\text{NH}_3$  concentrations (nitrate-saturated). Also shown are the  $\text{NH}_3$  and  $\text{HNO}_3$  concentrations from the high and low emissions cases, demonstrating why there is a large change in sensitivity: the high emissions case is nitrate-saturated, so that large changes in emissions yielded little change in  $\text{PM}_{2.5}$ , whereas the low emissions case is nitrate-limited, implying far greater sensitivity to  $\text{NO}_x$  emissions. A broad area in the northern Midwest presents conditions for which the line between nitrate-limited and nitrate-saturated is sharp, and nitrate limitation occurs to some degree across the US in the winter low emissions case.

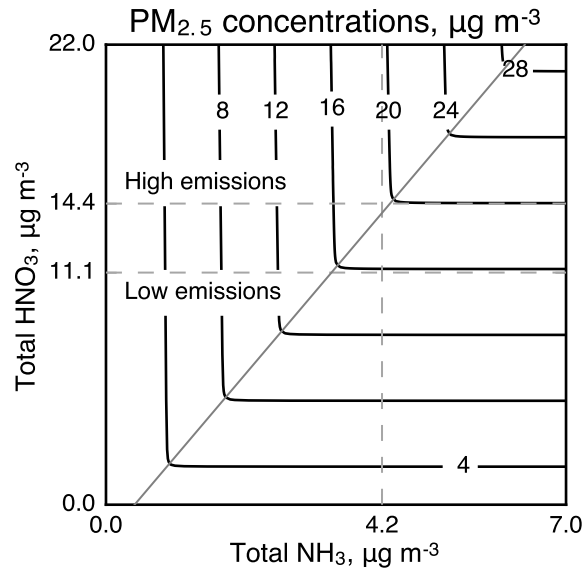


Figure 4-5: Total  $\text{PM}_{2.5}$  concentrations as a function of total available ammonia and nitrate as calculated by ISORROPIA II. The temperature, relative humidity, and total sulfate concentration ( $-8.4^\circ\text{C}$ , 83%,  $1.23 \mu\text{g m}^{-3}$ ) are fixed at values representative of the northern Midwest in January. The dashed gray lines show the average total ammonia and nitrate concentrations for the region (high emissions for  $\text{NH}_3$ , high and low emissions for  $\text{HNO}_3$ ). The solid gray line is the neutrality line, at which the total ammonia can fully neutralize both the sulfate and the available nitrate.

The transition to a nitrate-limited regime affects daily air quality as well as the monthly average. Figure 4-6 shows the fraction of daily-average  $\text{PM}_{2.5}$  concentrations above a given threshold value, using grid cells over the same northern Midwest domain used to generate figure 4-5. The 2012 case has fewer exceedances than the 2005 case for any threshold concentration. In particular, 1.8% of the grid cell-days exceed the NAAQS 24-hour average value of  $35 \mu\text{g m}^{-3}$  in the 2005 case, compared to 1.2% in the 2012 case. Since inorganic aerosols are only a fraction of  $\text{PM}_{2.5}$ , a threshold of  $20 \mu\text{g m}^{-3}$  might be more appropriate for the inorganic aerosols alone. For that threshold, the fraction of exceedances are 13% and 9%. For grid cell-days that exceed  $20 \mu\text{g m}^{-3}$  in the 2005 case, the average  $\text{PM}_{2.5}$  reduction in the 2012 case is 13.2%, compared to the domain and monthly average reduction of 12.9%. Thus emissions reductions have led to improvements in daily air quality metrics as well as the monthly average.

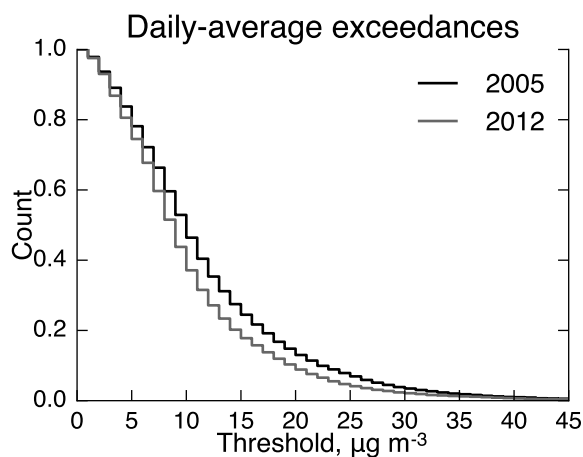


Figure 4-6: Fraction of grid cell-days with daily-average concentrations above the given threshold. These values are for the same northern Midwest domain as used in figure 4-5.

#### 4.4.2 Kinetics of $\text{SO}_2$ oxidation

The oxidation rate of  $\text{SO}_2$  into  $\text{SO}_4^{2-}$  determines whether  $\text{PM}_{2.5}$  forms before  $\text{SO}_2$  is transported or deposited and hence directly affects  $\text{PM}_{2.5}$  sensitivities to  $\text{SO}_2$  emissions.  $\text{SO}_2$  oxidation occurs in both gas and aqueous phases (Seinfeld and Pandis, 2012). Gas-phase oxidation involves the reaction of  $\text{SO}_2$  with hydroxyl radicals (OH).

In the aqueous phase,  $\text{SO}_2$  diffuses into cloud droplets where it reacts with other soluble gases (mostly hydrogen peroxide,  $\text{H}_2\text{O}_2$ ) to form  $\text{SO}_4^{2-}$ . If cloud droplets evaporate instead of precipitate,  $\text{SO}_4^{2-}$  remains as  $\text{PM}_{2.5}$ . GEOS-Chem outputs the production rate of  $\text{SO}_4^{2-}$  from the gas-phase reaction and from three additional reactions (aqueous  $\text{H}_2\text{O}_2$ , aqueous  $\text{O}_3$ , and on sea salt particles) individually, allowing the formation pathway to be explored in detail.

The rate and location of  $\text{SO}_2$  oxidation depends on whether the OH or  $\text{H}_2\text{O}_2$  reaction dominates.  $\text{NO}_x$  concentrations determine relative concentrations of OH and the hydroperoxy radical  $\text{HO}_2$ , which reacts with itself to form  $\text{H}_2\text{O}_2$ . Lower  $\text{NO}_x$  concentrations promote less OH and more  $\text{H}_2\text{O}_2$ , favoring aqueous  $\text{SO}_2$  oxidation. More complex organic peroxy radicals can also produce  $\text{H}_2\text{O}_2$ , and their concentrations also increase as  $\text{NO}_x$  concentrations decrease.

We explored oxidation changes in the high and low emissions cases by examining the ratio of aqueous  $\text{H}_2\text{O}_2$  oxidation to total oxidation (figure 4-7). The low emissions case has a larger fraction of aqueous-phase  $\text{SO}_2$  oxidation, as expected from lower  $\text{NO}_x$  concentrations, in most of the domain in January and over much of the eastern US in July. The largest difference are around the Ohio River Valley, where  $\text{H}_2\text{O}_2$  oxidation is (61%, 53%) of total oxidation in (January, July) in the high emissions case and (74%, 63%) in the low emissions case. Table 4.2 lists the percent changes in column burdens of several species, averaged over the eastern US (east of  $99^\circ$  W). Concentrations of tropospheric  $\text{H}_2\text{O}_2$  are (3.5%, 6.1%) higher in (January, July) in the low emissions case than in the high emissions case while OH concentrations are (2.3%, 3.7%) lower, supporting the link between  $\text{NO}_x$  emissions and  $\text{SO}_2$  oxidation.

	$\text{H}_2\text{O}_2$	OH	$\text{HO}_2$	NO	$\text{NO}_2$	$\text{O}_3$
Jan	3.49	-2.25	2.67	-0.24	-0.86	0.18
Jul	6.06	-3.69	1.50	-0.01	-0.02	-1.15

Table 4.2: Percent changes in various oxidation-relevant species from the high emissions case to the low emissions case. The values being compared are averages over the eastern US (east of  $99^\circ$  W) of tropospheric column burdens (up to 40 hPa) of the species.

We also investigated whether increased aqueous-phase oxidation would lead to

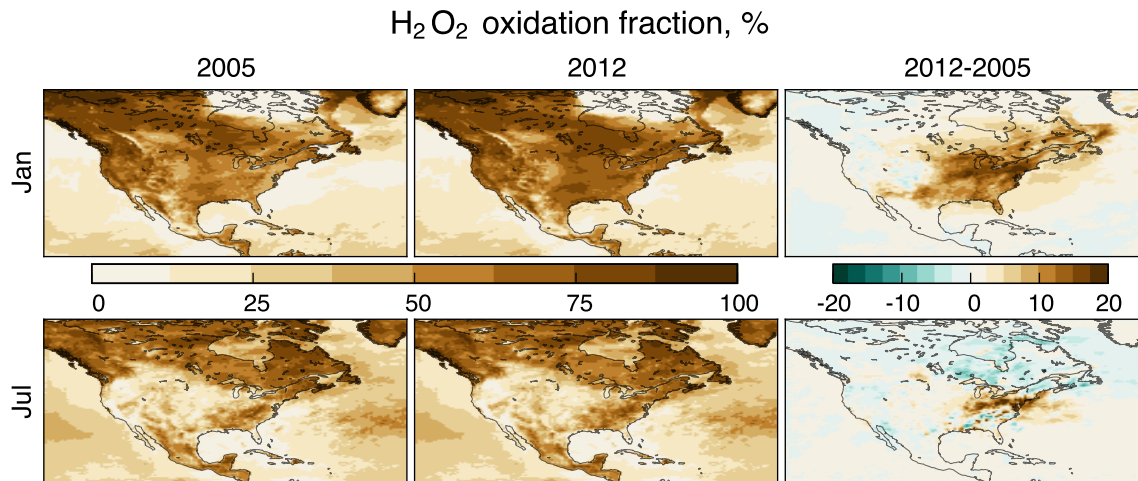


Figure 4-7: Ratio of aqueous oxidation by  $\text{H}_2\text{O}_2$  to total  $\text{SO}_2$  oxidation. Here, the oxidation rate is taken as the total kg S produced within the tropospheric column (up to 40 hPa) over the month of the simulation. The denominator of this fraction includes gas-phase OH oxidation; aqueous  $\text{H}_2\text{O}_2$  oxidation; aqueous  $\text{O}_3$  oxidation; and  $\text{O}_3$  oxidation on sea salt particles.

faster  $\text{SO}_2$  and  $\text{SO}_4^{2-}$  rainout due to more sulfur chemistry occurring within cloud droplets. The wet deposition rate is a measure of the speed of rainout. We have estimated this rate as the ratio of the monthly-total wet deposition to monthly-average column burden. Wet deposition rates of  $\text{SO}_4^{2-}$  are larger in the low emissions case than in the high emissions case by 12% and 15% in January and July, compared to 74% and 16% larger rates of aqueous  $\text{H}_2\text{O}_2$  oxidation. In addition, the differences in  $\text{PM}_{2.5}$  sensitivities to  $\text{SO}_2$  emissions between the high and low emissions cases are moderately spatially correlated ( $r^2 = 30\%$ ) with the differences in the  $\text{H}_2\text{O}_2$  fraction of oxidation. Thus, while slightly faster rainout occurs under lower  $\text{NO}_x$  emissions, it cannot compensate for the increase in aqueous oxidation.

We did not include the 25% decrease in CO emissions between 2005 and 2012 in our simulations. CO reacts with OH to form  $\text{HO}_2$  as the counterpart to  $\text{NO} + \text{HO}_2 \rightarrow \text{NO}_2 + \text{OH}$ . Lower CO emissions would lead to a larger OH/ $\text{HO}_2$  ratio, less  $\text{H}_2\text{O}_2$  production, and more gaseous  $\text{SO}_2$  oxidation. Thus, lower CO emissions could partially offset the shift to more aqueous-phase  $\text{SO}_2$  oxidation in our simulations. However, [Duncan et al. \(2010\)](#) suggest that much of the US is now in a  $\text{NO}_x$ -limited ozone formation regime and hence that  $\text{NO}_x$  exerts more control on  $\text{HO}_x$  partitioning

(and thus the  $\text{SO}_2$  oxidation pathway) than CO does.

### 4.4.3 Linearity of the system

Since  $\text{PM}_{2.5}$  sensitivities in the high and low emissions cases differ, this implies (by definition) that a constant-sensitivity model will have some error. Figure 4-8 shows the  $\text{PM}_{2.5}$  concentrations that would be predicted for the low emissions case, given the high emissions case sensitivities and concentrations. That is, it shows how a linear extrapolation from a few simulations, each slightly varying NEI05 emissions, would predict the results of the low emissions simulation. This kind of extrapolation is sometimes necessary as emissions inventories take years to compile and high-resolution air quality models are too computationally expensive to run over the entire range of potential emissions.

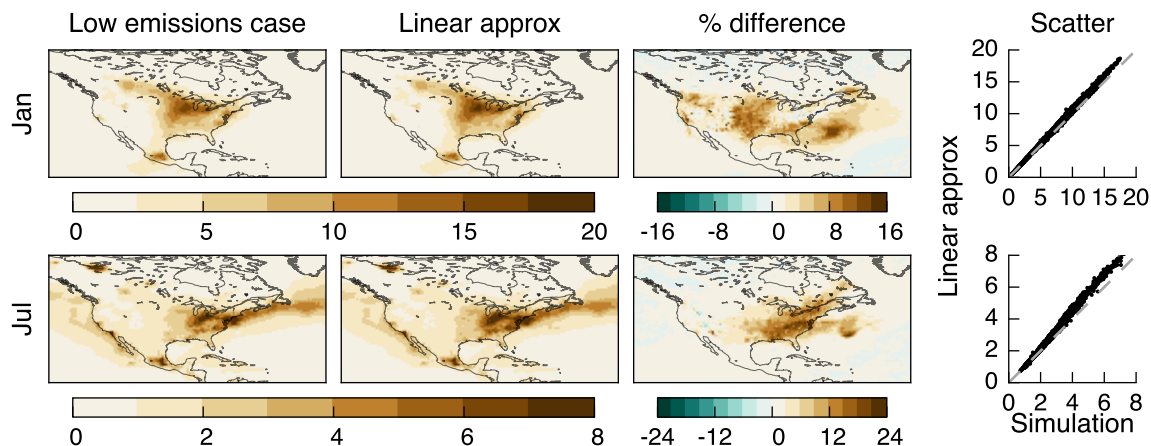


Figure 4-8: Modeled  $\text{PM}_{2.5}$  concentrations in the low emissions base case. The first column shows the full model results, as in figures 4-1 and 4-2. The second column is the linear extrapolation based on the concentrations and sensitivities in the high emissions case. The error in applying the linear extrapolation is highlighted as the fractional difference (third column) and deviation from the 1:1 line in a scatterplot comparison (fourth column). In the scatterplots, only points within the US are plotted.

The linear model shows deviations of 10% from the actual simulation in the central and southeast US in January. In July, the constant-sensitivity model deviates by 15% in most of the eastern US and by up to 25% in the mid-Atlantic coast. Elsewhere, the constant-sensitivity model is reasonably accurate. The constant-sensitivity model

consistently overestimates the concentrations, translating into an underestimate of the benefits of emissions reductions.

We have emphasized the errors in the constant-sensitivity model but the 15-25% overestimates of  $\text{PM}_{2.5}$  come from applying a linear model to roughly 50% changes in two of the three emitted species. The general agreement between the constant-sensitivity model and the full simulation is mainly due to the assumed lack of change in  $\text{NH}_3$  emissions. The large differences in  $\text{NH}_3$  sensitivities between the high and low emissions cases have no impact on the model predictions if  $\text{NH}_3$  emissions stay constant. If  $\text{NH}_3$  emissions were lowered from the low emissions case, however, then  $\text{PM}_{2.5}$  reductions would be much smaller than predicted from the constant-sensitivity model.

## 4.5 Discussion

Our study shows large differences in the sensitivities of  $\text{PM}_{2.5}$  concentrations to precursor emissions between two sets of simulations representing a 2005 baseline (high emissions) and a 2012 analogue (low emissions). We find that winter  $\text{NO}_x$  reductions represent a potential new opportunity for improving air quality, due to  $\text{PM}_{2.5}$  being more nitrate-limited under low emissions over much of the US, particularly the Midwest. Lower  $\text{NO}_x$  emissions also promote aqueous-phase  $\text{SO}_2$  oxidation, increasing the sensitivity of  $\text{PM}_{2.5}$  to  $\text{SO}_2$ . Sensitivities to  $\text{NH}_3$  emissions are lower in the low emissions case, primarily as a direct response to a less acidic atmosphere.

Results for winter in the northern Midwest are driven by the thermodynamic behavior of ammonium nitrate aerosols and are well-constrained for the meteorological conditions (i.e., cold and moist) that prevail there, where concentrations are highest. Figure 4-5 shows that nitrate availability will play a major role in determining  $\text{PM}_{2.5}$  in this region in the near future. Accounting for the high  $\text{NO}_3^-$  bias of the model can only push the system further into the nitrate-limited regime. Nevertheless, the large absolute sensitivities to winter  $\text{NO}_x$  emissions through  $\text{NO}_3^-$  formation are subject to the model bias. Several studies (Walker et al., 2012; Heald et al., 2012; Zhang et al.,

2012a) have shown that the standard GEOS-Chem simulation overestimates  $\text{HNO}_3$  and aerosol  $\text{NO}_3^-$  concentrations compared to both CASTNet and CSN measurements. There is evidence that certain types of  $\text{NO}_3^-$  measurements are biased low due to  $\text{HNO}_3$  volatilization from filters (Pakkanen et al., 1999; Schaap et al., 2004; Pathak et al., 2009), but adjusting for this does not always provide significant improvement (Squizzato et al., 2013). Studies with other air quality models (notably CAMx (Pinder et al., 2007) and CMAQ (Pinder et al., 2008; Dennis et al., 2008)) have emphasized the potential impact of  $\text{NH}_3$  emissions controls on  $\text{PM}_{2.5}$  concentrations, suggesting that our results are broadly consistent across models.

There are several possible sources of the nitrate bias in GEOS-Chem and other chemical transport models. The dependence of the rate of  $\text{N}_2\text{O}_5$  hydrolysis on aerosol water, nitrate, chloride, and organic content is uncertain, and nitric acid concentrations can be highly sensitive to the overall hydrolysis rate (Macintyre and Evans, 2010; Dennis et al., 2008; Bertram et al., 2009; Wen et al., 2014). Hydrolysis within GEOS-Chem includes limitation by nitrate, but this is a topic of ongoing research (Bertram et al., 2009; Wen et al., 2014; Chang et al., 2011; Simon et al., 2010; Hudson et al., 2007). GEOS-Chem produces more  $\text{HNO}_3$  from organic species reactions than other chemical mechanisms at low  $\text{NO}_x$  concentrations but performs comparably at high  $\text{NO}_x$  (Archibald et al., 2010). Heald et al. (2012) explore several other potential sources of bias, but no solution has yet been found. However, our thermodynamic analysis increases our confidence that the importance of  $\text{NO}_x$  emissions to winter  $\text{PM}_{2.5}$  is not an artifact of this model bias.

Model resolution can also affect model performance. Our simulations have a resolution of 55 km, compared to the 36 or 12 km resolution typical of regulatory models. Li et al. (2015) show differences in GEOS-Chem simulations of US  $\text{PM}_{2.5}$  at the nested and global resolutions. The maximum values for the three inorganic components are lower at low resolution, but the largest change (29%) is for  $\text{SO}_4^{2-}$  and changes are most substantial near cities. Thompson et al. (2014) show that  $\text{PM}_{2.5}$  within CAMx changes by 10% across model resolutions from 4–36 km. Pungler and West (2013) found that CMAQ simulations produce  $\text{PM}_{2.5}$  mortality estimates 11%

higher at 36 km resolution than at 12 km. Much coarser resolutions ( $>100$  km) show lower  $\text{PM}_{2.5}$  concentrations, but the relative changes are much larger for other components of  $\text{PM}_{2.5}$  than nitrate, sulfate, and ammonia. Our 55 km resolution is therefore sufficient for studying the regional response of inorganic  $\text{PM}_{2.5}$  to large, nation-wide changes in emissions, and the computational efficiency of the lower resolution allowed us to explore sensitivities (requiring several simulations for each case).

The change in sensitivity to  $\text{NH}_3$  emissions has several implications. First,  $\text{NH}_3$  emissions controls have been identified as a potentially cost-effective way to improve air quality (Pinder et al., 2007). We do not analyze the costs of emissions controls (though the costs of  $\text{SO}_2$  and  $\text{NO}_x$  controls have likely changed from the redistribution of sources) but the impacts of  $\text{NH}_3$  emissions controls could be much smaller than previously estimated. Second, previous studies comparing modeled and measured  $\text{PM}_{2.5}$  in the US (Henze et al., 2009; Heald et al., 2012; Zhang et al., 2012a; Dennis et al., 2008) have highlighted our generally poor understanding of the magnitude and seasonality of  $\text{NH}_3$  emissions. Decreased sensitivity to  $\text{NH}_3$  would limit the adverse effects of inaccurate emissions on model performance.

An alternative approach to our sensitivity analysis is to vary emissions based on economic sector (e.g., Caiazzo et al. (2013)). However, simultaneous emissions changes in multiple sectors will not have the impact on  $\text{PM}_{2.5}$  expected from changes in each sector individually. The changes in sensitivities presented here will help identify which sectors could be expected to have strong interactions. For example, broad agricultural  $\text{NH}_3$  and  $\text{NO}_x$  emissions can determine the neutralizing and oxidizing capacity of the background atmosphere and hence the impact of given coal  $\text{SO}_2$  emissions on  $\text{PM}_{2.5}$ .

Through this analysis, we find that lower  $\text{NO}_x$  and  $\text{SO}_2$  emissions lead to larger sensitivity to  $\text{SO}_2$ ; smaller sensitivity to  $\text{NH}_3$ ; and larger sensitivity to winter  $\text{NO}_x$  emissions in the US. These interactions provide new avenues for effective air quality regulations and emphasize the need to consider multiple pollutants simultaneously.

THIS PAGE INTENTIONALLY LEFT BLANK

# Chapter 5

## Direct radiative effects

Note: The work in this chapter is being submitted for publication in Journal of Geophysical Research – Atmospheres.

### 5.1 Introduction

Aerosols scatter and absorb solar radiation, affecting the energy budget of the earth system and thereby affecting climate. Scattering aerosols are primarily hygroscopic and include the inorganic ions sulfate, nitrate, and ammonium; hydrophilic organic carbon; and fine sea salt. Absorbing aerosols include coarse (and dehydrated) sea salt and dust as well as elemental carbon. In addition to direct interactions with radiation, aerosols affect cloud albedo (Twomey, 1974), cloud lifetime (Albrecht, 1989), and precipitation type (Rosenfeld et al., 2008). These direct and indirect effects contribute to changes in climate.

Radiative impacts can be quantified in a number of ways. Here, I use the same terminology as Heald et al. (2014): the direct radiative effect (DRE) of an atmospheric species is the instantaneous change in tropospheric radiation that would occur if that species were removed, without allowing the rest of the climate system to adjust. The DRE can be computed directly by using multiple radiative transfer evaluations. In contrast, the radiative forcing (RF) of an atmospheric species is the change in DRE since the pre-industrial era. This can be further split into the instantaneous

RF (IRF), which keeps all other climate components fixed, and the adjusted RF (ARF), which allows stratospheric temperatures and downwelling radiation to adjust. The most recent IPCC report (IPCC, 2013), based on the work of Lohmann et al. (2010), suggests using a ‘radiative forcing perturbation’ in which all atmospheric and land surface components (but not sea surface temperatures or sea ice) are allowed to respond. The goal in all of the adjusted forcings is to separate components of the climate system that respond quickly from slower ‘feedback’ mechanisms. These differences in terminology are presented here so that previous studies can be compared with the proper context.

The radiative effects of certain emissions have been well-studied, especially CO<sub>2</sub>. Myhre et al. (1998) gives simple relationships between concentrations of CO<sub>2</sub> and other greenhouse gases and their ARF. At concentrations of 400 ppm, the CO<sub>2</sub> ARF is 1.9 W m<sup>-2</sup> and its sensitivity to *concentrations* is 0.013 W m<sup>-2</sup> ppm<sup>-1</sup>. Matthews et al. (2009) shows that for timescales beyond 20 years, the sensitivity of global-mean temperatures to cumulative carbon emissions in their model is roughly constant, primarily due to cancellation between decreasing carbon uptake rates and decreasing radiative forcing sensitivity to CO<sub>2</sub> as emissions increase. The recent IPCC report (Collins et al., 2013) gives a best estimate of 1.5–2.0 K PgC<sup>-1</sup> for the medium-term (~20 year) global mean surface temperature sensitivity to cumulative carbon emissions. These numbers provide context for the radiative effects of other emissions, as CO<sub>2</sub> is by far the dominant long-term forcing agent.

The radiative effects of tropospheric O<sub>3</sub> precursor emissions are more complex than for CO<sub>2</sub>. Naik et al. (2005) looked at changes in both O<sub>3</sub> concentrations and CH<sub>4</sub> lifetime due to reductions in NO<sub>x</sub> emissions from nine global regions, including both the spatial and temporal patterns of the forcing. They find that the global-mean sensitivity of IRF to North American NO<sub>x</sub> emissions is 0.12 and -0.29 mW m<sup>-2</sup>/TgN yr<sup>-1</sup> for O<sub>3</sub> and CH<sub>4</sub>, respectively.<sup>1</sup> West et al. (2007) expanded on this work by looking at 30% global anthropogenic emissions reductions of CH<sub>4</sub>, NO<sub>x</sub>, CO, and non-methane

---

<sup>1</sup>The signs of these sensitivities are important; the O<sub>3</sub> sensitivity is positive because NO<sub>x</sub> reductions lead to O<sub>3</sub> reductions and hence reduce the O<sub>3</sub>-related forcing, but they increase CH<sub>4</sub> lifetime and hence increase CH<sub>4</sub>-related forcing.

volatile organic carbon species (NMVOC) and found global-average IRF sensitivities of 2.1,  $-0.25$ , 2.2 and  $0.52 \text{ mW m}^{-2}/\text{Tg yr}^{-1}$ , respectively. [Stevenson et al. \(2013\)](#) reviewed the ARF due to changes in  $\text{O}_3$ ,  $\text{CH}_4$ , and  $\text{CO}_2$  in the Atmospheric Chemistry and Climate Model Intercomparison Program models, including using 6 models for attribution of ARF to global anthropogenic precursor emissions. They find net ARF sensitivities of 2.77,  $-3.48$ , 0.370 and  $0.754 \text{ mW m}^{-2}$  to global emissions of  $\text{CH}_4$ ,  $\text{NO}_x$ ,  $\text{CO}$ , and NMVOC, respectively. They also note an additional  $127 \text{ mW m}^{-2}$  of forcing – 13% of the total ARF – due to nonlinear interactions between emissions, especially the change in  $\text{CH}_4$  atmospheric lifetime. In contrast, [Shindell \(2005\)](#) find that nonlinearities in ozone formation did not strongly impact the IRF of  $\text{O}_3$  and  $\text{CH}_4$  in their model because of this quantity’s strong relation to near-tropopause, remote  $\text{O}_3$  concentrations.

The impacts of emissions on aerosol DRE have also been studied. [Unger et al. \(2006\)](#) report that the total DRE of ozone precursor emissions may actually be dominated by their influence on  $\text{SO}_2$  oxidation rates. For projected emissions between 1995 and 2030, they find that changes in ozone precursors increase the DRE of  $\text{O}_3$  by  $0.35 \text{ W m}^{-2}$  over India and China, but also magnify the negative DRE of sulfate by  $-0.61 \text{ W m}^{-2}$  in the same area. The global average changes are much smaller, reflecting the local nature of these pollutants. [Shindell et al. \(2009\)](#) found a similar magnification of the ARF<sup>2</sup> from  $\text{CH}_4$ ,  $\text{CO}$ , and  $\text{NO}_x$  emissions when their effects on aerosols are included. [Shindell et al. \(2008\)](#) performs similar gas-and-aerosol experiments focusing on three economic sectors in both North America and developing Asia. Their sector approach precludes an estimate of the sensitivity to a single species, but they do show how North American industry and power sector emissions induce large but opposite DREs from aerosol and gaseous species. [Unger et al. \(2010\)](#) used a similar sector-based approach, emphasizing the evolution of IRF with time.

Relatively few studies have used experiments that allow for direct sensitivity calculations. [Shindell et al. \(2009\)](#) finds that the ARF sensitivity to global emissions

---

<sup>2</sup>It is not explicitly stated whether they studied the IRF or the ARF, but their comparison to IPCC AR4 values suggest ARF.

is 3.0, 0.26,  $-3.6$ ,  $-12.0$  and  $-14.0 \text{ mW m}^{-2} / \text{Tg yr}^{-1}$  for  $\text{CH}_4$ ,  $\text{CO}$ ,  $\text{NO}_x$ ,  $\text{SO}_2$ , and  $\text{NH}_3$ , respectively. They also show that including aerosol effects in ARF calculations increases the magnitude of the sensitivity to emissions (positive sensitivity for  $\text{CH}_4$  and  $\text{CO}$ , negative for  $\text{NO}_x$ ) relative to gas-only effects. For regional impacts, [Saikawa et al. \(2009\)](#) explored changes in Chinese emissions between 2000 and 2030 in different economic scenarios. The sensitivity of global-mean ARF to Chinese  $\text{SO}_2$  emissions,  $-3.5 \text{ mW m}^{-2} / \text{Tg yr}^{-1}$ , is roughly constant across scenarios.

Large changes in emissions can lead to nonlinear responses that are not represented in climate models without interactive chemistry. In particular, the Representative Concentration Pathways (RCPs) developed for the recent IPCC report are matched to emissions inventories for 2000-2005 and use integrated assessment model projections from 2005 onward ([Vuuren et al., 2011](#)). The RCPs, and by extension many of the most up-to-date climate projections, may be missing these large, recent changes in US aerosol precursor emissions. [Leibensperger et al. \(2012b\)](#) combine GEOS-Chem simulations with a general circulation model, comparing results with and without US aerosol precursor emissions. They find that US precursor emissions decrease surface temperatures in the eastern US, with the largest effects on extreme temperatures in summer and fall. Precursor emissions also decrease cloud cover and soil moisture availability in the eastern US. Climate impacts studies that are concerned with human heat stress (e.g. [Frumhoff and McCarthy \(2007\)](#)) or drought and agriculture ([Trnka et al., 2004](#); [Luo et al., 2005](#); [Tang et al., 2010](#)) may need to consider these recent changes in precursor emissions and their radiative effects.

In chapter 4 I showed how recent US emissions changes impacted the processes of inorganic aerosol formation. These same processes also affect aerosol radiative properties and hence the aerosol DRE. There are two factors that make the response of DRE to emissions distinct from that of surface concentrations. First, optical properties of aerosols depend much more strongly on relative humidity than the health effects do. High humidity can promote aerosol condensation, but only the dry aerosol mass is considered detrimental to human health. Particle size is critical to optical properties, so aerosol water content directly affects the radiative effect. Second, we

could focus entirely on concentrations over the US when considering air quality, but much of the radiative effects occur over the oceans.

This study extends the sensitivity calculations in Holt et al. (2015) to inorganic aerosol DRE. Section 5.2 briefly describes the chemical transport and radiative transfer models used. Section 5.3 presents the resulting estimates of the DRE, along with the sensitivity of the DRE to emissions. Section 5.4 explores the meaning and implications of these changes in sensitivities.

## 5.2 Methods

The goal of this work is to understand how US emissions of the inorganic aerosol precursors  $\text{NO}_x$ ,  $\text{SO}_2$ , and  $\text{NH}_3$  impact aerosol radiative effects. The impact of  $\text{NO}_x$  emissions is quantified as the sensitivity

$$\text{Sens}(\text{NO}_x) = \frac{\text{DRE}(\text{NO}_x^0 + \Delta\text{NO}_x) - \text{DRE}(\text{NO}_x^0 - \Delta\text{NO}_x)}{2\Delta\text{NO}_x} \quad (5.1)$$

and similarly for  $\text{SO}_2$  and  $\text{NH}_3$  emissions. Here,  $\text{NO}_x^0$  represents a base level of emissions and  $\Delta\text{NO}_x$  represents an additional amount of emissions. We calculated sensitivities centered around estimates for the base years of 2005 and 2012, with a focus on differences in sensitivities between these two cases.

The sensitivities defined above require both chemical and radiative quantities under a suite of emissions. Section 5.2.1 describes the chemical transport model used and the emissions applied. Section 5.2.2 broadly describes the radiative transfer model and our approach to estimating DRE. Section 5.2.3 compares our DRE estimation method to a fully coupled version of GEOS-Chem.

### 5.2.1 Chemical transport model GEOS-Chem

We used the GEOS-Chem model (Bey et al., 2001; Liu et al., 2001) version 9-02<sup>3</sup>. This model simulates ozone-NOx-hydrocarbon-aerosol chemistry and transport (Park

---

<sup>3</sup>Available at <http://geos-chem.org/>

et al., 2004). GEOS-Chem has previously been used to explore both regional atmospheric chemistry in the US (Henze et al., 2009; Heald et al., 2012; Walker et al., 2012; Zhang et al., 2012a) and atmospheric composition impacts on climate (Leibensperger et al., 2012a,b; Mickley et al., 2012; Heald et al., 2014).

Our results are from nested-grid simulations over the United States, allowing high spatial resolution of aerosol concentrations. In GEOS-Chem nested-grid simulations, a specified domain is modeled using the native resolution of the driving meteorological fields (Chen et al., 2009). In our simulations, the GEOS-5.2.0 meteorology was used with a resolution of  $0.5^\circ$  latitude by  $0.67^\circ$  longitude. The North American domain covers  $140^\circ$ – $40^\circ$  W and  $10^\circ$ – $70^\circ$  N. Boundary conditions come from global simulations at  $2^\circ \times 2.5^\circ$  resolution. The vertical grid for the chemistry includes 36 hybrid- $\sigma$  tropospheric layers extending up to 78.5 hPa (roughly 17.8 km) and 11 stratospheric layers extending up to 0.01 hPa. The timestep is 20 minutes for reactions and 10 minutes for transport.

The primary dataset used for US emissions is the EPA National Emissions Inventory for 2005 (NEI05). In the simulations used for sensitivity analysis, these emissions are scaled by a fixed fraction at every point; only the national, monthly total emissions are varied with no change in spatial or temporal structure. The EPA provides national, annual total emissions estimates for every year (US Environmental Protection Agency, 2014b) in addition to the national inventories every 3 years. To create the 2012 base case, we scaled US emissions within NEI05 to match the 42% and 62% decreases in national total  $\text{NO}_x$  and  $\text{SO}_2$  emissions between 2005 and 2012<sup>4</sup>. Table 2.5 shows the domain-total emissions of each species in the 2005 and 2012 base cases as well as the change in emissions applied to calculate sensitivities. In addition to  $\text{NO}_x$  and  $\text{SO}_2$ , CO emissions also decreased by 25.5% between 2005 and 2012, and we discuss the possible impact of this species on our results in section 5.4.

---

<sup>4</sup>Since starting this work, the EPA has revised its emissions estimates, resulting in a smaller decline in  $\text{NO}_x$  (33%) and a slightly larger decline in  $\text{SO}_2$  (64%).

## 5.2.2 Radiative transfer model RRTMG

To calculate aerosol DRE, we used the shortwave component of the Rapid Radiative Transfer Model for GCMs, version 3.9 (RRTMG, [Iacono et al. \(2008\)](#)). We use RRTMG as an off-line, post-processing tool, estimating DRE from monthly-average inorganic aerosol burden. However, RRTMG has also been integrated into GEOS-Chem by [Heald et al. \(2014\)](#) (hereafter H14) to compute radiative fluxes on-line with chemical transport. The next section compares our off-line approach to their on-line model results.

The primary outputs we use from the GEOS-Chem simulations are the monthly-average inorganic aerosol concentrations. The three components nitrate, sulfate, and ammonium are assumed to have the same optical properties, so we use the total dry aerosol mass concentrations (units of  $\mu\text{g aerosol (mol dry air)}^{-1}$ , derived from ppbv) for each simulation. Concentration values are saved in the 38 lowest model layers, which extend up to 40 hPa ( $\sim 22$  km).

For aerosol optical properties, we use a similar approach to the one detailed in H14. This approach treats aerosol optical properties for radiative transfer in the same manner as the photolysis module in GEOS-Chem. Briefly, aerosol optical properties are interpolated from a look-up table of extinction coefficient, single-scattering albedo, and 32 phase function coefficients to the relative humidity of the model grid cell. The look-up tables store these data for seven different relative humidities and 281 wavelengths from 250 to 4000 nm. The look-up tables are generated from a Mie scattering code ([Mishchenko et al., 1999](#)) and the Global Aerosol Data Set ([Köpke et al., 1997](#)) refractive indices for water-soluble species. These optical properties are aggregated to the 14 wavenumber bins used by RRTMG, weighted by the solar spectrum from [ASTM E490-00a \(2014\)](#).

The key solar input to RRTMG is the cosine of the solar zenith angle,  $\mu$ . For each latitude and month, we calculate the daytime-mean solar declination of the sun over that month. This daytime-mean accounts for points that are perpetually daytime or perpetually nighttime. (None of the points in the  $10\text{--}70^\circ$  N domain are perpetually

daytime or nighttime for all of January or July.) This average declination is then used to make a typical ‘day’ for that latitude and month. The radiative transfer model is run for 12 times between sunrise and maximum sun height with 12 corresponding  $\mu$  values. Pressure, temperature, and gas and aerosol concentrations are fixed at their monthly-average values for each time. The radiative fluxes and DRE values we show are the averages over these 12 points multiplied by the daytime-fraction for the month.

Additional inputs to RRTMG are either set as defaults or read directly from the GEOS-5.2.0 meteorology used for the simulations. Meteorological inputs include pressure, temperature, specific humidity, and surface albedo. For absorbing gas concentrations, we use the default values typical of midlatitude summer for ozone, oxygen, methane, and nitrous oxide. For carbon dioxide, we use a constant mixing ratio of 380 ppm typical of the year 2005. Water vapor concentration is calculated from the meteorological specific humidity. The surface albedo field from GEOS-5.2.0 is the energy-weighted average, appropriate for the shortwave spectral range. We apply the same albedo for direct and diffuse radiation in the UV/visible and near-IR ranges.

### 5.2.3 Off-line calculation validation

In this work, we used RRTMG as an off-line, post-processing tool rather than as an on-line radiative transfer module. In doing so, some of the inputs to RRTMG that would be instantaneous values have to be replaced with time-averaged inputs. The resulting off-line estimate thus has some level of error and bias relative to the on-line calculation.

There are three differences between the off-line approach used here and the on-line approach used by H14. First, the off-line approach uses fewer external data sources. H14 use climatological, horizontally and vertically varying profiles of absorbing gases; we use the midlatitude summer profiles for all points. Similarly, H14 use spectrally-varying albedo, where we use the energy-weighted averages from GEOS-5. Second, our approach uses monthly-mean values for meteorological quantities and aerosol concentrations. This reduces the number of radiative transfer calculations required,

	All		Land		Ocean	
	On-line	Off-line	On-line	Off-line	On-line	Off-line
JFM	-0.84	-0.87	-0.80	-0.85	-0.88	-0.88
AMJ	-1.38	-1.36	-1.49	-1.48	-1.29	-1.27
JAS	-1.11	-1.03	-1.36	-1.21	-0.92	-0.89
OND	-0.72	-0.72	-0.75	-0.73	-0.70	-0.71
Annual	-1.01	-1.00	-1.10	-1.07	-0.94	-0.94

Table 5.1: Domain-average DRE ( $\text{W m}^{-2}$ ) in the validation dataset. ‘On-line’ refers to the data from H14; ‘off-line’ refers to the post-processing approach used here.

but misses the effect of any covariance between concentrations and time of day. Third, the DRE in our approach is estimated as the difference between an atmosphere with gases and inorganic aerosols and an atmosphere with only gases. The DRE in H14 is the difference between an atmosphere with all species (gases and aerosols) and one without the aerosol species of interest. These differences in approaches lead to differences in estimates of DRE.

To quantify these differences, we applied our off-line approach to the monthly-average data provided by H14. We focus on the North American domain and divide the year (2010) into quarters: Jan/Feb/Mar, Apr/May/Jun, Jul/Aug/Sep, and Oct/Nov/Dec. Figures 5-1 and 5-2 compare the monthly-average DRE values from the on-line and off-line approaches as spatial maps and scatterplots, respectively. Table 5.1 lists the corresponding domain-averaged values.

There are two regions in which off-line DRE values do not quite match the on-line values. One region is north-central Canada in June and July. This region corresponds to a biomass burning event (wildfire) that occurred in 2010, leading to high concentrations of both inorganic and carbonaceous aerosols. In this region, the off-line DRE can be as large as  $-20 \text{ W m}^{-2}$ . The on-line DRE values, which include the competing effects of absorption and scattering, are rarely below  $-7 \text{ W m}^{-2}$ . The other region of mismatch is at high latitudes in spring. Large solar zenith angles and high-albedo ice and snow provide a much different radiative environment than seen at lower latitudes. Under these conditions, even primarily scattering aerosols can have a positive DRE because these aerosols increase the chance of absorption of light by the surface and

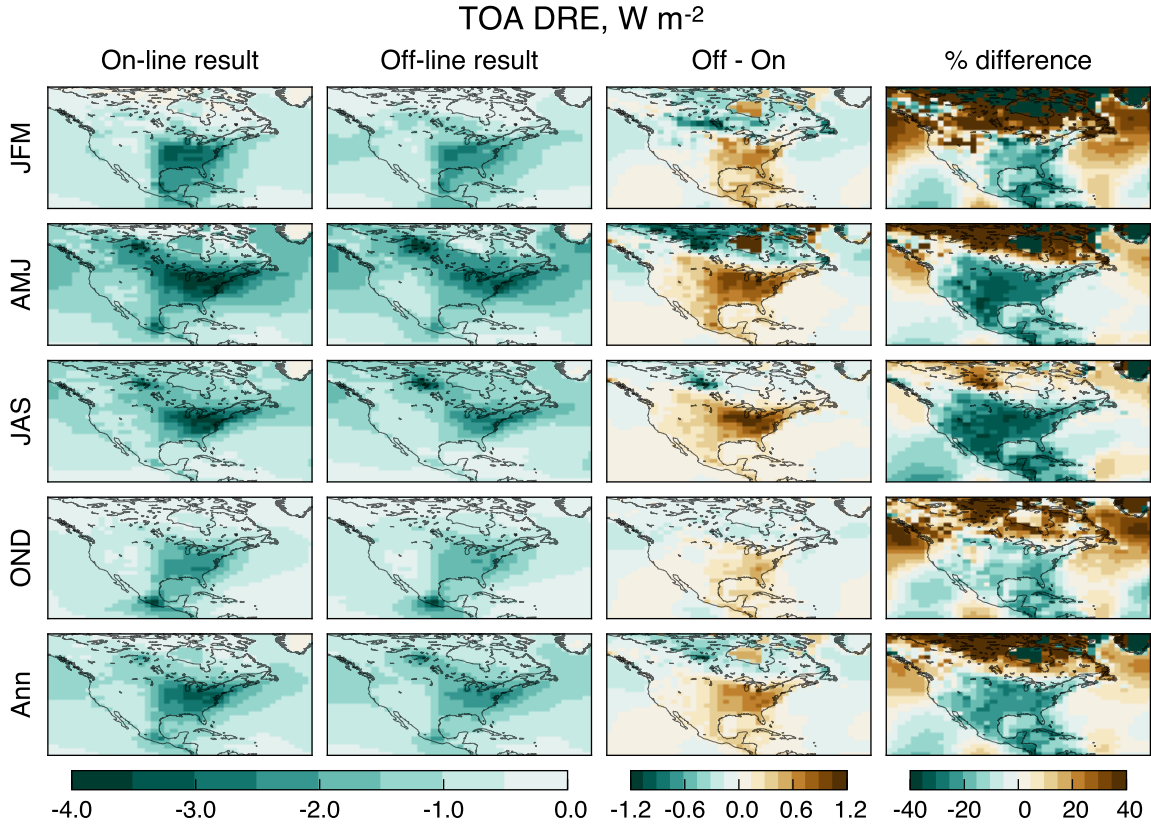


Figure 5-1: Inorganic aerosol DRE ( $W m^{-2}$ ) from the data of H14. The first column shows their results with on-line radiative transfer calculations. The second column shows the results from our off-line approach. The third and fourth columns show the absolute and fractional differences between these results. The data here have been aggregated into quarters of the year, with the annual average at the bottom.

by other aerosols. The post-processing approach reproduces some positive values, but not as many as the on-line approach.

The off-line approach shows overall agreement with the on-line calculations. We have found two sets of conditions – high absorbing aerosol concentrations and high-latitude spring – for which the approach is limited. However, the situations presented by these conditions are unlikely to be strongly affected by changes in US emissions. The off-line DRE estimates are too small over the US by 10-20%. This underestimate is relatively consistent across seasons, suggesting that it may be due to the neglect of other species (either aerosols or gases) rather than issues with averaging over a daily cycle. For the purposes of this work, i.e. calculating the sensitivity of inorganic aerosol DRE to US emissions, the off-line approach seems sufficient.

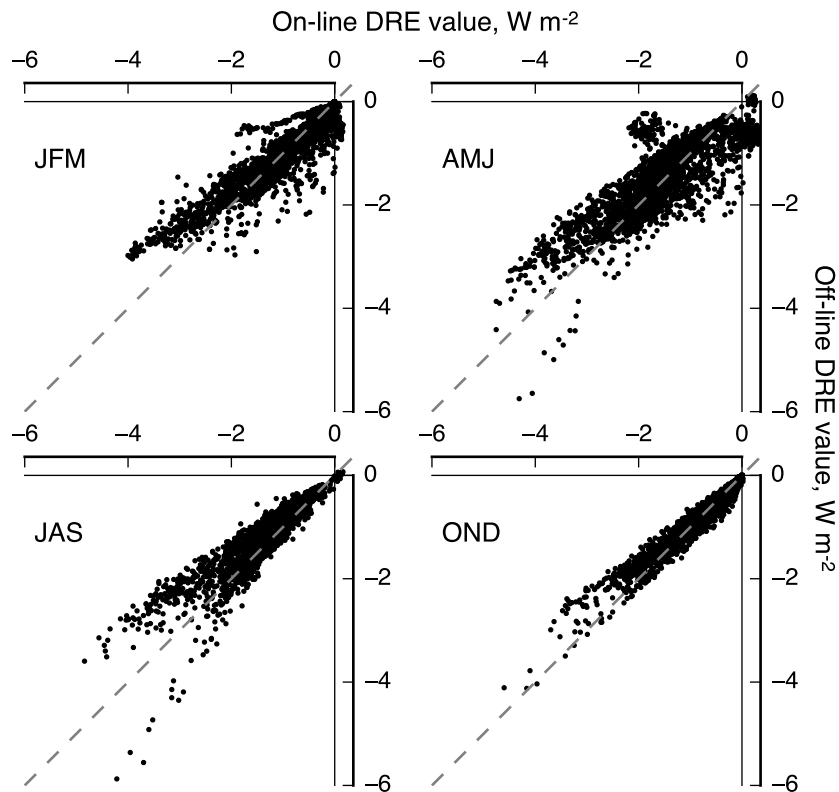


Figure 5-2: Comparison of the on-line (horizontal axis) and off-line (vertical axis) inorganic aerosol DRE. Each grid cell monthly average corresponds to a point, and the data are divided into quarters of the year (JFM=Jan/Feb/Mar, etc.). The dashed gray line is the 1:1 line. In the JAS averages, off-line DRE values extend to  $-20 \text{ W m}^{-2}$  due to a biomass burning event in late June and early July.

### 5.3 DRE and its sensitivity to emissions

In this section, we present estimates of the monthly-average inorganic aerosol DRE over the North American domain. We will first describe the DRE in the 2005 and 2012 base cases, including its spatial structure. Then we will cover the DRE sensitivities to emissions, with emphasis on domain-averaged quantities. Throughout this section, ‘DRE’ will mean the top-of-atmosphere radiative effect of inorganic aerosols relative to a gas-only atmosphere unless explicitly specified otherwise.

### 5.3.1 Base-case DRE

There are seasonal variations in both the value of the DRE in each case and in the differences between the 2005 and 2012 cases. In January, the largest DRE values occur over the southeastern US and southern Mexico (figure 5-3, top row). The DRE magnitude decreases quickly between the east coast and central Atlantic. However, the largest differences in January DRE between the 2005 and 2012 cases occur over the ocean. In July, large values of DRE occur over much of eastern North America, and there is a clear tongue of advection across the Atlantic (figure 5-3, bottom row). The July differences in DRE between the 2005 and 2012 cases extend a similar distance across the ocean as in January, but these differences now include much more of the nearby land surface.

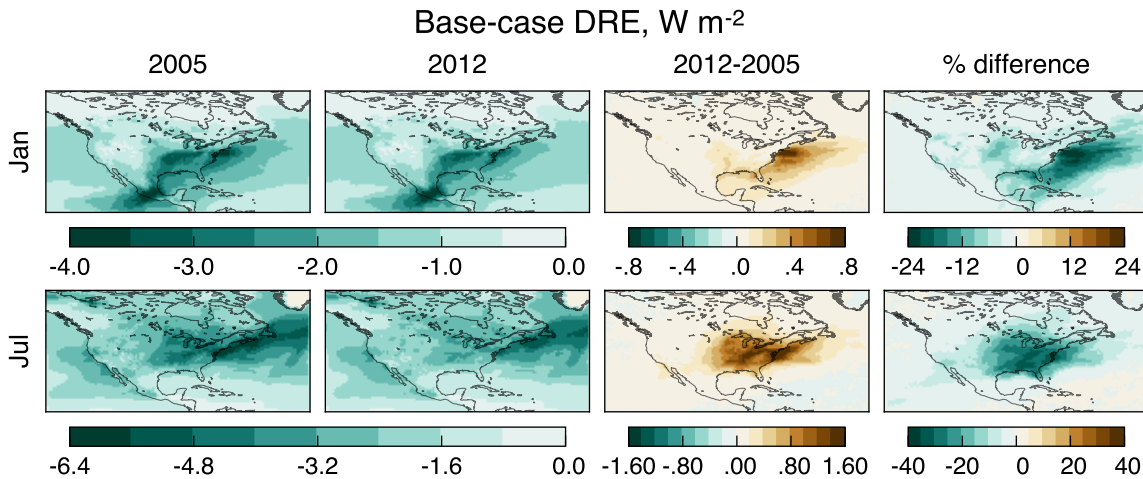


Figure 5-3: Inorganic aerosol DRE ( $\text{W m}^{-2}$ ) in the 2005 and 2012 base cases for January and July, along with the absolute and fractional differences between the cases.

Table 5.2 lists the domain-average DREs in the base cases and their differences, including over land and over ocean. The DRE over land is larger than over ocean in the summer, and *vice versa* in winter. There is remarkably little change in DRE over land in winter compared to summer, whereas the changes in ocean DRE in winter and in summer are comparable.

The changes in DRE are associated with changes in concentrations of each aerosol species throughout the atmosphere. These changes are shown in figure 5-4, averaged

	Jan				Jul			
	2005	2012	Diff	% diff	2005	2012	Diff	% diff
Total	-1.22	-1.16	59.4	-4.9	-2.20	-2.04	160.4	-7.3
Land	-1.06	-1.02	42.5	-4.0	-2.38	-2.12	262.1	-11.0
Ocean	-1.31	-1.24	69.8	-5.3	-2.09	-2.00	98.4	-4.7

Table 5.2: Domain-average DRE in the base-case simulations. The 2005 and 2012 values are in  $\text{W m}^{-2}$ ; the differences are in  $\text{mW m}^{-2}$ .

over land and over ocean. In January, the decreases in sulfate concentrations are limited to the lower troposphere, below about 600 hPa. The July decreases extend up to the tropopause. Ammonium concentrations show a similar pattern, but with July decreases limited to 400 hPa and below. Nitrate concentrations near the surface are actually larger in the 2012 case than 2005, except for July over land. Nitrate concentrations throughout the atmosphere are also larger in the 2012 case. This is most notable in summer, where nitrate concentrations near the tropopause are large. The total aerosol mass in each model layer (when averaged over this domain) is smaller in the 2012 case than the 2005 case except between about 350 and 150 hPa over ocean in July and over land in both January and July. As a result, total column burden and column AOD decrease from 2005 to 2012.

### 5.3.2 DRE sensitivities

For each base emissions case, we use six additional simulations with increased or decreased emissions of  $\text{NO}_x$ ,  $\text{SO}_2$ , or  $\text{NH}_3$ . The sensitivity values presented here are calculated using equation 5.1. The numerator in that expression is the average top-of-atmosphere DRE over the North American domain. The denominator is the total change in mass of US anthropogenic emissions, measured as mass of N for  $\text{NO}_x$  and  $\text{NH}_3$  and mass of S for  $\text{SO}_2$ . These sensitivities are plotted in figure 5-6.

In January, the sensitivity to  $\text{NO}_x$  emissions has the largest relative change between the 2005 and 2012 scenarios. The domain-average sensitivity to  $\text{NO}_x$  is larger by a factor of 5 in the 2012 case than the 2005 case. Most of the increase in sensitivity is over land, though sensitivity over ocean increases as well. Sensitivity to  $\text{SO}_2$

emissions increases as well: by 14.6% over land and 2.7% overall. These increases in sensitivity to  $\text{NO}_x$  and  $\text{SO}_2$ , which are the precursors to nitric and sulfuric acid, are consistent with a decrease in sensitivity to  $\text{NH}_3$ , the precursor to the base ammonium hydroxide. DRE sensitivity to  $\text{NH}_3$  decreases by 15.1% over land and 12.0% overall.

In July, the sensitivities to  $\text{SO}_2$  and  $\text{NH}_3$  show larger relative differences between the 2005 and 2012 cases than they did in January. These changes are concentrated over land, with sensitivity to  $\text{SO}_2$  increasing by 17.9% and sensitivity to  $\text{NH}_3$  decreasing by 24.3%. Sensitivity to  $\text{NO}_x$  increases as well – by 23.0% over land – but not as dramatically as the quintupling seen in January.

## 5.4 Discussion

The relative changes in sensitivities between the 2005 and 2012 cases indicates how accurate a simple scaling of aerosol radiative effects to emissions would be. Using the DRE from the July 2005 case; the sensitivities to each emission from that case; and the changes in emissions from 2005 to 2012, a simple scaling predicts a DRE value  $21.4 \text{ mW m}^{-2}$  larger than the actual DRE from the July 2012 case. Zeroing out all US emissions, based on 2005 sensitivities, gives a residual DRE of  $-1.83 \text{ W m}^{-2}$ . A rough estimate of the ‘attributable’ DRE from US emissions is the 2005 DRE minus this value, or  $-374.5 \text{ mW m}^{-2}$ . Thus the error from scaling the domain-average net radiative flux is about 5.7% of the total DRE attributable to US emissions. This is equivalent to underestimating the reduction in July  $\text{SO}_2$  emissions by 30.6 GgS, or 10.6% of US emissions in July 2005. In winter, simply scaling to US emissions gives a DRE value  $10.3 \text{ mW m}^{-2}$  too large, which is 7.1% of the possible change in DRE and equivalent to an additional 39.3 GgS reduction in  $\text{SO}_2$  emissions (13.6% of January 2005 US emissions).

These results can be compared to those from [Holt et al. \(2015\)](#) for surface concentrations in the context of air quality. Scaling the US-average surface concentrations from 2005 to 2012 using the sensitivities from the 2005 case results in overestimates of surface concentrations of 8.7% and 5.9% of the ‘US-attributable’ concentrations in

January and July, respectively. The US SO<sub>2</sub> emission equivalents are 342 GgS (118% of 2005) in January and 32 GgS (11% of 2005) in July. In other words, the reductions in wintertime fine particulate matter between 2005 and 2012 likely could not have been achieved with SO<sub>2</sub> reductions alone. The fractional overestimates in scaling are thus similar for DRE and surface concentrations, but how these overestimates translate into specific emissions reductions is different for these two impacts.

The large increase in sensitivity to winter NO<sub>x</sub> emissions implies that a future scaling of DRE to NO<sub>x</sub> emissions would be more inaccurate than the results shown above. If NO<sub>x</sub> emissions decreased by another 50 GgN beyond 2012 levels (17.6% of 2012 emissions), the differences in estimates based on scaling from 2005 values and from 2012 values is 13.0 mW m<sup>-2</sup>, 9.0% of the attributable DRE and equivalent to 48.3 GgS (44.0% of 2012 US emissions). Therefore as SO<sub>2</sub> emissions decrease and NO<sub>x</sub> sensitivities increase, the error made in not including NO<sub>x</sub> sensitivity changes becomes larger than the uncertainty expected for US SO<sub>2</sub> emissions.

The sensitivity of DRE to precursor emissions can be divided in two parts: the sensitivity of DRE to column aerosol burden, and the sensitivity of column burden to precursor emissions. Symbolically,

$$\text{Sens}(\text{DRE}, \text{Emissions}) = \text{Sens}(\text{DRE}, \text{Burden}) \times \text{Sens}(\text{Burden}, \text{Emissions}).$$

The fractional changes in sensitivities then (nearly) add together to give the total sensitivity:

$$\frac{\Delta\text{Sens}(\text{DRE}, \text{Emissions})}{\text{Sens}(\text{DRE}, \text{Emissions})} \approx \frac{\Delta\text{Sens}(\text{DRE}, \text{Burden})}{\text{Sens}(\text{DRE}, \text{Burden})} + \frac{\Delta\text{Sens}(\text{Burden}, \text{Emissions})}{\text{Sens}(\text{Burden}, \text{Emissions})}. \quad (5.2)$$

These fractional changes are listed in table 5.3. Note that the sensitivity of DRE to column burden is also referred to as the normalized radiative forcing (e.g. by [Haywood and Boucher \(2000\)](#)). This decomposition of sensitivities thus approximately separates the nonlinearities of chemical formation and transport of aerosols from the nonlinearities of radiative transfer.

In July, the fractional changes in sensitivity of DRE to burden are relatively small

Sensitivity of quantity: to variable	Jan			Jul		
	DRE: Emissions	Burden: Emissions	DRE: Burden	DRE: Emissions	Burden: Emissions	DRE: Burden
Species						
NO <sub>x</sub> , GgN	397.7	35.3	267.9	21.3	0.3	21.0
SO <sub>2</sub> , GgS	2.7	2.6	0.1	11.2	0.5	10.6
NH <sub>3</sub> , GgN	-12.0	3.0	-14.6	-16.9	2.2	-18.7

Table 5.3: Fractional changes in sensitivities between 2005 and 2012 cases, %. The column labels specify the sensitivity of the top quantity to changes in the bottom variable. For example, the second column is the sensitivity of DRE to changes in aerosol column burden. The three columns correspond to the three terms in equation 5.2.

for each emitted species; changes in column burden account for most of the changes in overall sensitivity. This is consistent with a fixed, linear relationship between DRE and inorganic aerosol burden and a constant normalized radiative forcing.

In January, however, changes in sensitivity of DRE to burden are larger than they were in July and make a noticeable contribution to the overall sensitivity of DRE to precursor emissions. In particular, the changes in DRE sensitivity to SO<sub>2</sub> emissions are almost entirely due to changes in the DRE-burden relationship. Finally, note that changes in the various sensitivities to NO<sub>x</sub> and SO<sub>2</sub> emissions are all of the same sign, but changes in sensitivities to NH<sub>3</sub> emissions are not. The same decrease in total mass of NH<sub>3</sub> emissions leads to smaller changes in total burden and total DRE in the 2012 case than in the 2005 case. However, DRE became *more* impacted by a given change in column burden. For NH<sub>3</sub> emissions, the changes in these sensitivities partially cancel rather than add.

Three mechanisms could be causing changes in the DRE-burden sensitivity. First, a change in the horizontal structure of aerosol burden could change the domain-average DRE-burden sensitivity. A targeted decrease in aerosols at points where they have the largest effect (e.g. over low-albedo oceans) would change the domain-average DRE-burden sensitivity. The January DRE-burden sensitivity does change much more over ocean than over land, with maximum changes of about 4%. Second, a change in vertical structure would also change the domain-average DRE-burden

sensitivity for the same reason: a disproportionate decrease in aerosols where they are most radiatively effective. In January, the aerosol concentration response to emissions is limited to the lower troposphere (800 hPa and below), whereas in July the response can reach 600 hPa and above. Third, the relationship between DRE and column burden could be intrinsically nonlinear because of a high optical depth. Inorganic aerosol optical depths in January peak at around 0.25 in January. While not particularly large, this value could be enough to induce a nonlinear radiative response when combined with the low solar zenith angles of winter. All three of these mechanisms are possible explanations for changes in DRE sensitivity to emissions beyond the nonlinear responses in concentrations alone.

All of the quantities presented here involve the aerosol direct radiative effect, not the aerosol direct radiative forcing. For a radiative forcing calculation, fluxes in the present-day (PD) and pre-industrial (PI) atmospheres are compared. For radiative effect, atmospheres with and without aerosols are compared. Figure 3 of H14 shows spatial maps of the DRE and DRF for 2010 from their simulations. Overall, DRF is uniformly small over the western US, eastern Pacific, and most of the northern Atlantic; most of the aerosol DRE in these areas is due to natural aerosols. In global averages, the DRF and DRE values for nitrate and ammonium are similar, whereas the DRF for sulfate is about half of the DRE. In sensitivity calculations, fluxes from two present-day atmospheres are being compared for both DRE and DRF, so the DRE and DRE sensitivities to precursor emissions are identical.

Part of this difference between DRF and DRE is due to pre-industrial precursor emissions being much lower than present-day emissions. Another part is due to pre-industrial oxidant concentrations being different from present-day. [Tsigaridis et al. \(2006\)](#) find an overall 74% increase in  $O_3$ ; a factor of 4 increase in  $NO_x$ ; and a 48% increase in  $H_2O_2$  between the PI and PD atmospheres. [Naik et al. \(2013\)](#) show that OH concentrations in the northern midlatitudes increased by 35% near the surface and decreased by 11% in the upper troposphere between PI and PD. A decrease in upper-tropospheric  $SO_2$  oxidation would lead to a longer  $SO_2$  atmospheric lifetime, but could also lead to less rainout once sulfate is produced. Such effects on lifetime

lead to a different spatial distribution of aerosols in the PI atmosphere in addition to lower total burdens and make comparing DRE and DRF values difficult. However, the results from H14 suggest that the DRF in the eastern US would be similar to but smaller than the DRE values shown here, whereas DRF in the western US and Pacific is small.

In this work, we focus on the response of inorganic aerosols to the direct precursors  $\text{NO}_x$ ,  $\text{SO}_2$ , and  $\text{NH}_3$ . However, US emissions of carbon monoxide decreased by 25.5% between 2005 and 2012. Carbon monoxide and other volatile organic species affect the concentrations of tropospheric ozone, hydrogen peroxide, and hydroxyl radicals, which are all oxidizers of  $\text{SO}_2$ . [Duncan et al. \(2010\)](#) suggest that decreased  $\text{NO}_x$  emissions led to increased sensitivity of ozone production rates to  $\text{NO}_x$ . Hence,  $\text{NO}_x$  would have a larger influence on the  $\text{SO}_2$  oxidation pathway than carbon monoxide or other organic species. However, their results are from satellite measurements over land, where direct oxidation of  $\text{SO}_2$  by ozone is negligible compared to other pathways. Oxidation by ozone is much more substantial over oceans. The changes in aerosol DRE over ocean in winter are primarily due to changes in sulfate concentrations, and these concentrations could be affected by changing carbon monoxide emissions.

## 5.5 Conclusion

In this study we extended the sensitivity analysis from [Holt et al. \(2015\)](#) to radiative impacts of US inorganic aerosol precursor emissions. We combined outputs from the chemical transport model GEOS-Chem with offline calculations of radiative transfer with RRTMG. From the 2005 National Emissions Inventory, we scale US precursor emissions of  $\text{NO}_x$ ,  $\text{SO}_2$ , and  $\text{NH}_3$  to match 2012 total emissions to create a year 2012 case. Emissions of these species were then increased and decreased around each base case, and the differences are used to calculate sensitivities. All simulations used a nested grid over the North American domain ( $140^\circ\text{--}40^\circ$  W,  $10^\circ\text{--}70^\circ$  N), boundary conditions from a global simulation, and meteorology from January or July of 2005.

We estimate that top-of-atmosphere, inorganic aerosol, direct radiative effects over

the North American domain decreased by 59 and 160  $\text{mW m}^{-2}$  in January and July, respectively, between 2005 and 2012. The majority of the change in summer DRE is over land, whereas DRE over ocean plays a larger role in the change in winter.

Between the 2005 and 2012 scenarios, sensitivities to  $\text{NO}_x$  and  $\text{SO}_2$  emissions increase while sensitivity to  $\text{NH}_3$  emissions decrease, consistent with the sensitivities of surface  $\text{PM}_{2.5}$  concentrations. In particular, sensitivity to January  $\text{NO}_x$  emissions increases by a factor of 5 between the 2005 and 2012 cases. The sensitivity of DRE to a precursor is typically larger over land than over ocean; the exception is  $\text{SO}_2$  in January. Changes in sensitivity are also concentrated over land, although sensitivity of DRE over ocean to January  $\text{NO}_x$  emissions shows an appreciable increase in magnitude between 2005 and 2012.

We find that simply scaling the DRE to total emissions based on the 2005 sensitivities leads to a domain-average DRE that is too large by 21.4  $\text{mW m}^{-2}$  in July and 10.3  $\text{mW m}^{-2}$  in January. These values are 5.7% and 7.1% of the estimated US-attributable DRE. Fractional overestimates of a similar size are seen in US-average surface aerosol concentrations. These DRE overestimates are also equivalent to additional  $\text{SO}_2$  emissions reductions of 39.3 GgS (13.6% of 2005) in January and 30.6 GgS (10.6% of 2005) in July. The increased sensitivity to  $\text{NO}_x$  emissions, especially in winter, suggests that further scaling would be more inaccurate.

The sensitivity of DRE to emissions can be separated into the sensitivities of DRE to aerosol burden and of aerosol burden to emissions. We find that in July, the majority of changes in DRE-emissions sensitivity can be attributed to changes in burden-emissions sensitivity. This perspective is consistent with a constant normalized radiative forcing. In January, however, the DRE-burden sensitivity can be an appreciable portion of the overall change. The changes in DRE-burden sensitivity could be due to nonlinearities in radiative transfer or to changes in horizontal or vertical structure of the aerosol burden.

Analysis of near-term or regional climate impacts often relies on the available global climate model runs, many of which are based on the RCPs. These RCPs may not include the full extent of US  $\text{NO}_x$  and  $\text{SO}_2$  emissions reductions over the last

decade. Our results show how well simply scaling aerosol radiative effects to precursor emissions, without adjusting for changes in chemistry and transport, might predict aerosol DRE around North America. Analyses that could be strongly influenced by aerosol DRE should consider using datasets forced by more recent emissions estimates.

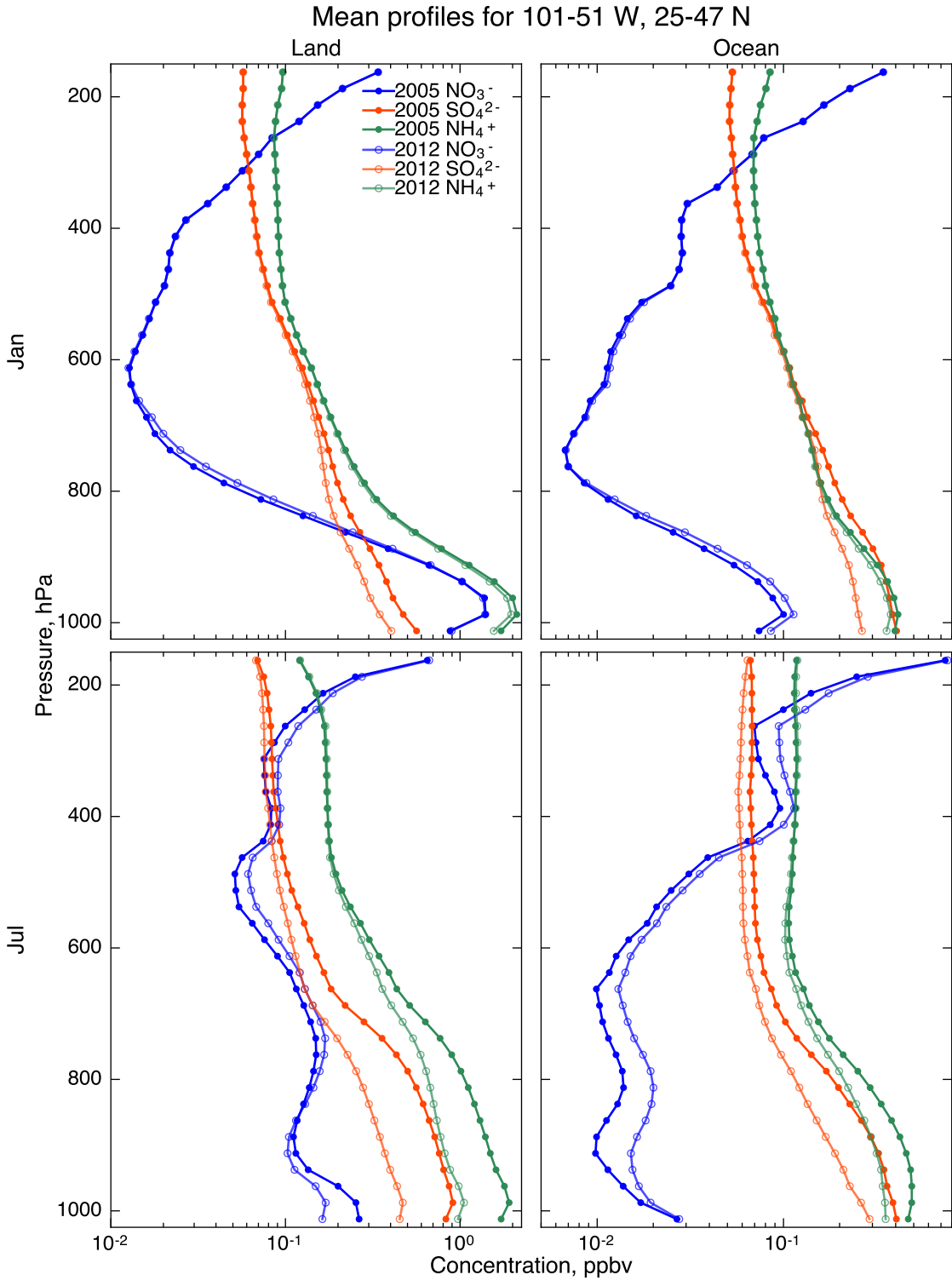


Figure 5-4: Vertical profiles of concentrations (mixing ratios, in ppbv) in the base cases. The top and bottom rows show January and July; the left and right columns are averages over land and over ocean. The blue, orange, and green lines show nitrate, sulfate, and ammonium concentrations. Dark, filled circles denote 2005 values and lighter, empty circles denote 2012. The profiles are averages over 101°-51° W and 25°-47° N; this domain is pictured in figure 5-5.

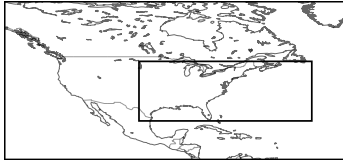


Figure 5-5: The domain used for the profiles in figure 5-4 with coastlines and country borders for orientation.

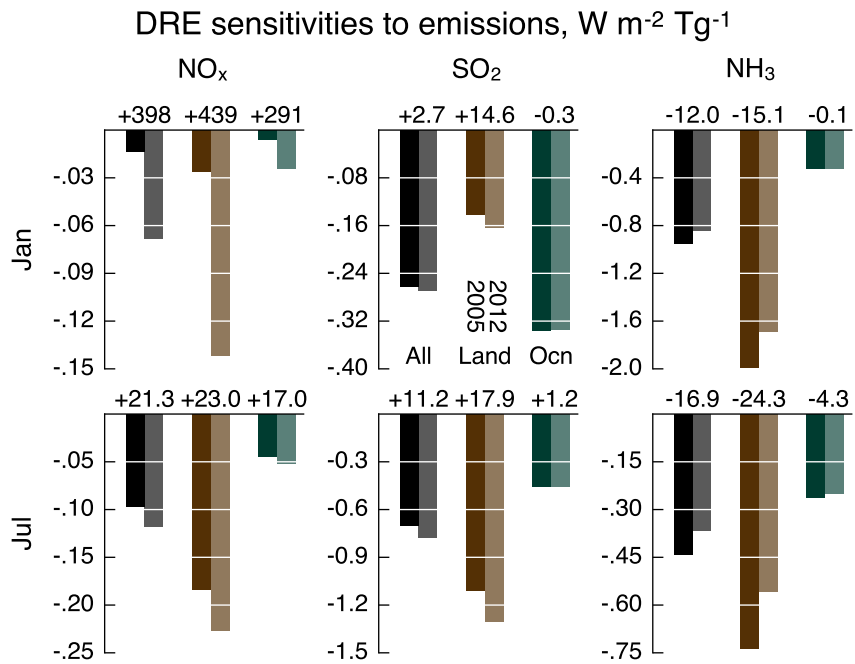


Figure 5-6: Domain-average DRE sensitivities to each precursor emission and for each month. In each plot, the three pairs of bars show averages over the full domain, over land, and over ocean. Within each pair, the left value is the sensitivity from the 2005 case and the right bar from the 2012 case. The numbers printed above each pair are the fractional (%) changes from 2005 to 2012. The units are given as  $W\ m^{-2}\ (TgN)^{-1}$  for NO<sub>x</sub> and NH<sub>3</sub> and  $W\ m^{-2}\ (TgS)^{-1}$  for SO<sub>2</sub>.

# Chapter 6

## Conclusions

### 6.1 Discussion

The work presented in this thesis was aimed at understanding how sensitivities to emissions may have changed over the last decade. From a scientific perspective, changes in sensitivity reflect nonlinearities in the behavior of the system. These nonlinear interactions give a system its complexity, so they are often the main focus of research. From a policy perspective, sensitivities help describe how effective a policy will be. To maintain effective policy, one must therefore understand how and why the sensitivities change.

This work has explored the sensitivities of two quantities – surface  $\text{PM}_{2.5}$  concentrations and aerosol direct radiative effect – to US emissions. Specifically, I studied inorganic aerosols, composed of  $\text{NO}_3^-$ ,  $\text{SO}_4^{2-}$ , and  $\text{NH}_4^+$ , and their immediate precursors  $\text{NO}_x$ ,  $\text{SO}_2$ , and  $\text{NH}_3$ . The physical processes that caused the changes in sensitivities were determined through analysis of the thermodynamics, chemical kinetics, and radiative aspects of the aerosol.

One key result of this work is that  $\text{NO}_3^-$  may now play a much larger role in both air quality and climate forcing than it did in 2005. Modeled surface aerosols in the winter northern Midwest transitioned from  $\text{NH}_3$ -limited to  $\text{NO}_3^-$ -limited as emissions were decreased, with a corresponding rise in sensitivity to  $\text{NO}_x$  emissions. Even in summer, some urban areas could be experiencing higher aerosol  $\text{NO}_3^-$  concentrations.

In the colder mid-troposphere, aerosol  $\text{NO}_3^-$  readily forms even in summer, leading to a broad area of relatively high sensitivity of aerosol DRE to  $\text{NO}_x$  emissions.

Another key result is that  $\text{SO}_2$  oxidation has shifted towards more aqueous  $\text{H}_2\text{O}_2$  oxidation and increased in rate. In our low-emissions (2012) simulations, OH concentrations are lower and  $\text{H}_2\text{O}_2$  concentrations are higher than in the high-emissions simulations. The fraction of  $\text{SO}_2$  oxidation that occurs via the aqueous  $\text{H}_2\text{O}_2$  path is also increased. Since aqueous oxidation is generally faster than gas-phase oxidation, the overall oxidation rate also increased. Thus, while  $\text{SO}_4^{2-}$  concentrations have decreased, sensitivities to  $\text{SO}_2$  emissions have generally increased, both for surface  $\text{PM}_{2.5}$  concentrations and DRE. Because  $\text{NO}_x$  concentrations strongly control  $\text{HO}_x$  partitioning, this result represents a crucial interaction between  $\text{NO}_x$  and  $\text{SO}_2$  emissions.

A consequence of these results is that sensitivities to  $\text{NH}_3$  emissions are much lower in the low-emissions case than in the high-emissions case. With lower  $\text{SO}_4^{2-}$  and total nitrate concentrations, less of the atmosphere is ammonia-limited in terms of aerosol formation. However, sensitivity to  $\text{NH}_3$  emissions could still be considered high, especially in winter, since the per-ton sensitivities to  $\text{NH}_3$  are typically an order of magnitude larger than for  $\text{NO}_x$  and  $\text{SO}_2$ . The impact of  $\text{NH}_3$  emissions controls would be smaller now than 10 years ago, but such controls may still be an effective way to improve air quality.

Various events led to the decline in US emissions between 2005 and 2012. [Russell et al. \(2012\)](#) cites the 2009 recession (global economics); a shift in electricity generation from coal to natural gas (national economics); and new vehicle emissions standards (direct policy action) as contributors to the decline. There are thus a variety of exogenous and endogenous contributors in addition to the direct impact of policy. The speed of the change in emissions emphasizes the need to understand and frequently re-evaluate what we think the sensitivities – and hence policy impacts – are. This is true not just for air quality and human health, but also for climate impacts, especially on the regional scale.

## 6.2 Future work

There are several ways this work can be expanded upon. One straightforward way is to include more variation in optical properties as aerosol composition varies. Each of the inorganic ions in the aerosol have slightly different refractive indices, which are all very different from the refractive index of water. The species also have different hygroscopicities, so aerosol water content also varies with composition. Allowing the optical properties to change in response to changing composition could lead to some subtle but measurable differences in the resulting DRE.

Throughout, the focus was on inorganic aerosols and their direct precursor emissions, as these quantities are directly linked. Changes in, and sensitivities to, CO and volatile organic carbon emissions were thus ignored. These species act opposite to  $\text{NO}_x$  in determining  $\text{HO}_x$  partitioning and overall oxidant concentrations. While the study of [Duncan et al. \(2010\)](#) suggests that changes in  $\text{NO}_x$  emissions would currently have a larger influence on oxidants, it would be useful to have a more direct verification of that behavior within this modeling framework.

Organic aerosols have also been ignored in this work, analogous to CO and VOC emissions. Organic aerosols, and especially secondary organic aerosols (SOA), are the focus of much of current atmospheric chemistry. SOA is directly linked to VOC emissions and depends on the speciation of those emissions. A thorough analysis of SOA sensitivities would thus introduce many more parameters than the three ( $\text{NO}_x, \text{SO}_2, \text{NH}_3$  emissions) I have used. Natural emissions also influence SOA more than they do inorganic aerosol, so SOA sensitivities may need to be calculated under a range of such natural emissions. The atmospheric lifetime of SOA is linked to its solubility, its carbon:oxygen ratio, and thus to oxidant concentrations, so  $\text{NO}_x$  emissions would still need to be included in SOA sensitivities. In addition to these complications, SOA formation itself is still highly uncertain and may not be represented well in any given chemical transport model. The methodology I have used in this work could in principle be applied to organic aerosols as well, but it would be extremely difficult.

In calculating sensitivities and creating different scenarios, I used a straightforward scaling of total anthropogenic US emissions. This approach provides a good conceptual picture of the regional impacts of the decline in emissions. However, it does not represent any specific change in economics or policy that would be employed in reality. Emissions from different economic sectors have different temporal and spatial distributions. They also have different chemical speciation. For example, it may be unphysical to independently vary power plant  $\text{SO}_2$  and  $\text{NO}_x$  emissions; it may also be unphysical to simultaneously vary power plant  $\text{SO}_2$  and transportation  $\text{SO}_2$  emissions<sup>1</sup>. Another type of sensitivity analysis, using adjoint models or another approach that produces field sensitivities, would be more suitable to studying the impacts of specific changes in emissions.

To isolate the changes in chemistry that lead to the changes in sensitivities, I used fixed meteorology from two months of 2005. However, aerosol  $\text{NO}_3^-$  concentrations vary strongly with temperature. Soil emissions of  $\text{NO}_x$  and  $\text{NH}_3$  and marine emissions of DMS also vary with surface temperature, as well as other meteorological factors (e.g. wind speed, photosynthetically active radiation). In addition, the increase in  $\text{SO}_2$  oxidation rate depends on the frequency and location of non-precipitating clouds. With the most fundamental mechanisms identified, it would be productive to explore the importance of meteorological and climate variability in these sensitivities.

The climate impacts work of this thesis was limited to the aerosol direct radiative effect, a quantity that can be computed within the framework of a chemical transport model. Within a full climate model, the influence of the recent emissions decline may turn out to be broader. The direct radiative effects of changing aerosol concentrations would influence soil moisture and evaporation; surface energy balance; and temperatures throughout the atmospheric column through radiative adjustment. Changing aerosol concentrations would also appear as indirect effects on the brightness and lifetime of clouds. These aspects of the climate impacts can only be assessed with a

---

<sup>1</sup>That different economic sectors have different emissions profiles is an even more fundamental issue for SOA sensitivities than for inorganic aerosols. Transportation is a large component of US  $\text{NO}_x$  emissions, but the associated VOC emissions depend on the type of vehicle driven. Whether commercial transport (trucks) and personal transport (cars) are varied independently is therefore a much larger issue for SOA than for inorganics.

model of atmospheric circulation, not just one with transport of chemicals.

## 6.3 Final notes

The work presented in this thesis involved the application of a framework of sensitivity analysis to questions of atmospheric chemistry. Sensitivity analysis is useful because it can help provide answers to questions about the benefits (or disbenefits) of changes in emissions, whether those changes are policy-driven or not. In addition, sensitivity analysis describes the behavior of a system. The sensitivities of an air quality metric and a climate forcing metric are shown to have changed in less than a decade. I hope that both the air quality and climate communities appreciate the importance and rapidity of this change and can be prepared for more like it in the future.

THIS PAGE INTENTIONALLY LEFT BLANK

# Appendix A

## Normalizing sensitivities

Throughout this work, I have been using the term ‘sensitivity’ to refer to the (exact or approximate) partial derivative

$$S^0 = \frac{\partial f}{\partial x}$$

where  $x$  is an input variable and  $f(x)$  is an output variable. For surface  $\text{PM}_{2.5}$  concentration sensitivity to  $\text{NO}_x$  emissions, the resulting units for  $S^0$  are  $\mu\text{g m}^{-3} (\text{Gg N})^{-1}$ , where the mass of emissions in the denominator is the change in total US anthropogenic  $\text{NO}_x$  emissions in a given month.

This definition of the sensitivity is straightforward to calculate and can be readily compared between different estimation methods. However, it lacks the context needed to be able to directly compare sensitivities across species, locations, and times. For example, the sensitivity of surface  $\text{PM}_{2.5}$  concentrations in the northern Midwest to winter  $\text{NH}_3$  emissions is much larger than the sensitivity to winter  $\text{SO}_2$  emissions or to summer  $\text{NH}_3$  emissions. However, the actual amount of winter  $\text{NH}_3$  emissions is also much smaller than the other two; that 1 Gg decrease in winter  $\text{NH}_3$  emissions represents a much larger fraction of the total anthropogenic emissions.

From a policy perspective, a regulation for a given industry may mandate a specific emissions reduction, and the sensitivity  $S^0$  given above provides a measure of the effectiveness of that mandate. In contrast, an emissions control device for commercial vehicles may reduce emissions by a fixed fraction. In that case,  $S^0$  does not directly

provide a measure of the policy effectiveness. The fractional change in emissions could also be more closely related to the economic costs of the change in emissions. A 200 kt reduction in the 1300 kt of winter  $\text{NO}_x$  emissions may seem difficult, but there was a 400 kt reduction between 2005 and 2012. A 200 kt reduction in the 170 kt of winter  $\text{NH}_3$  emissions, in contrast, is physically impossible. The normalized sensitivity may allow for an easier comparison between sensitivities to sources and species that have very different total emissions. It could thus be argued that a policy-relevant sensitivity would use the fractional change in emissions as the denominator:

$$S^1 = \frac{\partial f}{(\partial x)/x} = x \frac{\partial f}{\partial x} = x \cdot S^0.$$

For the surface concentration example, the units of  $S^1$  would be  $\mu\text{g m}^{-3}$  or  $\mu\text{g m}^{-3} / \%$ .

By a similar argument, using the fractional change in concentrations

$$S^2 = \frac{(\partial f)/f}{\partial x} = \frac{1}{f} \frac{\partial f}{\partial x} = \frac{S^0}{f}$$

could also lead to a more policy-relevant sensitivity. Areas where  $\text{PM}_{2.5}$  concentrations are already low are much less likely to have high sensitivities to emissions; there simply isn't as much room for change. People in these areas may still be interested in seeing which actions would most improve or degrade their air quality, though. Figures such as 4-3 and 4-4 do not make that comparison easy, as changes in those low-sensitivity areas are hard to identify.

Finally, these normalizations can be combined, resulting in

$$S^3 = \frac{(\partial f)/f}{(\partial x)/x} = \frac{x}{f} \frac{\partial f}{\partial x} = \frac{x}{f} S^0.$$

This quantity is common in economics, where it is referred to as the 'elasticity'. This quantity is fully dimensionless, though often written with units of  $\% / \%$ . Because it is dimensionless and scale-free, this definition of sensitivity can be used to compare a diverse set of inputs and outputs.

To say that a system has constant sensitivity means different things for different normalizations for sensitivity. The constant-sensitivity ('linear') models associated

with each of the above definitions are:

$$f^0(x) = S^0 \cdot (x - x_0) + f_0$$

$$f^1(x) = S^1 \cdot \ln(x/x_0) + f_0$$

$$f^2(x) = f_0 \cdot \exp(S^2(x - x_0))$$

$$f^3(x) = f_0 \cdot (x/x_0)^{(S^3)}$$

where  $x_0$  is some reference value for  $x$  and  $f_0 = f(x_0)$  is the reference value for  $f$ . If there are physical constraints on the variables, then that leads to limitations in what kind of constant-sensitivity model can be used. Some such constraints are:

- $f > 0$ . PM<sub>2.5</sub> concentrations cannot be negative, so any model of PM<sub>2.5</sub> concentrations should not give negative results. This is automatically true of  $f^2$  for all values of  $x$ , and true of  $f^3$  for positive values of  $x$ . It may or may not be true of  $f^0$  depending on the specific sensitivity and base values. For  $f^1$ , this constraint implies that  $x$  cannot be much smaller than  $x_0$  if  $S^1 > 0$ .
- Positive and negative sensitivities. If we know *a priori* that the sensitivity is strictly positive, then the constraint  $f > 0$  is easy to satisfy. If the sensitivity can have either sign, then the constraints for some models change. A negative  $S^0$  means that  $x$  cannot be too large or else  $f^0 < 0$ ; a negative  $S^3$  means that  $f^3$  explodes as  $x$  decreases.
- Behavior of  $f$  near  $x = 0$ . Model  $f^1$  cannot be applied to small values of  $x$ . Model  $f^3$  can be applied, but only if  $S^3$  is positive and we know that  $f(x = 0) = 0$ . In these two sensitivities, it is imperative to specify whether  $x$  refers to anthropogenic or total emissions; we expect that  $f(x = 0) > 0$  if  $x$  refers to anthropogenic emissions only. In contrast, the models  $f^0$  and  $f^2$  are unchanged by this distinction, as the difference  $x - x_0$  is unchanged.

As these examples should show, the question of whether one normalization of sensitivity is more appropriate than another depends critically on both what questions

one hopes to answer with the results and what can be assumed about the behavior of the system.

The last item in the list above highlights a fundamental tension in choosing which normalization to use. As mentioned before, the fractional change in anthropogenic emissions might be policy-relevant. However, the mass balance within the system depends most directly on total emissions. One could say that the most *physically*-relevant sensitivity would not be normalized. For this reason, I found that I was only able to understand and describe the mechanisms that control sensitivities and their changes over time by studying the non-normalized sensitivities.

For the numerator, non-normalized sensitivities seemed most appropriate for the particular impacts studied here. The work of [Dockery et al. \(1993\)](#) and others suggests that mortality and morbidity rates associated with  $\text{PM}_{2.5}$  decline linearly as  $\text{PM}_{2.5}$  concentrations decrease, even down to low concentrations.<sup>1</sup> Similarly, climate impacts can be expected to depend most closely on the total energy imbalance of the earth system, rather than the relative imbalance at a particular location.

---

<sup>1</sup>Nonlinear exposure-response behavior has been noted by [Pope et al. \(2011\)](#) and others, but mostly for concentrations higher than expected for US ambient air pollution.

# Bibliography

- J. Aitken. 1. On Dust, Fogs, and Clouds. *Proceedings of the Royal Society of Edinburgh*, 11:14–18, 1882. ISSN 0370-1646. doi: 10.1017/S0370164600046666. URL [http://journals.cambridge.org/abstract/\\_S0370164600046666](http://journals.cambridge.org/abstract/_S0370164600046666).
- B. A. Albrecht. Aerosols, Cloud Microphysics, and Fractional Cloudiness. *Science*, 245 (4923):1227–1230, sep 1989. ISSN 0036-8075. doi: 10.1126/science.245.4923.1227. URL <http://www.sciencemag.org/content/245/4923/1227>.
- A. Ångström. On the Atmospheric Transmission of Sun Radiation and on Dust in the Air. *Geografiska Annaler*, 11:156–166, 1929. doi: 10.2307/519399. URL <http://www.jstor.org/stable/519399?seq=1{#}page{ }scan{ }tab{ }contents>.
- A. S. Ansari and S. N. Pandis. Response of Inorganic PM to Precursor Concentrations. *Environmental Science & Technology*, 32(18):2706–2714, sep 1998. ISSN 0013-936X. doi: 10.1021/es971130j. URL <http://dx.doi.org/10.1021/es971130j>.
- A. Archibald, M. Jenkin, and D. Shallcross. An isoprene mechanism intercomparison. *Atmospheric Environment*, 44(40):5356–5364, dec 2010. ISSN 13522310. doi: 10.1016/j.atmosenv.2009.09.016. URL <http://www.sciencedirect.com/science/article/pii/S135223100900781X>.
- ASTM E490-00a. Standard Solar Constant and Zero Air Mass Solar Spectral Irradiance Tables. Technical report, ASTM International, West Conshohocken, PA, 2014. URL <http://www.astm.org/Standards/E490.htm>.
- T. H. Bertram and J. A. Thornton. Toward a general parameterization of N<sub>2</sub>O<sub>5</sub> reactivity on aqueous particles: the competing effects of particle liquid water, nitrate and chloride. *Atmospheric Chemistry and Physics*, 9(21):8351–8363, nov 2009. ISSN 1680-7324. doi: 10.5194/acp-9-8351-2009. URL <http://www.atmos-chem-phys.net/9/8351/2009/acp-9-8351-2009.html>.
- T. H. Bertram, J. A. Thornton, T. P. Riedel, A. M. Middlebrook, R. Bahreini, T. S. Bates, P. K. Quinn, and D. J. Coffman. Direct observations of N<sub>2</sub>O<sub>5</sub> reactivity on ambient aerosol particles. *Geophysical Research Letters*, 36:No. L19803, oct 2009. ISSN 0094-8276. doi: 10.1029/2009GL040248. URL <http://doi.wiley.com/10.1029/2009GL040248>.

- I. Bey, D. J. Jacob, R. M. Yantosca, J. A. Logan, B. D. Field, A. M. Fiore, Q. Li, H. Y. Liu, L. J. Mickley, and M. G. Schultz. Global modeling of tropospheric chemistry with assimilated meteorology: Model description and evaluation. *Journal of Geophysical Research*, 106(D19):23073–23095, oct 2001. ISSN 0148-0227. doi: 10.1029/2001JD000807. URL <http://doi.wiley.com/10.1029/2001JD000807>.
- T. C. Bond, S. J. Doherty, D. W. Fahey, P. M. Forster, T. Berntsen, B. J. DeAngelo, M. G. Flanner, S. Ghan, B. Kärcher, D. Koch, S. Kinne, Y. Kondo, P. K. Quinn, M. C. Sarofim, M. G. Schultz, M. Schulz, C. Venkataraman, H. Zhang, S. Zhang, N. Bellouin, S. K. Guttikunda, P. K. Hopke, M. Z. Jacobson, J. W. Kaiser, Z. Klimont, U. Lohmann, J. P. Schwarz, D. Shindell, T. Storelvmo, S. G. Warren, and C. S. Zender. Bounding the role of black carbon in the climate system: A scientific assessment. *Journal of Geophysical Research: Atmospheres*, 118(11):5380–5552, jun 2013. ISSN 2169897X. doi: 10.1002/jgrd.50171. URL <http://doi.wiley.com/10.1002/jgrd.50171>.
- F. Caiazzo, A. Ashok, I. A. Waitz, S. H. Yim, and S. R. Barrett. Air pollution and early deaths in the United States. Part I: Quantifying the impact of major sectors in 2005. *Atmospheric Environment*, 79:198–208, nov 2013. ISSN 13522310. doi: 10.1016/j.atmosenv.2013.05.081. URL <http://www.sciencedirect.com/science/article/pii/S1352231013004548>.
- W. L. Chang, P. V. Bhave, S. S. Brown, N. Riemer, J. Stutz, and D. Dabdub. Heterogeneous Atmospheric Chemistry, Ambient Measurements, and Model Calculations of N<sub>2</sub>O<sub>5</sub>: A Review. *Aerosol Science and Technology*, 45(6):665–695, apr 2011. ISSN 0278-6826. doi: 10.1080/02786826.2010.551672. URL <http://dx.doi.org/10.1080/02786826.2010.551672>.
- D. Chen, Y. Wang, M. B. McElroy, K. He, R. M. Yantosca, and P. Le Sager. Regional CO pollution and export in China simulated by the high-resolution nested-grid GEOS-Chem model. *Atmospheric Chemistry and Physics*, 9(11):3825–3839, jun 2009. ISSN 1680-7324. doi: 10.5194/acp-9-3825-2009. URL <http://www.atmos-chem-phys.net/9/3825/2009/acp-9-3825-2009.html>.
- A. J. Cohen, H. Ross Anderson, B. Ostro, K. D. Pandey, M. Krzyzanowski, N. Künzli, K. Gutschmidt, A. Pope, I. Romieu, J. M. Samet, and K. Smith. The global burden of disease due to outdoor air pollution. *Journal of toxicology and environmental health. Part A*, 68(13-14):1301–7, jan 2006. ISSN 1528-7394. doi: 10.1080/15287390590936166. URL <http://www.tandfonline.com/doi/abs/10.1080/15287390590936166>.
- M. Collins, R. Knutti, J. Arblaster, J.-L. Dufresne, T. Fichet, P. Friedlingstein, X. Gao, W. Gutowski, T. Johns, G. Krinner, M. Shongwe, C. Tebaldi, A. Weaver, and M. Wehner. Long-term Climate Change: Projections, Commitments and Irreversibility. In T. Stocker, D. Qin, G.-K. Plattner, M. Tignor, S. Allen, J. Boschung, A. Nauels, Y. Xia, V. Bex, and P. Midgley, editors, *Climate Change 2013: The Physical Science Basis. Contribution of Working Group I to the Fifth Assessment*

- Report of the Intergovernmental Panel on Climate Change*, chapter 12, page 1535. Cambridge University Press, Cambridge, United Kingdom and New York, NY, USA, 2013. URL <https://www.ipcc.ch/report/ar5/wg1/>.
- B. V. Constantin and S. R. H. Barrett. *Application of the complex step method to chemistry-transport modeling*. Sm, Massachusetts Institute of Technology, 2014.
- R. L. Dennis, P. V. Bhave, and R. W. Pinder. Observable indicators of the sensitivity of PM<sub>2.5</sub> nitrate to emission reductions. Part II: Sensitivity to errors in total ammonia and total nitrate of the CMAQ-predicted non-linear effect of SO<sub>2</sub> emission reductions. *Atmospheric Environment*, 42(6):1287–1300, feb 2008. ISSN 13522310. doi: 10.1016/j.atmosenv.2007.10.036. URL <http://www.sciencedirect.com/science/article/pii/S1352231007009478>.
- D. W. Dockery, C. A. Pope, X. Xu, J. D. Spengler, J. H. Ware, M. E. Fay, B. G. Ferris, and F. E. Speizer. An association between air pollution and mortality in six U.S. cities. *The New England journal of medicine*, 329(24):1753–9, dec 1993. ISSN 0028-4793. doi: 10.1056/NEJM199312093292401. URL <http://www.nejm.org/doi/full/10.1056/NEJM199312093292401?#t=article>.
- E. Drury, D. J. Jacob, R. J. D. Spurr, J. Wang, Y. Shinozuka, B. E. Anderson, A. D. Clarke, J. Dibb, C. McNaughton, and R. Weber. Synthesis of satellite (MODIS), aircraft (ICARTT), and surface (IMPROVE, EPA-AQS, AERONET) aerosol observations over eastern North America to improve MODIS aerosol retrievals and constrain surface aerosol concentrations and sources. *Journal of Geophysical Research*, 115(D14):D14204, jul 2010. ISSN 0148-0227. doi: 10.1029/2009JD012629. URL <http://doi.wiley.com/10.1029/2009JD012629>.
- B. N. Duncan, Y. Yoshida, J. R. Olson, S. Sillman, R. V. Martin, L. Lamsal, Y. Hu, K. E. Pickering, C. Retscher, D. J. Allen, and J. H. Crawford. Application of OMI observations to a space-based indicator of NO<sub>x</sub> and VOC controls on surface ozone formation. *Atmospheric Environment*, 44(18):2213–2223, jun 2010. ISSN 13522310. doi: 10.1016/j.atmosenv.2010.03.010. URL <http://www.sciencedirect.com/science/article/pii/S1352231010002050>.
- R. M. Errico. What Is an Adjoint Model? *Bulletin of the American Meteorological Society*, 78(11):2577–2591, nov 1997. ISSN 0003-0007. doi: 10.1175/1520-0477(1997)078<2577:WIAAM>2.0.CO;2. URL [http://journals.ametsoc.org/doi/abs/10.1175/1520-0477\(1997\)078{T1\textless}2577:WIAAM{T1\textgreater}2.0.CO;2](http://journals.ametsoc.org/doi/abs/10.1175/1520-0477(1997)078{T1\textless}2577:WIAAM{T1\textgreater}2.0.CO;2).
- N. Fann, C. M. Fulcher, and B. J. Hubbell. The influence of location, source, and emission type in estimates of the human health benefits of reducing a ton of air pollution. *Air quality, atmosphere, & health*, 2(3):169–176, sep 2009. ISSN 1873-9318. doi: 10.1007/s11869-009-0044-0. URL <http://www.pubmedcentral.nih.gov/articlerender.fcgi?artid=2770129&tool=pmcentrez&rendertype=abstract>.

- N. Fann, K. R. Baker, and C. M. Fulcher. Characterizing the PM<sub>2.5</sub>-related health benefits of emission reductions for 17 industrial, area and mobile emission sectors across the U.S. *Environment international*, 49:141–51, nov 2012. ISSN 1873-6750. doi: 10.1016/j.envint.2012.08.017. URL <http://www.ncbi.nlm.nih.gov/pubmed/23022875>.
- N. Fann, C. M. Fulcher, and K. Baker. The Recent and Future Health Burden of Air Pollution Apportioned Across U.S. Sectors. *Environmental science & technology*, mar 2013. ISSN 1520-5851. doi: 10.1021/es304831q. URL <http://www.ncbi.nlm.nih.gov/pubmed/23506413>.
- V. E. Fioletov, C. A. McLinden, N. Krotkov, M. D. Moran, and K. Yang. Estimation of SO<sub>2</sub> emissions using OMI retrievals. *Geophysical Research Letters*, 38(21):n/a–n/a, nov 2011. ISSN 00948276. doi: 10.1029/2011GL049402. URL <http://doi.wiley.com/10.1029/2011GL049402>.
- B. Ford and C. L. Heald. An A-train and model perspective on the vertical distribution of aerosols and CO in the Northern Hemisphere. *Journal of Geophysical Research*, 117(D6):D06211, mar 2012. ISSN 0148-0227. doi: 10.1029/2011JD016977. URL <http://doi.wiley.com/10.1029/2011JD016977>.
- C. Fountoukis and A. Nenes. ISORROPIA II: a computationally efficient thermodynamic equilibrium model for K-Ca-Mg-NH<sub>4</sub>-Na-SO<sub>4</sub>-NO<sub>3</sub>-Cl-H<sub>2</sub>O aerosols. *Atmospheric Chemistry and Physics*, 7(17):4639–4659, may 2007. ISSN 1680-7324. doi: 10.5194/acp-7-4639-2007. URL <http://www.atmos-chem-phys.net/7/4639/2007/files/13/FountoukisandNenes-2007-ISORROPIAIIacomputationallyefficientthermody.pdf>.
- P. Frumhoff and J. McCarthy. Confronting Climate Change in the U.S. Northeast: Science, impacts, and Solutions. . . . *US Northeast: science . . .*, 2007. URL <http://www.cabdirect.org/abstracts/20083177506.html>.
- I. M. Gelfand and S. V. Fomin. *Calculus of Variations*. Prentice-Hall, Englewood Cliffs, NJ, 1963. ISBN 9780486414485.
- A. Hakami. Nonlinearity in atmospheric response: A direct sensitivity analysis approach. *Journal of Geophysical Research*, 109:No. D15303, 2004. ISSN 0148-0227. doi: 10.1029/2003JD004502. URL <http://doi.wiley.com/10.1029/2003JD004502>.
- A. Hakami, M. T. Odman, and A. G. Russell. High-Order, Direct Sensitivity Analysis of Multidimensional Air Quality Models. *Environmental Science & Technology*, 37(11):2442–2452, jun 2003. ISSN 0013-936X. doi: 10.1021/es020677h. URL <http://dx.doi.org/10.1021/es020677h>.
- J. Haywood and O. Boucher. Estimates of the direct and indirect radiative forcing due to tropospheric aerosols: A review. *Reviews of Geophysics*, 38(4):513, 2000.

ISSN 8755-1209. doi: 10.1029/1999RG000078. URL <http://doi.wiley.com/10.1029/1999RG000078>.

- C. L. Heald, J. L. J. Collett, T. Lee, K. B. Benedict, F. M. Schwandner, Y. Li, L. Clarisse, D. R. Hurtmans, M. Van Damme, C. Clerbaux, P.-F. Coheur, S. Philip, R. V. Martin, and H. O. T. Pye. Atmospheric ammonia and particulate inorganic nitrogen over the United States. *Atmospheric Chemistry and Physics*, 12(21):10295–10312, may 2012. ISSN 1680-7324. doi: 10.5194/acp-12-10295-2012. URL <http://www.atmos-chem-phys.net/12/10295/2012/files/101/Healdetal.-2012-Atmosphericammoniaandparticulateinorganicznitr.pdf>.
- C. L. Heald, D. A. Ridley, J. H. Kroll, S. R. H. Barrett, K. E. Cady-Pereira, M. J. Alvarado, and C. D. Holmes. Contrasting the direct radiative effect and direct radiative forcing of aerosols. *Atmospheric Chemistry and Physics*, 14(11):5513–5527, jun 2014. ISSN 1680-7324. doi: 10.5194/acp-14-5513-2014. URL <http://www.atmos-chem-phys.net/14/5513/2014/acp-14-5513-2014.html>.
- D. K. Henze, A. Hakami, and J. H. Seinfeld. Development of the adjoint of GEOS-Chem. *Atmospheric Chemistry and Physics*, 7(9):2413–2433, may 2007. ISSN 1680-7324. doi: 10.5194/acp-7-2413-2007. URL <http://www.atmos-chem-phys.org/7/2413/2007/acp-7-2413-2007.html>.
- D. K. Henze, J. H. Seinfeld, and D. T. Shindell. Inverse modeling and mapping US air quality influences of inorganic PM<sub>2.5</sub> precursor emissions using the adjoint of GEOS-Chem. *Atmospheric Chemistry and Physics*, 9(16):5877–5903, aug 2009. ISSN 1680-7324. doi: 10.5194/acp-9-5877-2009. URL <http://www.atmos-chem-phys.net/9/5877/2009/>.
- J. Holt, N. E. Selin, and S. Solomon. Changes in inorganic fine particulate matter sensitivities to precursors due to large-scale us emissions reductions. *Environmental Science and Technology*, 49(8):4834–4841, 2015. ISSN 15205851. doi: 10.1021/acs.est.5b00008.
- J. Holt, S. Solomon, and N. E. Selin. Sensitivity of inorganic aerosol radiative effects to US emissions. *Journal of Geophysical Research*, In prep, 2016.
- R. C. Hudman, N. E. Moore, A. K. Mebust, R. V. Martin, A. R. Russell, L. C. Valin, and R. C. Cohen. Steps towards a mechanistic model of global soil nitric oxide emissions: implementation and space based-constraints. *Atmospheric Chemistry and Physics*, 12(16):7779–7795, aug 2012. ISSN 1680-7324. doi: 10.5194/acp-12-7779-2012. URL <http://www.atmos-chem-phys.net/12/7779/2012/acp-12-7779-2012.html>.
- P. K. Hudson, J. Schwarz, J. Baltrusaitis, E. R. Gibson, and V. H. Grassian. A spectroscopic study of atmospherically relevant concentrated aqueous nitrate solutions. *The journal of physical chemistry. A*, 111(4):544–8, feb 2007. ISSN 1089-5639. doi: 10.1021/jp0664216. URL <http://dx.doi.org/10.1021/jp0664216>.

- M. J. Iacono, J. S. Delamere, E. J. Mlawer, M. W. Shephard, S. A. Clough, and W. D. Collins. Radiative forcing by long-lived greenhouse gases: Calculations with the AER radiative transfer models. *Journal of Geophysical Research: Atmospheres*, 113(D13):D13103, jul 2008. ISSN 0148-0227. doi: 10.1029/2008JD009944. URL <http://doi.wiley.com/10.1029/2008JD009944>.
- IPCC. Climate Change 2013: The Physical Science Basis. Contribution of Working Group I to the Fifth Assessment Report of the Intergovernmental Panel on Climate Change. Technical report, IPCC, Cambridge, United Kingdom and New York, NY, USA, 2013. URL <https://www.ipcc.ch/report/ar5/wg1/>.
- D. Koch and A. D. Del Genio. Black carbon semi-direct effects on cloud cover: review and synthesis. *Atmospheric Chemistry and Physics*, 10(16):7685–7696, aug 2010. ISSN 1680-7324. doi: 10.5194/acp-10-7685-2010. URL <http://www.atmos-chem-phys.net/10/7685/2010/>.
- P. Köpke, M. Hess, I. Schult, and E. P. Shettle. *Global aerosol data set*. Max Planck Institute for Meteorology, Hamburg, Germany, rep. 243 edition, 1997.
- L. B. Lave and E. P. Seskin. An Analysis of the Association between U.S. Mortality and Air Pollution. *Journal of the American Statistical Association*, 68(342):284–290, jun 1973. ISSN 0162-1459. doi: 10.1080/01621459.1973.10482421. URL <http://www.tandfonline.com.libproxy.mit.edu/doi/abs/10.1080/01621459.1973.10482421>.
- E. M. Leibensperger, L. J. Mickley, D. J. Jacob, and S. R. Barrett. Intercontinental influence of NO<sub>x</sub> and CO emissions on particulate matter air quality. *Atmospheric Environment*, 45(19):3318–3324, jun 2011. ISSN 13522310. doi: 10.1016/j.atmosenv.2011.02.023. URL <http://www.sciencedirect.com/science/article/pii/S1352231011001579>.
- E. M. Leibensperger, L. J. Mickley, D. J. Jacob, W.-T. Chen, J. H. Seinfeld, A. Nenes, P. J. Adams, D. G. Streets, N. Kumar, and D. Rind. Climatic effects of 1950–2050 changes in US anthropogenic aerosols. Part 1: Aerosol trends and radiative forcing. *Atmospheric Chemistry and Physics*, 12(7):3333–3348, apr 2012a. ISSN 1680-7324. doi: 10.5194/acp-12-3333-2012. URL <http://www.atmos-chem-phys.net/12/3333/2012/acp-12-3333-2012.html>.
- E. M. Leibensperger, L. J. Mickley, D. J. Jacob, W.-T. Chen, J. H. Seinfeld, A. Nenes, P. J. Adams, D. G. Streets, N. Kumar, and D. Rind. Climatic effects of 1950–2050 changes in US anthropogenic aerosols. Part 2: Climate response. *Atmospheric Chemistry and Physics*, 12(7):3349–3362, apr 2012b. ISSN 1680-7324. doi: 10.5194/acp-12-3349-2012. URL <http://www.atmos-chem-phys.net/12/3349/2012/acp-12-3349-2012.html>.
- Y. Li, D. K. Henze, D. Jack, and P. L. Kinney. The influence of air quality model resolution on health impact assessment for fine particulate matter and

- its components. *Air Quality, Atmosphere & Health*, feb 2015. ISSN 1873-9318. doi: 10.1007/s11869-015-0321-z. URL <http://link.springer.com/10.1007/s11869-015-0321-z>.
- H. Liu, D. J. Jacob, I. Bey, and R. M. Yantosca. Constraints from  $^{210}\text{Pb}$  and  $^7\text{Be}$  on wet deposition and transport in a global three-dimensional chemical tracer model driven by assimilated meteorological fields. *Journal of Geophysical Research: Atmospheres*, 106(D11):12109–12128, jun 2001. ISSN 2156-2202. doi: 10.1029/2000JD900839. URL <http://onlinelibrary.wiley.com/doi/10.1029/2000JD900839/abstractfiles/128/Liuetal.-2001-Constraintsfrom210Pband7Beonwetdepositiona.pdf>.
- S. Liu and X.-Z. Liang. Observed Diurnal Cycle Climatology of Planetary Boundary Layer Height. *Journal of Climate*, 23(21):5790–5809, nov 2010. ISSN 0894-8755. doi: 10.1175/2010JCLI3552.1. URL <http://journals.ametsoc.org/doi/abs/10.1175/2010JCLI3552.1>.
- U. Lohmann, L. Rotstayn, T. Storelvmo, A. Jones, S. Menon, J. Quaas, A. M. L. Ekman, D. Koch, and R. Ruedy. Total aerosol effect: radiative forcing or radiative flux perturbation? *Atmospheric Chemistry and Physics*, 10(7):3235–3246, apr 2010. ISSN 1680-7324. doi: 10.5194/acp-10-3235-2010. URL <http://www.atmos-chem-phys.net/10/3235/2010/>.
- Q. Luo, R. N. Jones, M. Williams, B. Bryan, and W. Bellotti. Probabilistic distributions of regional climate change and their application in risk analysis of wheat production. *Climate Research*, 29:41–52, 2005.
- H. L. Macintyre and M. J. Evans. Sensitivity of a global model to the uptake of  $\text{N}_2\text{O}_5$  by tropospheric aerosol. *Atmospheric Chemistry and Physics*, 10(15):7409–7414, aug 2010. ISSN 1680-7324. doi: 10.5194/acp-10-7409-2010. URL <http://www.atmos-chem-phys.net/10/7409/2010/acp-10-7409-2010.html>.
- M. MacLeod, H. von Waldow, P. Tay, J. M. Armitage, H. Wöhrnschimmel, W. J. Riley, T. E. McKone, and K. Hungerbühler. BETR global – a geographically-explicit global-scale multimedia contaminant fate model. *Environmental pollution (Barking, Essex : 1987)*, 159(5):1442–5, may 2011. ISSN 1873-6424. doi: 10.1016/j.envpol.2011.01.038. URL <http://www.sciencedirect.com/science/article/pii/S0269749111000601>.
- P. A. Makar, M. D. Moran, Q. Zheng, S. Cousineau, M. Sassi, A. Duhamel, M. Besner, D. Davignon, L.-P. Crevier, and V. S. Bouchet. Modelling the impacts of ammonia emissions reductions on North American air quality. *Atmospheric Chemistry and Physics*, 9(18):7183–7212, sep 2009. ISSN 1680-7324. doi: 10.5194/acp-9-7183-2009. URL <http://www.atmos-chem-phys.net/9/7183/2009/acp-9-7183-2009.html>.
- W. C. Malm, J. F. Sisler, D. Huffman, R. A. Eldred, and T. A. Cahill. Spatial and seasonal trends in particle concentration and optical extinction in the United

- States. *Journal of Geophysical Research*, 99(D1):1347, 1994. ISSN 0148-0227. doi: 10.1029/93JD02916. URL <http://doi.wiley.com/10.1029/93JD02916>.
- P. T. Manktelow, G. W. Mann, K. S. Carslaw, D. V. Spracklen, and M. P. Chipperfield. Regional and global trends in sulfate aerosol since the 1980s. *Geophysical Research Letters*, 34:No. L14803, jul 2007. ISSN 0094-8276. doi: 10.1029/2006GL028668. URL <http://doi.wiley.com/10.1029/2006GL028668>.
- H. D. Matthews, N. P. Gillett, P. A. Stott, and K. Zickfeld. The proportionality of global warming to cumulative carbon emissions. *Nature*, 459(7248):829–32, jun 2009. ISSN 1476-4687. doi: 10.1038/nature08047. URL <http://dx.doi.org/10.1038/nature08047>.
- R. A. McCormick and J. H. Ludwig. Climate Modification by Atmospheric Aerosols. *Science*, 156(3780):1358–1359, jun 1967. ISSN 0036-8075. doi: 10.1126/science.156.3780.1358. URL <http://science.sciencemag.org.libproxy.mit.edu/content/156/3780/1358.abstract>.
- L. Mickley, E. Leibensperger, D. Jacob, and D. Rind. Regional warming from aerosol removal over the United States: Results from a transient 2010-2050 climate simulation. *Atmospheric Environment*, 46:545–553, jan 2012. ISSN 13522310. doi: 10.1016/j.atmosenv.2011.07.030. URL <http://www.sciencedirect.com/science/article/pii/S1352231011007722>.
- M. I. Mishchenko, J. M. Dlugach, E. G. Yanovitskij, and N. T. Zakharova. Bidirectional reflectance of flat, optically thick particulate layers: an efficient radiative transfer solution and applications to snow and soil surfaces. *Journal of Quantitative Spectroscopy and Radiative Transfer*, 63(2-6):409–432, sep 1999. ISSN 00224073. doi: 10.1016/S0022-4073(99)00028-X. URL <http://www.sciencedirect.com/science/article/pii/S002240739900028X>.
- N. Z. Muller. Linking Policy to Statistical Uncertainty in Air Pollution Damages Linking Policy to Statistical Uncertainty in Air Pollution Damages. *The B.E. Journal of Economic Analysis & Policy*, 11(1):No. 32, 2011.
- N. Z. Muller and R. Mendelsohn. Measuring the damages of air pollution in the United States. *Journal of Environmental Economics and Management*, 54(1):1–14, jul 2007. ISSN 00950696. doi: 10.1016/j.jeem.2006.12.002. URL <http://linkinghub.elsevier.com/retrieve/pii/S0095069607000095>.
- N. Z. Muller and R. Mendelsohn. Efficient Pollution Regulation: Getting the Prices Right, 2009. URL <http://www.jstor.org/stable/25592534>.
- N. Z. Muller, R. Mendelsohn, and W. Nordhaus. Environmental accounting for pollution in the United States economy. *American Economic Review*, 101(August):1649–1675, 2011. doi: 10.1257/aer.101.5.1649. URL <http://www.ingentaconnect.com/content/aea/aer/2011/00000101/00000005/art00001>.

- G. Myhre, E. J. Highwood, K. P. Shine, and F. Stordal. New estimates of radiative forcing due to well mixed greenhouse gases. *Geophysical Research Letters*, 25(14): 2715–2718, jul 1998. ISSN 00948276. doi: 10.1029/98GL01908. URL <http://doi.wiley.com/10.1029/98GL01908>.
- G. Myhre, B. H. Samset, M. Schulz, Y. Balkanski, S. Bauer, T. K. Berntsen, H. Bian, N. Bellouin, M. Chin, T. Diehl, R. C. Easter, J. Feichter, S. J. Ghan, D. Hauglustaine, T. Iversen, S. Kinne, A. Kirkevåg, J.-F. Lamarque, G. Lin, X. Liu, M. T. Lund, G. Luo, X. Ma, T. van Noije, J. E. Penner, P. J. Rasch, A. Ruiz, Ø. Seland, R. B. Skeie, P. Stier, T. Takemura, K. Tsigaridis, P. Wang, Z. Wang, L. Xu, H. Yu, F. Yu, J.-H. Yoon, K. Zhang, H. Zhang, and C. Zhou. Radiative forcing of the direct aerosol effect from AeroCom Phase II simulations. *Atmospheric Chemistry and Physics*, 13(4):1853–1877, feb 2013. ISSN 1680-7324. doi: 10.5194/acp-13-1853-2013. URL <http://www.atmos-chem-phys.net/13/1853/2013/acp-13-1853-2013.html>.
- V. Naik, D. Mauzerall, L. Horowitz, M. D. Schwarzkopf, V. Ramaswamy, and M. Oppenheimer. Net radiative forcing due to changes in regional emissions of tropospheric ozone precursors. *Journal of Geophysical Research*, 110(D24):D24306, 2005. ISSN 0148-0227. doi: 10.1029/2005JD005908. URL <http://doi.wiley.com/10.1029/2005JD005908>.
- V. Naik, L. W. Horowitz, A. M. Fiore, P. Ginoux, J. Mao, A. M. Aghedo, and H. Levy. Impact of preindustrial to present-day changes in short-lived pollutant emissions on atmospheric composition and climate forcing. *Journal of Geophysical Research: Atmospheres*, 118(14):8086–8110, jul 2013. ISSN 2169897X. doi: 10.1002/jgrd.50608. URL <http://doi.wiley.com/10.1002/jgrd.50608>.
- T. A. Pakkanen, R. E. Hillamo, M. Aurela, H. V. Andersen, L. Grundahl, M. Ferm, K. Persson, V. Karlsson, A. Reissell, O. Røyset, I. Fløisand, P. Oyola, and T. Ganko. Nordic intercomparison for measurement of major atmospheric nitrogen species. *Journal of Aerosol Science*, 30(2):247–263, feb 1999. ISSN 00218502. doi: 10.1016/S0021-8502(98)00039-1. URL <http://www.sciencedirect.com/science/article/pii/S0021850298000391>.
- R. J. Park, D. J. Jacob, B. D. Field, R. M. Yantosca, and M. Chin. Natural and trans-boundary pollution influences on sulfate-nitrate-ammonium aerosols in the United States: Implications for policy. *Journal of Geophysical Research: Atmospheres*, 109:No. D15204, may 2004. ISSN 2156-2202. doi: 10.1029/2003JD004473. URL <http://doi.wiley.com/10.1029/2003JD004473>.
- R. K. Pathak, W. S. Wu, and T. Wang. Summertime PM<sub>2.5</sub> ionic species in four major cities of China: nitrate formation in an ammonia-deficient atmosphere. *Atmospheric Chemistry and Physics*, 9(5):1711–1722, mar 2009. ISSN 1680-7324. doi: 10.5194/acp-9-1711-2009. URL <http://www.atmos-chem-phys.net/9/1711/2009/acp-9-1711-2009.html>.

- F. Paulot and D. J. Jacob. Hidden Cost of U.S. Agricultural Exports: Particulate Matter from Ammonia Emissions. *Environmental Science & Technology*, 48(2): 903–908, dec 2013. ISSN 0013-936X. doi: 10.1021/es4034793. URL <http://dx.doi.org/10.1021/es4034793>.
- R. W. Pinder, P. J. Adams, S. N. Pandis, and A. B. Gilliland. Temporally resolved ammonia emission inventories: Current estimates, evaluation tools, and measurement needs. *Journal of Geophysical Research: Atmospheres*, 111:No. D16310, 2006. doi: 10.1029/2005JD006603. URL <http://onlinelibrary.wiley.com/doi/10.1029/2005JD006603/full>.
- R. W. Pinder, P. J. Adams, and S. N. Pandis. Ammonia Emission Controls as a Cost-Effective Strategy for Reducing Atmospheric Particulate Matter in the Eastern United States. *Environmental Science & Technology*, 41(2):380–386, may 2007. ISSN 0013-936X. doi: 10.1021/es060379a. URL <http://www.ncbi.nlm.nih.gov/pubmed/17310695>.
- R. W. Pinder, R. L. Dennis, and P. V. Bhave. Observable indicators of the sensitivity of PM<sub>2.5</sub> nitrate to emission reductions. Part I: Derivation of the adjusted gas ratio and applicability at regulatory-relevant time scales. *Atmospheric Environment*, 42(6):1275–1286, feb 2008. ISSN 13522310. doi: 10.1016/j.atmosenv.2007.10.039. URL <http://www.sciencedirect.com/science/article/pii/S1352231007009508>.
- R.-E. Plessix. A review of the adjoint-state method for computing the gradient of a functional with geophysical applications. *Geophysical Journal International*, 167(2):495–503, nov 2006. ISSN 0956540X. doi: 10.1111/j.1365-246X.2006.02978.x. URL <http://gji.oxfordjournals.org/content/167/2/495.shorthhttp://gji.oxfordjournals.org/cgi/doi/10.1111/j.1365-246X.2006.02978.x>.
- C. A. {III}. Pope. Review: Epidemiological Basis for Particulate Air Pollution Health Standards. *Aerosol Science and Technology*, 32(1):4–14, may 2000. ISSN 0278-6826. doi: 10.1080/027868200303885. URL <http://www.tandfonline.com/doi/full/10.1080/027868200303885http://www.tandfonline.com/doi/abs/10.1080/027868200303885files/70/Pope-2000-ReviewEpidemiologicalBasisforParticulateAir.pdf>.
- C. A. {III}. Pope, R. T. Burnett, M. C. Turner, A. Cohen, D. Krewski, M. Jerrett, S. M. Gapstur, and M. J. Thun. Lung Cancer and Cardiovascular Disease Mortality Associated with Ambient Air Pollution and Cigarette Smoke: Shape of the Exposure–Response Relationships, 2011. URL <http://ehp.niehs.nih.gov/1103639/>.
- E. M. Pungler and J. J. West. The effect of grid resolution on estimates of the burden of ozone and fine particulate matter on premature mortality in the United States. *Air quality, atmosphere, & health*, 6(3), sep 2013. ISSN 1873-9318. doi: 10.1007/s11869-013-0197-8. URL <http://www.pubmedcentral.nih.gov/articlerender.fcgi?artid=3862082{&}tool=pmcentrez{&}rendertype=abstract>.

- H. O. T. Pye, H. Liao, S. Wu, L. J. Mickley, D. J. Jacob, D. K. Henze, and J. H. Seinfeld. Effect of changes in climate and emissions on future sulfate-nitrate-ammonium aerosol levels in the United States. *Journal of Geophysical Research: Atmospheres*, 114:No. D01205, may 2009. ISSN 2156-2202. doi: 10.1029/2008JD010701. URL <http://onlinelibrary.wiley.com/doi/10.1029/2008JD010701/abstractfiles/109/Pyetal.-2009-Effectofchangesinclimateandemissionsonfutu.pdf>.
- D. Rosenfeld, U. Lohmann, G. B. Raga, C. D. O’Dowd, M. Kulmala, S. Fuzzi, A. Reissell, and M. O. Andreae. Flood or drought: how do aerosols affect precipitation? *Science (New York, N.Y.)*, 321(5894):1309–13, sep 2008. ISSN 1095-9203. doi: 10.1126/science.1160606. URL <http://www.sciencemag.org/content/321/5894/1309.figures-only>.
- A. R. Russell, L. C. Valin, and R. C. Cohen. Trends in OMI NO<sub>2</sub> observations over the United States: effects of emission control technology and the economic recession. *Atmospheric Chemistry and Physics*, 12(24):12197–12209, dec 2012. ISSN 1680-7324. doi: 10.5194/acp-12-12197-2012. URL <http://www.atmos-chem-phys.net/12/12197/2012/acp-12-12197-2012.html>.
- E. Saikawa, V. Naik, L. W. Horowitz, J. Liu, and D. L. Mauzerall. Present and potential future contributions of sulfate, black and organic carbon aerosols from China to global air quality, premature mortality and radiative forcing. *Atmospheric Environment*, 43(17):2814–2822, jun 2009. ISSN 13522310. doi: 10.1016/j.atmosenv.2009.02.017. URL <http://www.sciencedirect.com/science/article/pii/S135223100900137X>.
- M. Schaap, M. van Loon, H. M. ten Brink, F. J. Dentener, and P. J. H. Builtjes. Secondary inorganic aerosol simulations for Europe with special attention to nitrate. *Atmospheric Chemistry and Physics*, 4(3):857–874, jun 2004. ISSN 1680-7324. doi: 10.5194/acp-4-857-2004. URL <http://www.atmos-chem-phys.net/4/857/2004/acp-4-857-2004.html>.
- J. H. Seinfeld and S. N. Pandis. *Atmospheric Chemistry and Physics: From Air Pollution to Climate Change*. John Wiley & Sons, New York, 2012. ISBN 1118591364. URL <http://books.google.com/books?hl=en&lr=&id=YH2K9eWsZ0cC&pgis=1>.
- D. Shindell, J.-F. Lamarque, N. Unger, D. Koch, G. Faluvegi, S. Bauer, M. Ammann, J. Cofala, and H. Teich. Climate forcing and air quality change due to regional emissions reductions by economic sector. *Atmospheric Chemistry and Physics*, 8(23):7101–7113, dec 2008. ISSN 1680-7324. doi: 10.5194/acp-8-7101-2008. URL <http://www.atmos-chem-phys.net/8/7101/2008/acp-8-7101-2008.html>.
- D. T. Shindell. An emissions-based view of climate forcing by methane and tropospheric ozone. *Geophysical Research Letters*, 32(4):L04803, 2005. ISSN 0094-8276. doi: 10.1029/2004GL021900. URL <http://doi.wiley.com/10.1029/2004GL021900>.

- D. T. Shindell, G. Faluvegi, D. M. Koch, G. A. Schmidt, N. Unger, and S. E. Bauer. Improved attribution of climate forcing to emissions. *Science (New York, N.Y.)*, 326(5953):716–8, oct 2009. ISSN 1095-9203. doi: 10.1126/science.1174760. URL <http://science.sciencemag.org.libproxy.mit.edu/content/326/5953/716.abstract>.
- H. Simon, Y. Kimura, G. McGaughy, D. Allen, S. Brown, D. Coffman, J. Dibb, H. Osthoff, P. Quinn, and J. Roberts. Modeling heterogeneous ClNO<sub>2</sub> formation, chloride availability, and chlorine cycling in Southeast Texas. *Atmospheric Environment*, 44(40):5476–5488, dec 2010. ISSN 13522310. doi: 10.1016/j.atmosenv.2009.09.006. URL <http://www.sciencedirect.com/science/article/pii/S1352231009007717>.
- H. Simon, K. R. Baker, and S. Phillips. Compilation and interpretation of photochemical model performance statistics published between 2006 and 2012. *Atmospheric Environment*, 61:124–139, dec 2012. ISSN 13522310. doi: 10.1016/j.atmosenv.2012.07.012. URL <http://www.sciencedirect.com/science/article/pii/S135223101200684X>.
- W. Squire and G. Trapp. Using Complex Variables to Estimate Derivatives of Real Functions. *SIAM Review*, 40(1):110–112, jan 1998. ISSN 0036-1445. doi: 10.1137/S003614459631241X. URL <http://epubs.siam.org/doi/abs/10.1137/S003614459631241X>.
- S. Squizzato, M. Masiol, A. Brunelli, S. Pistollato, E. Tarabotti, G. Rampazzo, and B. Pavoni. Factors determining the formation of secondary inorganic aerosol: a case study in the Po Valley (Italy). *Atmospheric Chemistry and Physics*, 13(4):1927–1939, feb 2013. ISSN 1680-7324. doi: 10.5194/acp-13-1927-2013. URL <http://www.atmos-chem-phys.net/13/1927/2013/acp-13-1927-2013.html>.
- D. S. Stevenson, P. J. Young, V. Naik, J.-F. Lamarque, D. T. Shindell, A. Voulgarakis, R. B. Skeie, S. B. Dalsoren, G. Myhre, T. K. Berntsen, G. A. Folberth, S. T. Rumbold, W. J. Collins, I. A. MacKenzie, R. M. Doherty, G. Zeng, T. P. C. van Noije, A. Strunk, D. Bergmann, P. Cameron-Smith, D. A. Plummer, S. A. Strode, L. Horowitz, Y. H. Lee, S. Szopa, K. Sudo, T. Nagashima, B. Josse, I. Cionni, M. Righi, V. Eyring, A. Conley, K. W. Bowman, O. Wild, and A. Archibald. Tropospheric ozone changes, radiative forcing and attribution to emissions in the Atmospheric Chemistry and Climate Model Intercomparison Project (ACCMIP). *Atmospheric Chemistry and Physics*, 13(6):3063–3085, mar 2013. ISSN 1680-7324. doi: 10.5194/acp-13-3063-2013. URL <http://www.atmos-chem-phys.net/13/3063/2013/acp-13-3063-2013.html>.
- S. Takahama, A. E. Wittig, D. V. Vayenas, C. I. Davidson, and S. N. Pandis. Modeling the diurnal variation of nitrate during the Pittsburgh Air Quality Study. *Journal of Geophysical Research*, 109:No. D16S06, 2004. ISSN 0148-0227. doi: 10.1029/2003JD004149. URL <http://doi.wiley.com/10.1029/2003JD004149>.

- G. Tang, B. Beckage, B. Smith, and P. a. Miller. Estimating potential forest NPP, biomass and their climatic sensitivity in New England using a dynamic ecosystem model. *Ecosphere*, 1(6):art18, dec 2010. ISSN 2150-8925. doi: 10.1890/ES10-00087.1. URL <http://www.esajournals.org/doi/abs/10.1890/ES10-00087.1>.
- T. M. Thompson and N. E. Selin. Influence of air quality model resolution on uncertainty associated with health impacts. *Atmospheric Chemistry and Physics*, 12(20):9753–9762, oct 2012. ISSN 1680-7324. doi: 10.5194/acp-12-9753-2012. URL <http://www.atmos-chem-phys.net/12/9753/2012/>.
- T. M. Thompson, R. K. Saari, and N. E. Selin. Air quality resolution for health impact assessment: influence of regional characteristics. *Atmospheric Chemistry and Physics*, 14(2):969–978, jan 2014. ISSN 1680-7324. doi: 10.5194/acp-14-969-2014. URL <http://www.atmos-chem-phys.net/14/969/2014/acp-14-969-2014.html>.
- D. Q. Tong, L. Lamsal, L. Pan, C. Ding, H. Kim, P. Lee, T. Chai, K. E. Pickering, and I. Stajner. Long-term NO<sub>x</sub> trends over large cities in the United States during the great recession: Comparison of satellite retrievals, ground observations, and emission inventories. *Atmospheric Environment*, 107:70–84, apr 2015. ISSN 13522310. doi: 10.1016/j.atmosenv.2015.01.035. URL <http://www.sciencedirect.com/science/article/pii/S1352231015000564>.
- M. Trnka, M. Dubrovský, D. Semerádová, and Z. Žalud. Projections of uncertainties in climate change scenarios into expected winter wheat yields. *Theoretical and Applied Climatology*, 77(3-4):229–249, mar 2004. ISSN 0177-798X. doi: 10.1007/s00704-004-0035-x. URL <http://link.springer.com/10.1007/s00704-004-0035-x>.
- K. Tsigaridis, M. Krol, F. J. Dentener, Y. Balkanski, J. Lathière, S. Metzger, D. A. Hauglustaine, and M. Kanakidou. Change in global aerosol composition since preindustrial times. *Atmospheric Chemistry and Physics*, 6(12):5143–5162, nov 2006. ISSN 1680-7324. doi: 10.5194/acp-6-5143-2006. URL <http://www.atmos-chem-phys.net/6/5143/2006/>.
- S. Twomey. Pollution and the planetary albedo. *Atmospheric Environment (1967)*, 8(12):1251–1256, dec 1974. ISSN 00046981. doi: 10.1016/0004-6981(74)90004-3. URL <http://www.sciencedirect.com/science/article/pii/0004698174900043>.
- N. Unger, D. T. Shindell, D. M. Koch, and D. G. Streets. Cross influences of ozone and sulfate precursor emissions changes on air quality and climate. *Proceedings of the National Academy of Sciences of the United States of America*, 103(12):4377–80, mar 2006. ISSN 0027-8424. doi: 10.1073/pnas.0508769103. URL <http://www.pnas.org/content/103/12/4377.full?sid=0718201d-d2b5-4bb0-8885-a8c7bf4bd7f1>.

- N. Unger, T. C. Bond, J. S. Wang, D. M. Koch, S. Menon, D. T. Shindell, and S. Bauer. Attribution of climate forcing to economic sectors. *Proceedings of the National Academy of Sciences of the United States of America*, 107(8):3382–7, feb 2010. ISSN 1091-6490. doi: 10.1073/pnas.0906548107. URL <http://www.pnas.org/content/107/8/3382.short>.
- US Environmental Protection Agency. Technical Support Document for the Proposed PM NAAQS Rule. Technical report, US Government, Research Triangle Park, NC, 2006.
- US Environmental Protection Agency. Chemical Speciation Network, 2014a. URL <https://www3.epa.gov/ttnamti1/speciepg.html>.
- US Environmental Protection Agency. National Emissions Inventory (NEI) air pollutant emissions trends data., 2014b. URL <https://www.epa.gov/air-emissions-inventories/air-pollutant-emissions-trends-data>.
- A. van Donkelaar, R. V. Martin, W. R. Leaitch, A. M. Macdonald, T. W. Walker, D. G. Streets, Q. Zhang, E. J. Dunlea, J. L. Jimenez, J. E. Dibb, L. G. Huey, R. Weber, and M. O. Andreae. Analysis of aircraft and satellite measurements from the Intercontinental Chemical Transport Experiment (INTEX-B) to quantify long-range transport of East Asian sulfur to Canada. *Atmospheric Chemistry and Physics*, 8(11):2999–3014, jun 2008. ISSN 1680-7324. doi: 10.5194/acp-8-2999-2008. URL <http://www.atmos-chem-phys.net/8/2999/2008/acp-8-2999-2008.html>.
- D. V. Vayenas, S. Takahama, C. I. Davidson, and S. N. Pandis. Simulation of the thermodynamics and removal processes in the sulfate-ammonia-nitric acid system during winter: Implications for PM2.5 control strategies. *Journal of Geophysical Research: Atmospheres*, 110:No. D07S14, may 2005. ISSN 2156-2202. doi: 10.1029/2004JD005038. URL <http://onlinelibrary.wiley.com/doi/10.1029/2004JD005038/abstract>.
- D. P. Vuuren, J. Edmonds, M. Kainuma, K. Riahi, A. Thomson, K. Hibbard, G. C. Hurtt, T. Kram, V. Krey, J.-F. Lamarque, T. Masui, M. Meinshausen, N. Nakicenovic, S. J. Smith, and S. K. Rose. The representative concentration pathways: an overview. *Climatic Change*, 109(1-2):5–31, aug 2011. ISSN 0165-0009. doi: 10.1007/s10584-011-0148-z. URL <http://link.springer.com/10.1007/s10584-011-0148-z>.
- J. M. Walker, S. Philip, R. V. Martin, and J. H. Seinfeld. Simulation of nitrate, sulfate, and ammonium aerosols over the United States. *Atmospheric Chemistry and Physics*, 12(22):11213–11227, nov 2012. ISSN 1680-7324. doi: 10.5194/acp-12-11213-2012. URL <http://www.atmos-chem-phys.net/12/11213/2012/acp-12-11213-2012.html>.
- L. Wen, J. Chen, L. Yang, X. Wang, X. Sui, L. Yao, Y. Zhu, J. Zhang, T. Zhu, and W. Wang. Enhanced formation of fine particulate nitrate at a rural site on

- the North China Plain in summer: the important roles of ammonia and ozone. *Atmospheric Environment*, 101:294–302, nov 2014. ISSN 13522310. doi: 10.1016/j.atmosenv.2014.11.037. URL <http://www.sciencedirect.com/science/article/pii/S1352231014009029>.
- J. West, A. Ansari, and S. Pandis. Marginal PM<sub>2.5</sub> : Nonlinear Aerosol Mass Response to Sulfate Reductions in the Eastern United States. *Journal of the Air & Waste Management Association*, 49(12):1415–1424, 1999. URL <http://www.tandfonline.com/doi/full/10.1080/10473289.1999.10463973>.
- J. J. West, A. M. Fiore, V. Naik, L. W. Horowitz, M. D. Schwarzkopf, and D. L. Mauzerall. Ozone air quality and radiative forcing consequences of changes in ozone precursor emissions. *Geophysical Research Letters*, 34(6):L06806, mar 2007. ISSN 0094-8276. doi: 10.1029/2006GL029173. URL <http://doi.wiley.com/10.1029/2006GL029173>.
- Y.-J. Yang, J. G. Wilkinson, and A. G. Russell. Fast, Direct Sensitivity Analysis of Multidimensional Photochemical Models. *Environmental Science & Technology*, 31(10):2859–2868, oct 1997. ISSN 0013-936X. doi: 10.1021/es970117w. URL <http://dx.doi.org/10.1021/es970117w>.
- L. Zhang, D. J. Jacob, E. M. Knipping, N. Kumar, J. W. Munger, C. C. Carouge, A. van Donkelaar, Y. X. Wang, and D. Chen. Nitrogen deposition to the United States: distribution, sources, and processes. *Atmospheric Chemistry and Physics*, 12(10):4539–4554, jul 2012a. ISSN 1680-7324. doi: 10.5194/acp-12-4539-2012. URL <http://www.atmos-chem-phys.net/12/4539/2012/files/105/Zhangetal.-2012-NitrogendepositiontotheUnitedStatesdistribu.pdf>.
- W. Zhang, S. L. Capps, Y. Hu, A. Nenes, S. L. Napelenok, and A. G. Russell. Development of the high-order decoupled direct method in three dimensions for particulate matter: enabling advanced sensitivity analysis in air quality models. *Geoscientific Model Development*, 5(2):355–368, mar 2012b. ISSN 1991-9603. doi: 10.5194/gmd-5-355-2012. URL <http://www.geosci-model-dev.net/5/355/2012/gmd-5-355-2012.html>.